UNIVERSITÀ DEGLI STUDI DI BERGAMO

Scuola di Alta formazione Dottorale

Corso di Dottorato in Ingegneria e Scienze Applicate

Ciclo XXIX

Settore scientifico disciplinare ING-IND/22 - Scienza e Tecnologia dei Materiali

CORROSION BEHAVIOR OF CARBON STEEL REBAR IN CALCIUM SULFOALUMINATE CSA-BASED SYSTEMS

Tesi di Dottorato

Simone Pellegrini

Matricola n. 54787

Tutor:

Chiar.mo Prof. Tommaso Pastore

Supervisore:

Chiar.ma Prof.ssa Marina Cabrini

Anno Accademico 2015/16

CONTENT

FIGURES INDEX

TABLES INDEX

ABSTRACT

The experimental work was carried out at University of Bergamo, Department of Engineering and Applied Sciences, and at Construction Material Testing Lab of University of Bergamo with the research group of Professor Tommaso Pastore, Professor Marina Cabrini and Eng. Sergio Lorenzi.

The experimental work concerning tests in solutions simulating the pore chemistry of CSA-based concretes were carried out in collaboration with the reasearch group of Professor Maria de Fátima Grilo da Costa Montemor and Eng. Yegor Morozov, from Instituto Superior Técnico – Universidade de Lisboa.

The use of ordinary binders to manufacture structural concrete for construction sector does not fully fit with the interests of cement industries, which are seeking to reduce the impact of cement production on environment, CO_2 emissions and consumption of raw materials and energy. Therefore, alternative binders are developed and studied, such as calcium sulfoaluminate (CSA) cement, which combines rapid hardening, high-early strength, with less CO_2 emission due to the lower temperature used for clinker production. Several studies regarding the mechanical and rheological properties of concretes manufactured with CSA cement are reported, whereas research on durability and corrosion behavior of carbon steel in such admixtures is still lacking. Compared with ordinary Portland cement (OPC), the hydration of CSA cement shows important difference that can influence durability of reinforced concrete structures, because it does not produce Ca(OH)2. Consequently, less alkaline pH is expected, which significantly affects corrosion behavior of steel reinforcing bars.

Furthermore, purpose of this work is the evaluation of the alkalinity level of concretes manufactured with CSA cement using pH sensible probes, pH indicators alternative to phenolphthalein and other techniques. Likewise, in order to investigate the corrosion behavior of carbon steel during different stages of hydration of calcium sulfoaluminate based cementitious systems, tests in simulating pore solutions at different pH and SO_4^{2-} concentration were carried out.

ACKNOWLEDGEMENTS

First, I would like to thank my father, the person to whom I dedicate this doctoral thesis, for letting me to become what I am.

Thanks to my mother, the strongest person that I have ever known.

Thanks to Silvia, for all the support, love and patience that she gave to me.

Thanks to Professors Tommaso Pastore and Marina Cabrini, thanks to Eng. Sergio Lorenzi, extraordinary colleagues and, above all, authentic friends.

Thanks to all of my friends, a special family that, day after day, can always surprise me and warm my heart.

CHAPTER 1

---

1 INTRODUCTION

The synergy between Portland cement-based concrete and carbon steel, both for mechanical and rheological properties and durability, led concrete to be the most used construction material. However, the impact on environment related to Portland cement production is huge and therefore, the trend in concrete manufacturing is changing. Between alternative hydraulic binder, calcium sulfoaluminate (CSA) cement deserves a special attention due to its characteristics, and mainly, for being a low-CO_2 emission alternative. However, it would be dangerous to assume that durability of CSA concretes is similar to that manufactured with ordinary Portland cement (OPC) and so, huge research must be done in order to outline a complete overview of the problem.

1.1 Trends of cement production

Cement is the most abundant man-made material with today's annual global production exceeding 4000 million of tons (Mt) with tendency to increase (Figure 1.1) [1] [2]. Most of the cement is manufactured in People's Republic of China (Figure 1.1), accounting for more than 55 % [1] [2] [3] [4] and the largest producers are LafargeHolcim (France), Anhui Conch Cement Company (People's Republic of China) and China National Building Material Company (People's Republic of China) with market shares of 6.8 % (287 Mt), 5.2 % (217 Mt) and 4.2 % (176 Mt) respectively [2] (Figure 1.2).
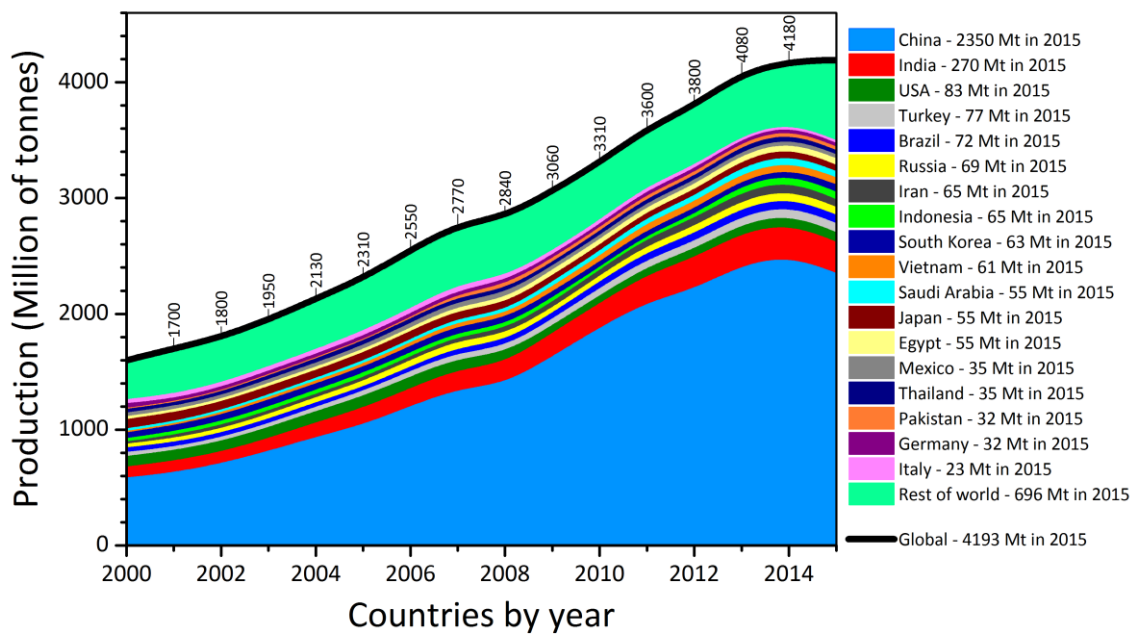
Figure 1.1: Cement production profile by country [1] [2].

- LafargeHolcim [287 Mt]
- Anhui Conch Cement Company [217 Mt]
- China National Building Material Company (CNBM) [176 Mt]
- HeidelbergCement [121 Mt]
- CEMEX S.A.B. de C.V. [87.1 Mt]
- Italcementi [76.6 Mt]
- China Resources Cement Holdings Limited (CRC) [71.0 Mt]
- Taiwan Cement Corporation [63.7 Mt]
- EUROCEMENT group [45.1 Mt]
- Votorantim Group [45.0 Mt]
- Cimpor - Cimentos de Portugal [28.1 Mt]
- Secil [9.75 Mt]
- Other [2970 Mt]

Figure 1.2: Main cement producers in 2015 [2].

Cement production is the largest contributor to the global carbon dioxide emissions, making up ca. 8 % [5]. The production of 1 ton of cement clinker – that represent 95% of cement mass - generates 800 kg of CO_2 [6] [7] and requires extensive energy consumption besides for clinker production, also for grinding. Further emissions are due to lime decomposition [1]. The production process consumes huge amount of fuel, which is approximately 2-3% of global primary energy [8].

Table 1.1 reports the specific consumption data in terms of raw material and energy required in order to produce 1 ton of Portland cement [9].

Table 1.1: Raw material and energy consumption to produce 1 ton of Portland cement [9].

Limestone	1.20 ton
Clay	0.30 ton
Gypsum	0.05 ton
Fossil fuel	0.07 ton
Electricity	103.00 kWh

Cement production also greatly contributes to the contamination of air with SO_x and NO_x, heavy metals and suspended particles.

Therefore, the use of ordinary binders in the field of the construction sector still does not fit in the interests of cement industries, which are constantly seeking for the solutions to reduce both energy consumption and greenhouse gas emission.

Although a significant number of waste materials is used to manufacture Portland cement, such as fly ash from coal combustion, blast furnace slag from iron production, bagasse ash from sugar industries and silica fume from ferrosilicon production, it only replaces a minor part of the clinker [8].

The main strategies include the optimization of clinker production, the use of alternative fuels and raw materials, the increase of grinding efficiency, but also the production of alternative cement products, based on new binders and their compositions with ordinary Portland cement (OPC). An interesting study carried out by the Cement Sustainability Initiative (CSI) of the World Business Council on Sustainable Development (WBCSD, 2009) revealed how the trend of cement production has changed since years. The share of blended cement has increased among countries compared to that of Portland cement therefore, average clinker fractions in cement production have decreased to $60 \div 80\%$ with a proportional decrease of CO_2 emissions per tonne of cement produced. The study evidences a decrease around 20% in CO_2 emissions per tonne of cement since 1980s [5].

The development of new binders on the stage of cementitious materials represents a clear separation from the "world" of Portland cement. Alternative binders do not benefit directly from the research and experience into OPC chemistry, reaction mechanisms, property development and durability. Therefore, they must be considered as new materials, in every way.

1.2 Durability of carbon steel bars in Ordinary Portland Cement (OPC) concrete

Concrete is the most common construction material and cement is the most important component that determines its mechanical, physical-chemical, service and other properties in both fresh and hardened state. The protectiveness of OPC cement with regard to carbon steel corrosion led concrete to dominate, over centuries, the scene in the field of construction materials: steel rebar gives tensile strength, while concrete combines high compressive strength properties and environmental internal conditions that are able to protect carbon steel from corrosion, allowing the fulfilment of durable structures. Such conditions are mainly achieved thanks to the formation of products during hydration of Portland cement constituents, which gives to the water in the pores of hardened concrete alkaline characteristics. Actually, the corrosion behavior of carbon steel is strongly dependent on the environment's pH (Figure 1.3), and it passivates above a limit usually assumed around 11.5. Thus, its corrosion rate becomes irrelevant, thanks to the formation of a protective oxide film on its surface, which blocks the metal dissolution.

Concretes manufactured with Portland cement have pH values above 12.5, due to the formation of calcium hydroxide which saturates the water of the pores, or higher, up to 13.5, due to the presence of alkaline sodium and potassium oxides. This condition of alkalinity is achieved immediately, since during the mixing, promoting a rapid passivation of carbon steel bars [10] [11], observable with the rapid increase of the corrosion potential of the steel (Figure 1.4).
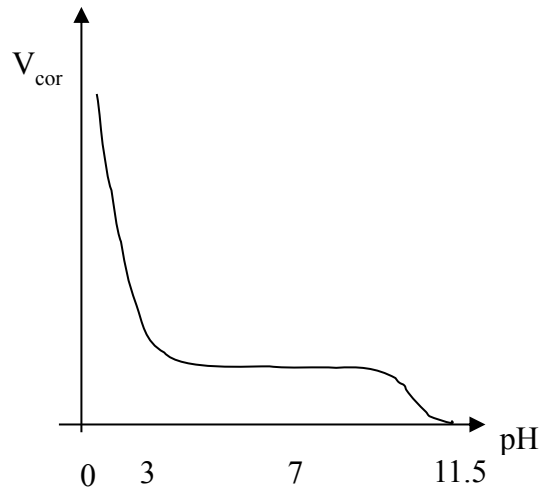
Figure 1.3: Effect of pH on corrosion rate of carbon steel in aqueous solutions (in absence of chlorides).
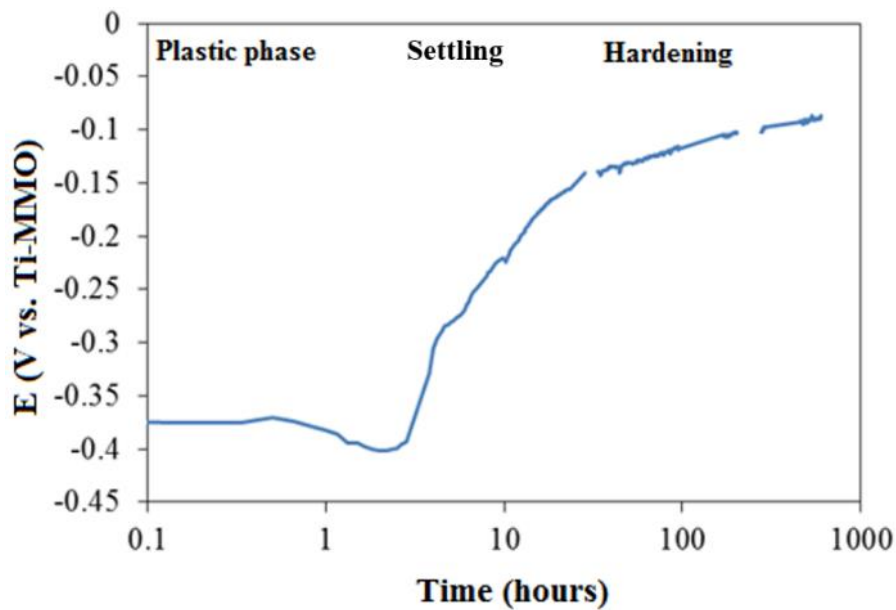
Figure 1.4: Kinetics of passive film formation on carbon steel bar in Portland cement mortar [10] [11].

However, the protectiveness of OPC concrete does not depend only on its pH, which is always higher - before the carbonation occurrence - than that required for steel passivation, but it is also ruled by its action on the critical chloride content. Furthermore, Portland cement is able to bind chloride ions, determining a reduction of free concentration, and it contrasts both chlorides penetration and carbonation through the concrete cover.

The pH achieved by hardened concrete, usually higher than 11.5, ensures an alkaline environment able to contrast chlorides. These ions are responsible for localized corrosion initiation. They can break the passive film promoting pitting at very restricted anodic area with penetrating attack that can reach, in humid concretes, magnitude of one mm/year. Pitting is the main cause of damage on reinforced structures exposed to marine environment and reinforced structure of highways motorways that come into contact with de-icing salts. In the past, the use of chloride salts as accelerator of cement hydration was responsible for serious damages and failures and nowadays, they have been forbidden for reinforced concrete.

The initiation of localized corrosion occurs after the chloride content in concrete overtakes a critical concentration at steel bars' surface, which depends on cement type and environmental condition. The critical chlorides concentration of Portland cement in structures exposed in atmosphere, which are characterized by high free corrosion potential values, is usually between 0.4% and 1% (chlorides wt. vs. cement mass). Higher concentrations are typical of concretes saturated of water, i.e. under conditions that promotes low free corrosion potential.

The main factors that influence the critical chlorides content are the alkalinity and the concrete-reinforcement interface characteristics [12] [13] [14] [15] [16]. The effect of alkalinity on localized corrosion initiation have been studied in several works [15] [16] [17] [18] [19] [20] [21] [22] and can be described in terms of chlorides-hydroxyl ions critical molar ratio, according to Equation 1.1.

Equation 1.1: Chlorides-hydroxyl ions critical molar ratio.

$$\frac{[Cl^-]}{[OH^-]^n} = k$$

The higher the pH, the higher the critical chloride concentration; according to the literature, it is common to assume chlorides-hydroxyl ions critical molar ratio of 0.6 (with unitary n exponent). Agreeing with this correlation, moving from a pH of 11.5, the minimum value for carbon steel passivation, to 12.5 and then to 13.5, the critical chlorides concentration increases of 1 and 2 orders of magnitude, respectively. Therefore, alkalinity

of Portland concrete can contrast efficiently the chlorides action, making localized corrosion possible only for chloride concentrations much higher - which can be only achieved after long time of exposure - compared to the initial level derived from concrete's components or mixing water.

Several authors evaluated the critical chlorides-alkalinity ratio analysing the pore solution: experimental work evidenced very scattered results, but the critical ratio was always greater than 2, and much higher compared to experimental results in alkaline solution [23]. This difference can be ascribed, according to Page [14], to the buffer ability of calcium hydroxide formed during cement's hydration. The presence of this phase directly in contact with carbon steel surface represents a reserve of alkalinity, which contrasts the pH drop due to localized corrosion initiation and pit formation at the steel/cement paste interface.

Only a small part of chlorides in concrete contributes for localized corrosion initiation. In fact, only free chlorides, which are dissolved inside the pore solution, participate actively while, a relevant part of them is bound to cement constituents, such as calcium-*chloro*-aluminate-hydrate and silicates-hydrate [24]. The analysis of the pore solution (with pH between 13 and 13.5) of concretes polluted with chlorides revealed critical concentrations greater than 0.2-0.6M.

Durability of concrete structures is ruled by hardened concrete properties. The chlorides penetration and carbonation are the two principal processes, which weaken the protective features of concrete over time. The carbonation reduces the pH of concrete owing to the reaction of CO_2 of atmosphere with the alkaline components of hydrated cement. Due to the progressive penetration of chlorides and carbonation through the cover, concrete loses its protectiveness towards carbon steel reinforcements and determines the initiation of corrosion after the protective passive film breaks. The penetration rate of this "de-passivation" front depends on the porosity of the matrix, on its size distribution and structure. In fact, it is well known that concrete durability firstly relies on mix design and proper curing of the concrete. However, the penetration is not only related on the pores' structure - concrete is quite far from being a mere porous septum, able to filter incoming species - but also on cement's constituents. They are able to bound incoming chlorides binding them and to slow down carbonation penetration, thanks to the alkalinity reserve

- that enhances buffering properties - guaranteed by the alkaline hydration products, in which calcium hydroxide is the most important and abundant participant.

1.2.1 Study of the passive film formation

Several authors studied the kinetics of formation of passive film on steel surface in alkaline environment simulating the pore solution or directly inside the concrete. Two electrochemical techniques have been used for this purpose: cyclic voltammetry (CV) and electrochemical impedance spectroscopy (EIS). Cyclic voltammetry has been used by Schrebler Guzmàn et al [25], to study the mechanism of passive film formation in de-aerated KOH 1M solution, by Cabrini et al [15] to study the effect of chlorides on carbon steel in alkaline solutions and by Hinatsu et al [26] in solutions of KOH, saturated $Ca(OH)_2$ and solution saturated with Portland cement. Lorenzi [10] [27] studied the formation of the passive film and the corrosion-erosion phenomena of carbon steel in contact with fresh mortar by means of cyclic voltammetry.

The typical shape of carbon steel voltammogram in environment is reported in Figure 1.5. The partial overlapping of some of the peaks and their variation make difficult to interpret the voltammogram. Generally, with increasing number of cycles during voltammetry, it is possible to observe a decrease of the width of the first anodic peaks, represented with roman numerals I and II, and first cathodic peak, represented with V, while the width of the anodic (III) and cathodic (IV) peaks increases with the number of cycles. Usually, the first anodic peak (I) stabilizes after 20 cycles.
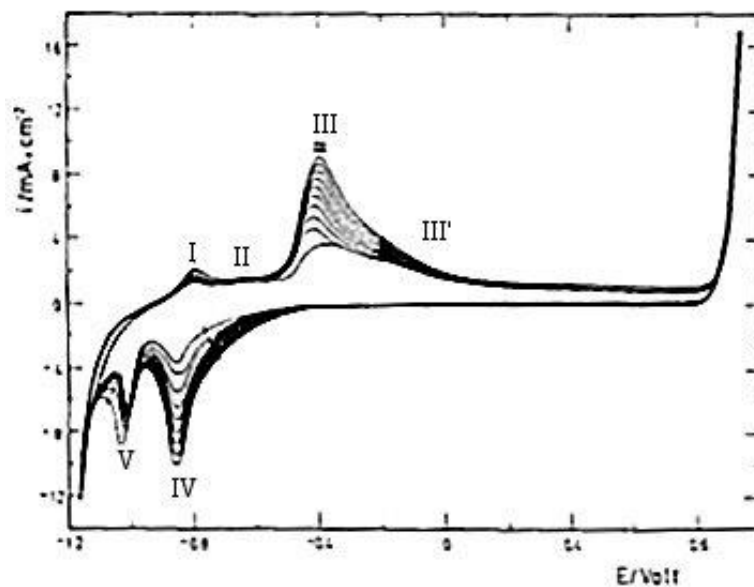
Figure 1.5: Carbon steel voltammogram in alkaline environment.

26

Authors interpreted these peaks according to the following mechanism: the stable product that is formed inside the potential interval within the current peaks I and II is $Fe(OH)_2$. Successively, it is oxidized to oxide $Fe^{(III)}$ (FeOOH) at peaks III and III'. They emphasize a complex structure of oxide, composed by an inner anhydrous part and an external hydrated layer, with other species - such as hydrated Fe_3O_4 – that can form by ageing. The full sequence of reactions is reported in Figure 1.6.

$$(1) \quad Fe + OH^- \underset{\leftarrow}{\overset{\rightarrow}{\rightleftharpoons}} \left[Fe(OH)\right]_{ad} + e^-$$

$$(2) \quad \left[Fe(OH)\right]_{ad} \underset{\leftarrow}{\overset{\rightarrow}{\rightleftharpoons}} \left[Fe(OH)\right]_{ad}^+ + e^-$$

$$(3) \quad \left[Fe(OH)\right]_{ad}^+ + OH^- \underset{\leftarrow}{\overset{\rightarrow}{\rightleftharpoons}} \left\{Fe(OH)_2\right\}$$

$$(4) \quad \left\{Fe(OH)_2\right\} + OH^- \underset{\leftarrow}{\overset{\rightarrow}{\rightleftharpoons}} HFeO_2^- + H_2O$$

$$(5) \quad HFeO_2^- + OH^- \underset{\leftarrow}{\overset{\rightarrow}{\rightleftharpoons}} FeO_2^{2-} + H_2O$$

$$(6) \quad \left\{Fe(OH)_2\right\} + OH^- \underset{\leftarrow}{\overset{\rightarrow}{\rightleftharpoons}} \left\{FeOOH\right\} + H_2O + e^-$$

$$(7) \quad \left\{FeOOH\right\} + \left\{FeOOH\right\} \underset{\leftarrow}{\overset{\rightarrow}{\rightleftharpoons}} \left\{Fe_2O_3 \cdot H_2O\right\}$$
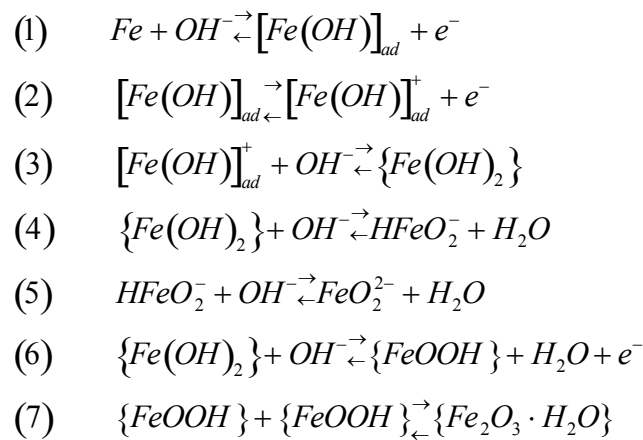
Figure 1.6: Reactions occurring on carbon steel surface in alkaline environment during cyclic voltammetry.

The reaction of the intermediate $[Fe(OH)]^+$ into the soluble species $Fe^{(II)}$ or $Fe(OH)_2$, according to reaction (3), is determined by the constant of ferrous ion and by the hydrogen ion activity at metal/solution interface. The current of peak I seems to be strictly related to $Fe(OH)_2$ formation (reactions (1), (2) and (3)). The existence of equilibria like those from reaction (3) to (5) promote a mechanism of precipitation/dissolution of $Fe(OH)_2$, especially in alkaline environments. The species $Fe(OH)_2$ is also related to peak II and its reduction occurs in correspondence of cathodic peak V, attested by the fact that the sum of the anodic charge of peaks I and II is the same of that of cathodic peak V. According to reaction (6), conjugated peaks III (III') and IV (IV') are localized in an interval of potential where it could be possible the formation of $Fe^{(III)}$.

Reaction (6) also entails the participation two reagents and the formation of two products that apparently involve stoichiometric equivalents, but that have different electrochemical

reactivity, producing therefore two contributes of anodic and cathodic current (peaks III, III'and IV, IV' respectively).

In the potential range included in these current peaks, species of not equilibrium are involved and consequently, structural transformation could be possible, giving birth to the ageing of the film. Such behavior can be explained with reaction (7), but long terms transformation can also occur, such as that from β-FeOOH to Fe_3O_4, or the conversion from δ-FeOOH to α-FeOOH and transformation from α-FeOOH to Fe_3O_4.

Several works also studied the formation of the film in solutions saturated with cement or pressure filtered from hardened concrete, while no studies have been reported yet of steel embedded in fresh concrete or mortar. According to Hinatsu et al [28] the cyclic voltammetry curves obtained in KOH solution, in saturated $Ca(OH)_2$ solution and in solution saturated with Portland cement have similar shape, with potential peaks almost identical, meaning that the general mechanism is the same. However, the current peaks observed after 100 cycles in solution saturated with cement are lower compared to those in NaOH 0.1M and KOH 0.1M solutions. The decrease of the height of the peaks in cement could be related to an increase of the film stability, due to the presence of $Ca(OH)_2$ within concrete's porosity. The presence of calcium leads to the deposition of a protective layer that contains iron and calcium, such as calcium ferrate $CaFe_2O_4$.

According to Foulkes et al [29], a gradual formation of oxide-hydroxide film of the steel electrode immersed in saturated water with cement can be developed by means of anodic and cathodic polarizations. This film, is made of two different layers: an external one, moderately thick, porous and hydrated containing $Fe^{(III)}$, and an inner one, thin, homogenous and mainly composed by $Fe^{(II)}$. The inner layer protect the steel from corrosion while, the external one does not have protective behavior, due to its porosity [30].

However, the film formed on steel surface during cyclic voltammetry is different from that formed spontaneously in concrete in free corrosion conditions. Cyclic voltammetry tests carried out on rebar in concrete at different ageing, without external polarization of the metal, are reported in literature in order to study the conditions for corrosion initiation, such as in presence of corrosion inhibitors.

Andrade et al [31] reported cyclic voltammetry curves carried out in hardened concrete, after 3 months or three years of exposure: the plots report less defined peaks, compared to tests in solution or in cement, probably due to the greater thickness of the oxide layer (5-10 µm) formed in concrete (Figure 1.7).
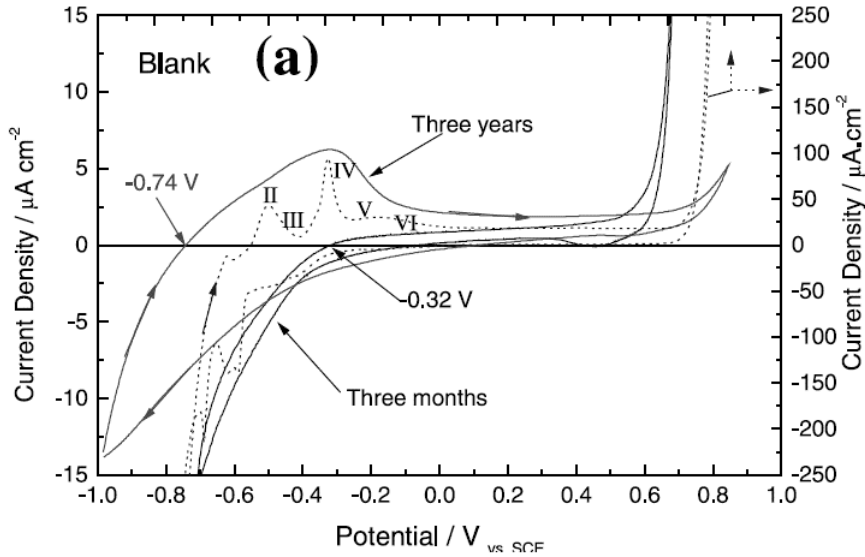
Figure 1.7: Cyclic voltammetry curves obtained in mortar after 3 months and 3 years of exposure [31].

The mechanism of passive film formation has been studied through the use of electrochemical impedance spectroscopy (EIS) technique by several authors [32] [33] [34] [35] [36] [37] [38] [39]. The steel–concrete system can be described in the form of an electrical circuit. A common and simple approach is the use of the simplified Randles circuit (Figure 1.8), which interprets and fits very well the EIS spectra for metal characterized by active behavior. This model includes the solution resistance R_s, a double layer capacitor C_{dl} in parallel with a charge transfer resistance (or polarization resistance R_p) [38].
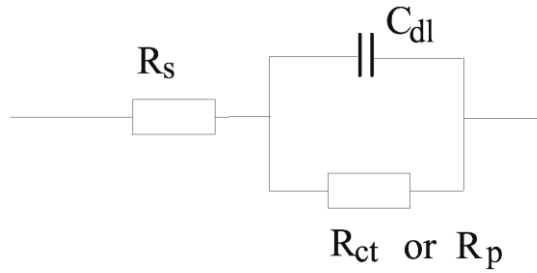
Figure 1.8: Simplified Randles equivalent circuit.

R_p can be directly associated with the steel corrosion current density [40] [41], according to Stern and Geary Equation 1.2:

Equation 1.2: Stern and Geary equation.

$$I_{corr}[mA] = \frac{k\ [mV]}{R_p\ [m\Omega]}$$

Where k is a constant, which can be assumed equal to 26 mV for active steel behavior.

According to the studies of cyclic voltammetry of carbon steel, the passive oxide film is characterized by a two-layer structure, that consist in an inner layer, which grows directly on steel surface, and an external layer precipitated by hydrolysis of cations expelled from the inner layer [34]. During the film growth at the interface oxide film/metal, metallic interstitial cations are produced, which are later consumed at the interface film/solution. Likewise, anionic vacation is formed at the interface film/metal and later consumed at film/solution interface. Therefore, under anodic polarization, a flux of oxygen vacation from metal/barrier layer interface to barrier layer/external layer and a flux of metallic interstitial cations moving in the opposite direction are present. In order to interpret the mechanism of passive film formation in alkaline environment of concrete pore solution, an equivalent circuit, made by a sequence of two RC circuits in parallel, has been proposed [25] [42]. The same model has been used by Andrade et al [31] to interpret EIS spectra after 3 months and 3 years of exposure in concrete. The majority of authors agrees with equivalent circuit reported in Figure 1.9(a) as the more representative and the best

for experimental data fitting whereas, in presence of diffusion phenomena, a Warburg element should be considered, as reported in Figure 1.9(b).
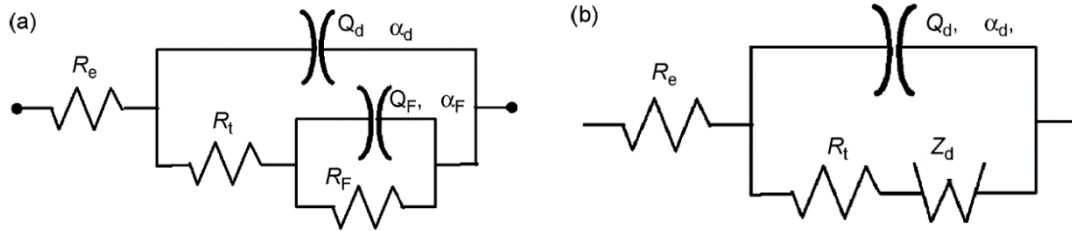
Figure 1.9: Equivalent circuits proposed in literature for EIS spectra fitting of steel in alkaline environment.

Figure 1.10 and Figure 1.11 show the Nyquist and Bode spectra of carbon steel immersed in alkaline solution (pH 13.2) at different ageing. Authors agree that, in alkaline environment, the equivalent circuit reported in Figure 1.9(a) is able to interpret the evolution of the passivity film formation: R_e correspond to the electrolyte resistance and R_t represents the charge transfer resistance. M. Sánchez et al [43] hypothesized the presence of two contributes: the capacitance of the passive layer (C_{SC}) and the capacity of the Helmholtz layer (C_H). The capacity (Q_d) can be calculated according to Equation 1.3:

Equation 1.3:

$$\frac{1}{Q_d} = \frac{1}{C_{SC}} + \frac{1}{C_H}$$

According to Sánchez et al [43], the value C_H can be calculated from that of the capacity Q_d by polarization of the sample to cathodic potentials, in order to free the surface of the metal from any kind of oxides. At low frequencies, the circuit in Figure 1.9(a), is related to a redox process involving passive species (such as oxidation of magnetite to $Fe^{(III)}$ oxide). Q_F is a pseudo Faraday capacitance, related to redox reversible processes that occur in correspondence of the passive film and R_F is the resistance of this faradaic reaction. The replacement of pure capacitors with constant phase elements (Q_d and Q_F) has the scope to consider that the surface of the electrode is not ideal. The values of the phase constants, αd e αF, are similar to time constants. The role of the parameters of the

constant phase element depends on the values of α, which are included in the interval 0≤α≤1, and can shift from an ideal capacitor to a Warburg element [44].

Intermediate values of α have been related to not homogeneity and to roughness of the electrode surface [45]. In literature, values of α around 0.90 are reported, in agreement with a behavior of the constant phase elements that is mainly capacitive.
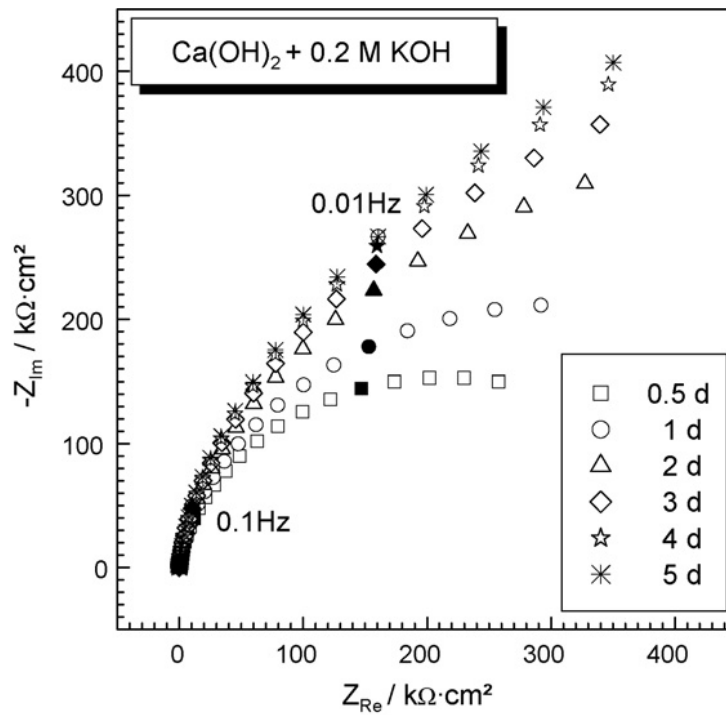
Figure 1.10: Evolution of Nyquist spectra in function of time of carbon steel in alkaline solution (pH 13.2).
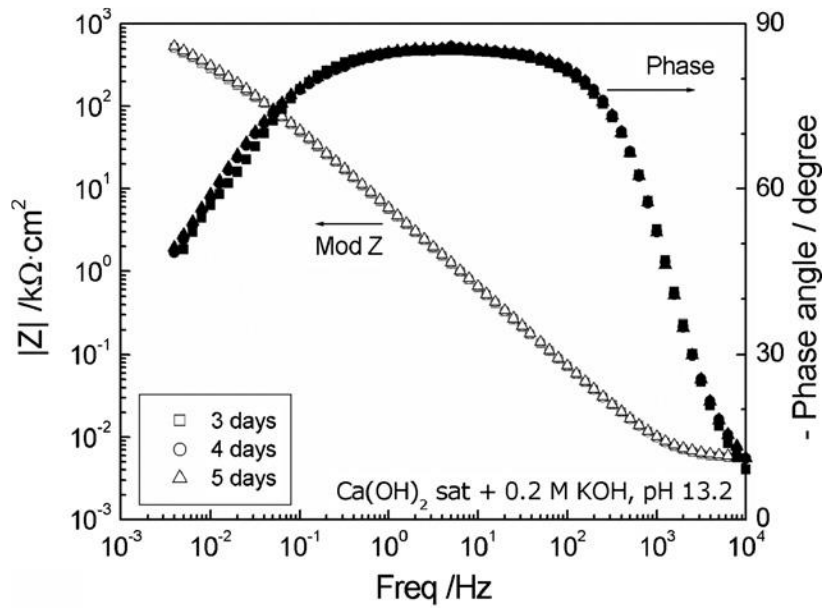
Figure 1.11: Evolution of Bode spectra after 3 days of exposure of carbon steel in alkaline solution (pH 13.2).

Monticelli et al reported a different equivalent circuit, which is a combination the previous models (Figure 1.12) [46].
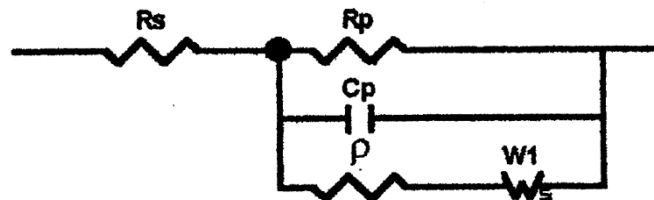
Figure 1.12: Equivalent circuit from Monticelli et al [46].

Figure 1.13 reports the evolution of charge transfer resistance, R_t, and the double layer capacitance Q_d, during the first days of immersion in alkaline solution. Their trend is similar to that of the corrosion potential: R_t increases exponentially with two time constants (one at 7 hours and the other after 2 days). The double layer capacitance decreases exponentially with two time constants (the first after 4 hours of exposure and the other after 1.5 days) and tends to reach a stationary state value of 34 µFcm-2, s0.95, which is typical for passive steel [47].
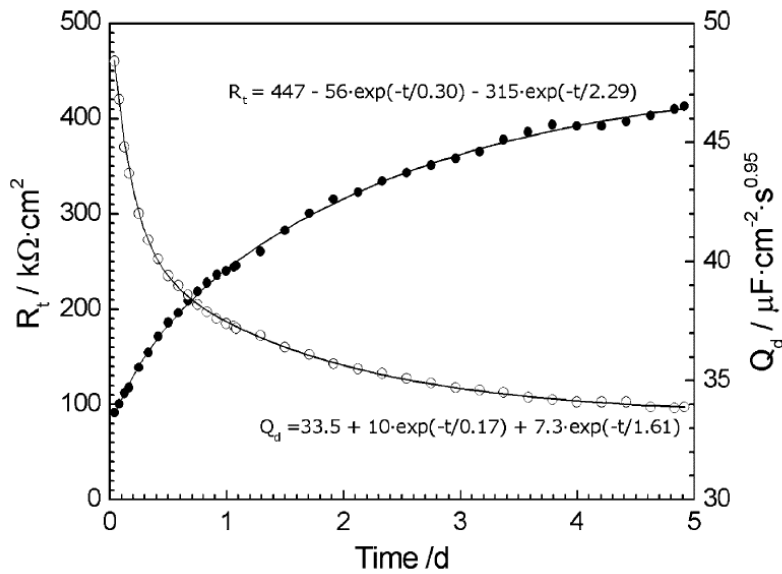
Figure 1.13: Evolution of Rt, related to charge transfer process, and Qd values obtained by EIS spectra data fitting at different time of immersion [47].

The difference between the two time constants can be related with the different processes involved on the rebar surface. At the first stage, a time constant around few hours should be related to the formation of oxide $Fe^{(II)}$ at the steel surface. Later, the presence of a second time constant, characterized by values around few days, could be related to the growth and reorganization of the passive film. The steady state of Q_d is achieved after three days of immersion, meaning that all the surface of the steel has been covered with oxide layer. However, the steady state of Q_d is not achieved, even after 5 days of exposure. This should be due to the change of the passive film resistance and therefore, to changes of the passive film composition. The principal modify of the passive film is related to the transformation of the $Fe^{(II)}$ oxide into magnetite, as suggested by the shift of the corrosion potential to more anodic values and by the increase of the R_t and R_F. Indeed, the resistivity of magnetite is greater compared to $Fe^{(II)}$ oxide. The second loop of the equivalent circuit in Figure 1.9(a), at low frequencies, can be related to the redox processes that occur inside the passive film and that involve the magnetite oxidation to $Fe^{(III)}$ oxide. Q_F decreases with time (Figure 1.14) reaching the steady state around 55 µFcm-2s0.95, after 3 days of immersion, and the α_F value approximately is 0.9. The time constant of the element $R_F x Q_F$ decreases exponentially over time, reaching a stationary value after 5 days, when

the passive film has reached a more stable composition, and as consequence an increment of its protective behavior is achieved. However, the composition of the passive film and the time necessary to reach stable conditions depend on the potential of the rebar: if the steel is polarized to anodic potentials, stationarity is reached in a shorter time and the film is more protective.
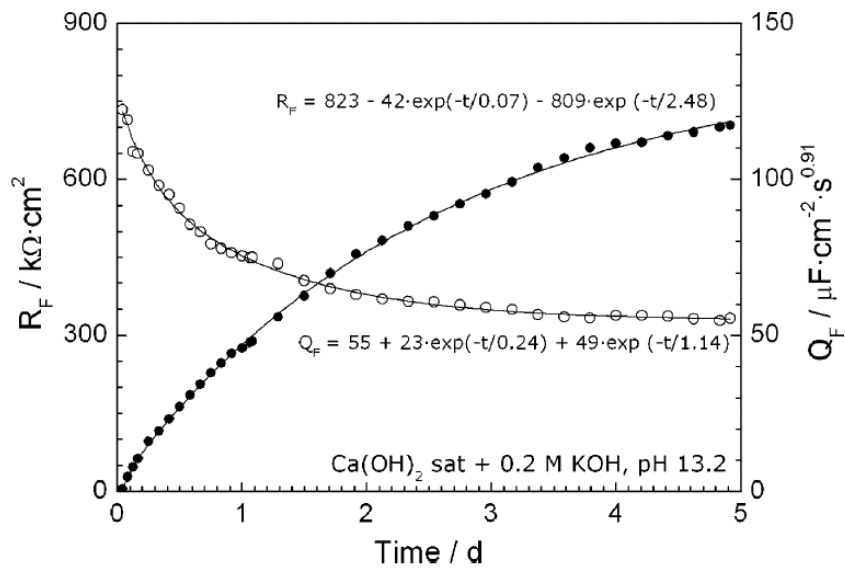
Figure 1.14: *Evolution of R_F, and Q_F values obtained by EIS spectra data fitting at different time of immersion* [47].

The equations shown in the figure are:

$$R_F = 823 - 42 \cdot \exp(-t/0.07) - 809 \cdot \exp(-t/2.48)$$

$$Q_F = 55 + 23 \cdot \exp(-t/0.24) + 49 \cdot \exp(-t/1.14)$$

Ca(OH)$_2$ sat + 0.2 M KOH, pH 13.2

1.3 Calcium Sulfoaluminate (CSA) cement

Among alternative hydraulic binders, calcium sulfoaluminate (ye'elimite $C_4A_3\bar{S}$) cements deserve a special attention due to their peculiar rheological-mechanical characteristics, and mainly, for being a promising low-CO_2 alternative to OPC.

Calcium Sulfoaluminate (CSA) cement has been developed in China in 1970s and its annual production is higher than 10^6 tons/year [48]. The main mineralogy of these binders is based on $4CaO\cdot3Al_2O_3\cdot SO_3$ (ye'elimite or tetracalcium trialuminate sulfate), which is the main constituent, calcium sulfate within the CSA clinker or added as $CaSO_4.2H_2O$ (gypsum) and a series of calcium silicates ($2CaO\cdot SiO_2$, $5CaO\cdot2SiO_2.SO_3$, $2CaO\cdot Al_2O_3\cdot SiO_2$, $CaO\cdot Al_2O_3\cdot2SiO_2$) and calcium aluminates ($3CaO\cdot Al_2O_3$, $4CaO\cdot Al_2O_3\cdot Fe_2O_3$, $12CaO\cdot7Al_2O_3$, $CaO\cdot Al_2O_3$) [9] [49].

CSA cement can be produced by calcium sulfate, bauxite and limestone at a temperature of about 1250°C, which is 200°C lower compared to that of Portland cement [50] [48] [51] [52] [53] [54]. Calcium sulfoaluminate cement releases only 0.56 g CO_2/ml of the cementing phase compared to 1.80 g CO_2/ml of the cementing phase to for alite [6] furthermore, grindability of this binder is easier than OPC. In Table 1.2 is reported a comparison between CO_2 emissions for CSA and Portland cements [9].

Table 1.2: CO₂ emissions for Portland and CSA cements production [9].

	CO_2 emissions from limestone calcination	CO_2 emissions from fuel	Total CO_2
Portland clinker [kg/(kg clinker)]	0.51	0.31	0.82
CSA clinker [kg/(kg clinker)]	0.16	0.18	0.34
Portland cement (95% clinker and 5% gypsum) [kg/(kg cement)]	0.48	0.29	0.77
CSA cement (85% clinker and 15% gypsum) [kg/(kg cement)]	0.14	0.15	0.29

Table 1.3 shows two compositions of commercial CSA cement [50], Table 1.4 and Table 1.5 report a comparison of mineralogical composition and chemical analysis between a CSA cement and a Portland cement. The main differences between CSA cement from

ordinary binders are the presence of calcium sulfoaluminate and the absence of tri-calcium [55] [56].

Therefore, huge differences in hydration processes will be present.

Table 1.3: Chemical composition of two commercial CSA cements [50].

	CaO wt. %	SiO2 wt. %	Al2O3 wt. %	Fe2O3 wt. %	MgO wt. %	Na2O wt. %	K2O wt. %	TiO2 wt. %	SO3 wt. %	L.O.I. wt. %
CSA-1	34.4	3.2	35.5	0.88	0.76	0.05	0.21	1.8	16.8	5.1
CSA-2	41.2	6.9	26.8	0.88	0.75	0.13	0.40	1.2	19.5	1.8

L.O.I.=Loss of Ignition

Table 1.4: Mineralogical composition of CSA and OPC cements obtained by Rietveld semi-quantitative XRD analyses [55].

Mineral phase	C_3S wt. %	C_2S wt. %	C_3A wt. %	C_4AF wt. %	C_4A_3S wt. %	Gypsum wt. %	Anhydrite wt. %	Calcite wt. %	Residual phases wt. %
OPC	57.4	10.2	4.5	9.4	-	3.6	-	13.5	1.4
CSA	-	21.7	9.3	3.9	42.4	11.3	4.9	6.0	0.5

Table 1.5: CSA and OPC chemical analysis [56].

Cement chemical analysis (%)	SiO_2	Al_2O_3	Fe_2O_3	CaO	MgO	K_2O	Na_2O	Total Cl-	Water soluble Cl-	SO_3	CaO_{free}
OPC	19.81	4.99	3.85	62.44	2.63	0.53	0.34	0.008	-	2.66	1.96
CSA*	15.52	13.08	5.20	50.33	1.62	0.05	0.03	0.007	0.005	14.21	0.14

*CSA cement was prepared in a laboratory electric furnace using: limestone (37%), bauxite (25.6%), siliceous earth (10.5%), an iron-rich industrial by-product (0.75%) and gypsum (25.4%).

1.3.1 Hydration of CSA cement

The main crystal products occurring during hydration are ettringite (AFt) and monosulfate (AFm), while the main gel products are C-S-H phase, Al_2O_3 (aqueous) and Fe_2O_3 (aqueous) [50] [54]

During CSA hydration, ettringite is formed rapidly according to Equation 1.4, in the absence of calcium hydroxide, or according to Equation 1.5, in the presence of calcium hydroxide.

Equation 1.4: Ettringite formation in the absence of calcium hydroxide

$$3CaO \cdot 3Al_2O_3 \cdot CaSO_4 + 2(CaSO_4 \cdot 2H_2O) + 34H_2O$$
$$\rightarrow 3CaO \cdot Al_2O_3 \cdot 3CaSO_4 \cdot 32H_2O + 4(Al \cdot OH_3)$$
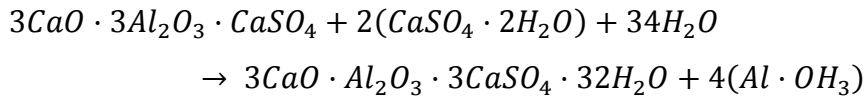
Equation 1.5: Ettringite formation in the presence of calcium hydroxide

$$3CaO \cdot 3Al_2O_3 \cdot CaSO_4 + 8(CaSO_4 \cdot 2H_2O) + 6Ca(OH)_2 + 74H_2O$$
$$\rightarrow 3(3CaO \cdot Al_2O_3 \cdot 3CaSO_4 \cdot 32H_2O)$$
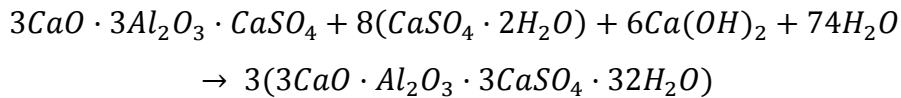
Both expansive and non-expansive sulfoaluminate cements can be produced, mainly depending on the lime concentration and on the presence of calcium hydroxide.

The ettringite formed in the presence of calcium hydroxide is characterized by great volume expansion and can be used to manufacture shrinkage-compensating concretes. Instead, when a CaO-deficient mixture is hydrated, most of the ettringite is formed before the full development of the skeletal structure and hardening of the paste, and therefore, no expansion is observed. Moreover, absence of calcium hydroxide is the responsible of the development of great compressive strength at early ages [57] [56]. Also, a low-alkali content promotes the non-expansive properties of sulfoaluminate cement [56].

After all calcium sulfoaluminate is consumed, monosulfate is formed with amorphous aluminium hydroxide, according to Equation 1.6.

The hydration of belite (C_2S) forms the gel products C-S-H, according to Equation 1.7.

Equation 1.6: Mono sulfate formation

$$CaO \cdot 3Al_2O_3 \cdot CaSO_4 + 18H_2O \rightarrow CaO \cdot Al_2O_3 \cdot CaSO_4 \cdot 12H_2O + 2(Al \cdot OH_3)$$
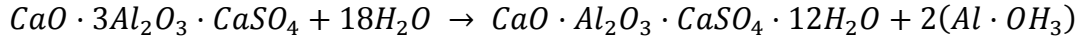
Equation 1.7: C-S-H gel products formation

$$2CaO \cdot SiO_2 + 2H_2O \rightarrow C - S - H + Ca(OH)_2$$
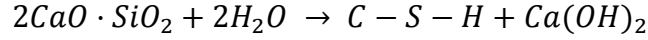
CSA cements have high hydration rates, high phase stability and greater amount of ettringite formed at early ages compared with OPC; during hydration considerable free water is consumed and a reduced capillary porosity is achieved [57]. The hydration of the calcium sulfoaluminate cements mainly depends on the amount and reactivity of the added calcium sulfate and it is maximum for addition around 30% [50].

Moreover, the hydration process is exothermic and releases a large amount of heat that leads to a relevant increase of the temperature.

Liao et al [54] showed maximum temperatures of paste around 70°C out during hydration of CSA cement pastes with 0.40 w/c ratio.

Thus, the technical behavior of CSA cements is dominated by their main component, $C_4A_3\bar{S}$ able to form, depending on the presence or absence of the calcium hydroxide, expansive or not expansive ettringite. These features can be used to manufacture shrinkage-compensating/self-stressing binders or rapid-hardening/dimensionally stable cements [58].

The pore sixe distribution of CSA cements has an important role in promoting mechanical performances at early ages and better impermeability properties. It is strongly dependent on the hydration reactions, which are very fast. The water is suddenly consumed and the hydration products decrease the interior pore space. Telesca et al compared calcium sulfoaluminate and Portland cement on pastes with water/solid mass ratio equal to 0.5, cured for 28 days. They observed completely different pore size distributions by mercury intrusion (Figure 1.15). Portland cement pastes at early ages (between 12 hours and 1 day) developed a unimodal (single peak - Figure 1.15 A/B) distribution related to a continuous network of capillary pores, characterized by pore radius decreasing from nearly 650 to 350 nm. After 28 days of curing, the pore radius decreased to about 150 nm and a region having smaller pores appeared (bimodal distribution, double peaks - Figure

1.15 A/B), further hydration products occluded the continuous network. CSA pastes revealed a bimodal distribution at early ages, in which the regions with a pore size about 25 nm are dominant, while the decrease of the total porosity is no more present at long ageing [59].
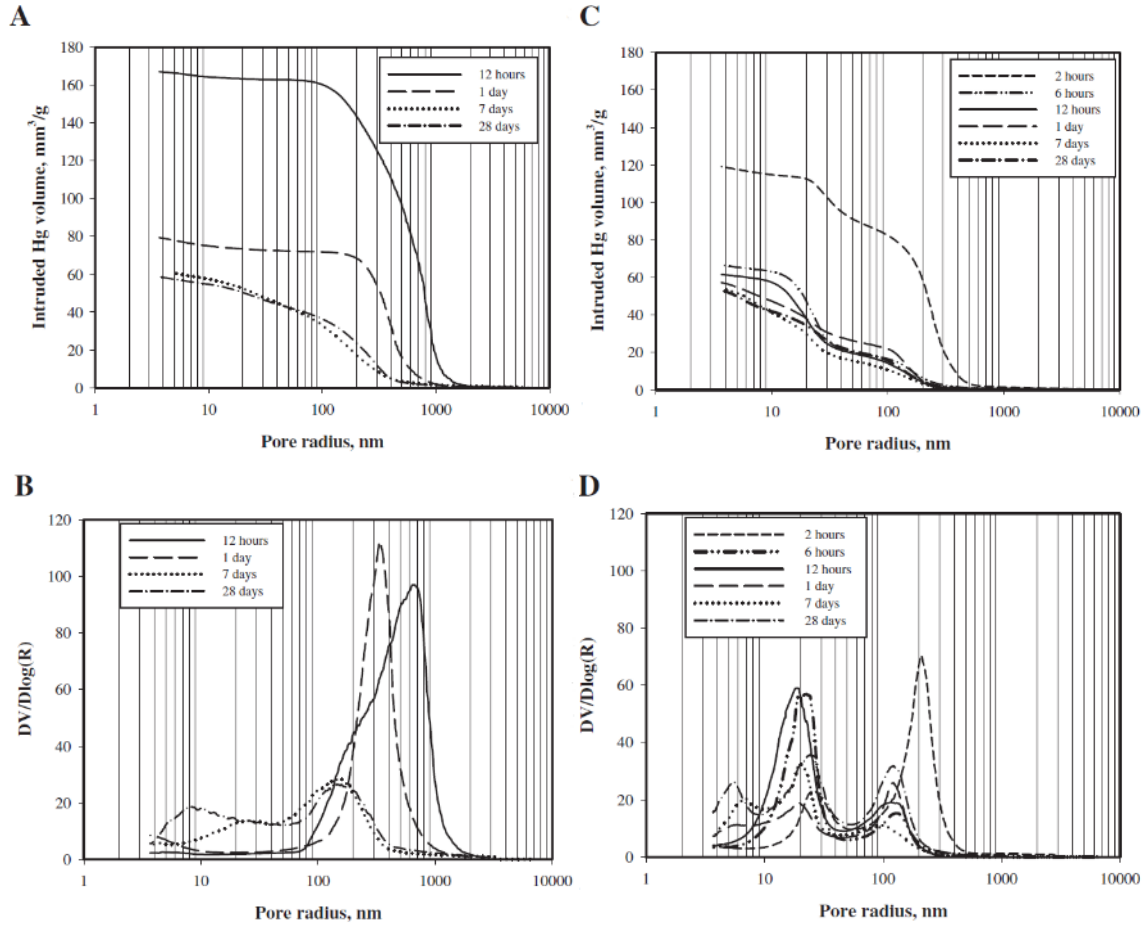
Figure 1.15: Intruded Hg volume vs. pore radius for cement pastes cured at various ages: (A) Portland cement, cumulative plot; (B) Portland cement, derivative plot; (C) sulfoaluminate cement, cumulative plot; (D) sulfoaluminate cement, derivative plot [59].

1.3.2 Mechanical and rheological properties of CSA based concretes

Huge literature is devoted to the study of the rheological-mechanical properties of CSA concretes [9] [49] [52] [53] [57]. The rapid formation of ettringite during hydration and the peculiar pore distribution of the hydrated system promote a rapid development of the mechanical properties. Compared to OPC, CSA concretes show higher compressive strengths at early ages, and a lower shrinkage. Moreover, the higher amount of water required to complete hydration, for the same w/c ratios, leads to a minor workability.

Ioannou et al [53] compared the rheological-mechanical properties of a calcium sulfoaluminate–anhydrite–fly ash cement combination (named GAF 15) with a Portland cement (CEM I) and a blastfurnace cement combination (III/A). Slump test was carried out at three different w/c ratios (0.35, 0.50 and 0.65) after 0, 5, 10, 15 and 20 min from the mixing, a superplasticizer was used for all the concretes (Figure 1.16). The authors report that GAF15 concrete required a little effort of water to reach Slump class S3. At lower w/c ratios the loss of slump for this concrete was greater than the reference mixes, due to the formation of rich amounts of ettringite in the cement matrix, which is characterized by a high water demand.
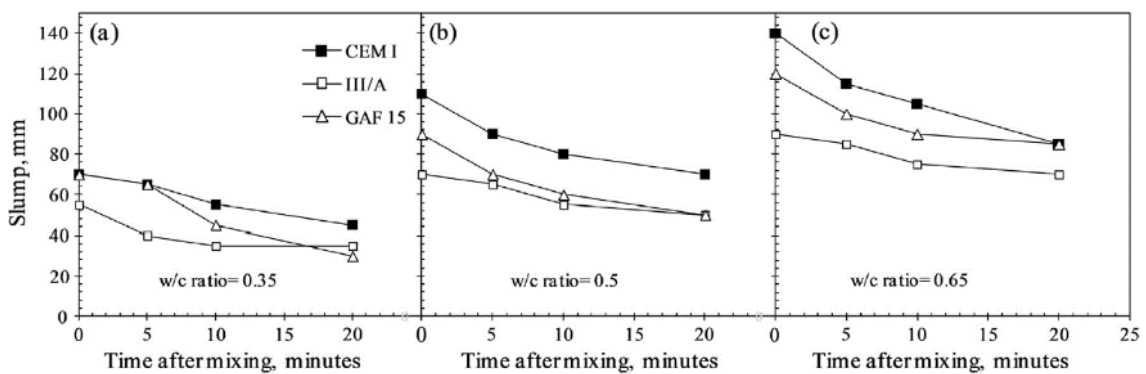
Figure 1.16: Slump of concretes at w/c ratio of (a) 0.35, (b) 0.5 and (c) 0.65 [53].

The 28-day cube strength of calcium sulfoaluminate–anhydrite–fly ash cement was similar to that of both reference concretes (for the same w/c ratio) but, at 7 days its compressive strength reached approximately 86-95% of 28-day one, indicating that early

strengths are a characteristic of CSA/calcium sulfate-based combinations (Figure 1.17) [53].
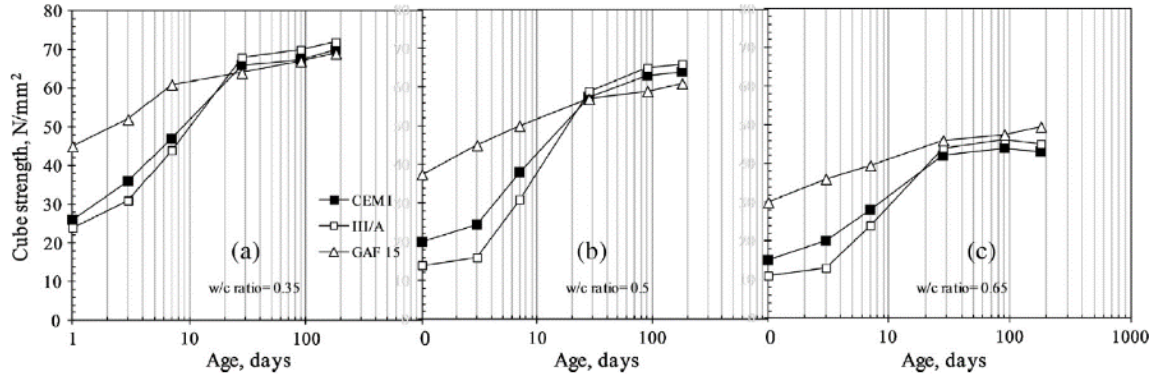
Figure 1.17: Cube strength development of concrete mixes at (a) w/c = 0.35; (b) w/c = 0.5 and (c) 0.65 [53].

Quilin [52] reported the compressive strength of a belite-based CSA concrete and of a calcium ferroaluminate concrete (FAC) with same w/c ratio of 0.56, in comparison with OPC and calcium aluminate cement (CAC) concretes. Figure 1.18 shows the compressive strength evolution as a percent of 28-day strength. The evolution was initially faster for FAC concrete than SAC concrete. However, the compressive strength of SAC concrete continued to increase up to 2 years, while that of FAC remained constant after three months. Early strength development for SAC and FAC concrete is faster than that of Portland cement concretes.
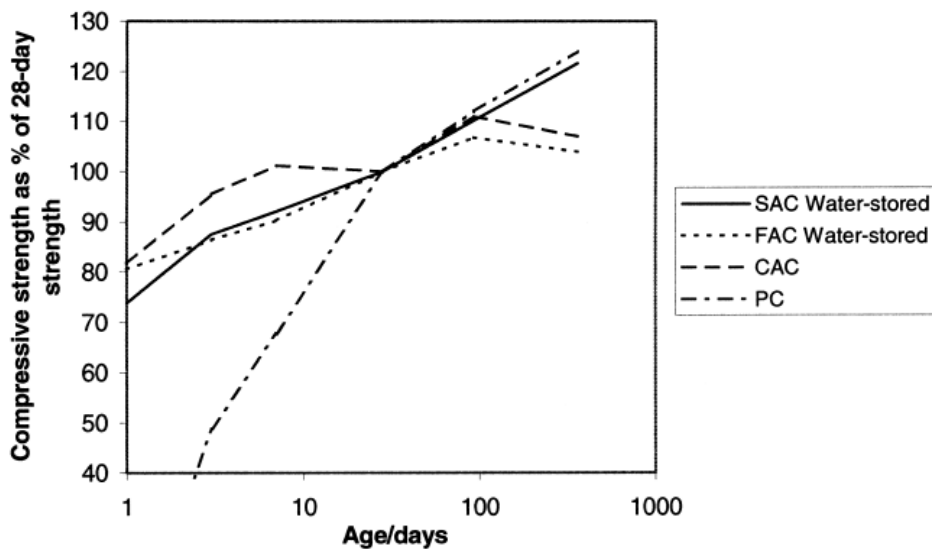
Figure 1.18: Compressive strength development in SAC, FAC, PC and CAC concrete as a % of 28-day strength [52].

Valenti [9] also reports a comparison between a CSA mortar (w/c = 0.50) and an OPC mortar (w/c = 0.45) and confirms that CSA cement develops higher early age compressive strength compared to OPC. Moreover, the author describes since the first hours after the mixing lower drying shrinkage for CSA mortar than that for Portland cement (Figure 1.19).
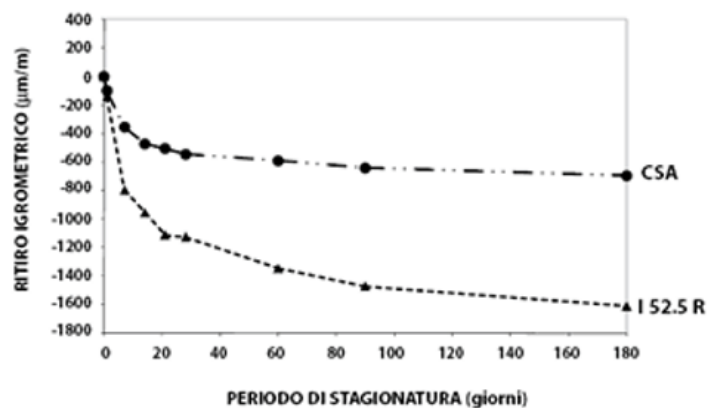
Figure 1.19: Drying shrinkage vs. time for CSA and CEM I 52.5R mortars [9].

Gastaldi et al [57] compared the behavior of a commercial CSA cement, two CSA-based mixes (MIX 1 and MIX 2, consisting of CSA clinker, natural gypsum and II/A-LL 42.5) and two Portland cements (CEM I 52.5 R, II/A-LL42.5 R). Compared to a high-strength and rapid-hardening Portland cements, they observe on commercial CSA cement higher compressive strength, especially within the first 24 hours of curing. Moreover, drying shrinkage was significantly lower. The two blends of CSA cement with Portland cement revealed a very low drying shrinkage and a mechanical strength higher than that of Portland cement alone at early ageing. The increase of the amount of Portland cement in the mix leads to a lower mechanical strength after 8 hours of curing and a more reduced drying shrinkage.

1.3.3 Durability of CSA cement based concretes

Substitution of Portland cement with new binders establish the necessity to verify the efficiency of their level of protection with respect to carbon steel bars, which depends on concrete's characteristics. The theme of durability in concretes manufactured with calcium sulfoaluminate cement has not been deeply investigated yet.

CSA concretes develop interesting properties, such as resistance to seawater sulfate attack, due to their high sulfate content [7] [48] [53]; however, the different hydration of $C_4A_3\bar{S}$, does not form Ca(OH)$_2$ and so, lower alkalinity levels are reached, with respect to Portland cement. Zhang et al [60] reported that the pH of hydration solution of CSA cement is low, around pH 10.6, and that also carbonation resistance capability is poor. Zhou et al [61] reports that CSA cements can be potential candidate for the encapsulation of wastes containing reactive materials, due to the low pH of the internal pore solution, which lies between 10 and 11.5.

Glasser et al [62] evaluated the chemical compositions of the pore solution expressed from commercial calcium sulfoaluminate-belite cement paste at different ageing, cured at 20°C, and measured the pH in the range 12.8-13.1; changes in concentrations of Na, K, Ca, Al, Si, Cl, Br and SO_4^{2-} were determined between 1 and 60 days of curing. The main components in the pore solution were Al and K, while Na, Ca, Cl, Br and SO_4^{2-} concentrations were low.

Winnefeld et al [50] determined the concentrations of the elements and the pH of the pore fluids extracted from two different CSA cement pastes with w/c ratios of 0.72 and 0.80 at different ageing (Table 1.6). Within the first hours of hydration, pore solution chemistry of CSA-1 is ruled by alkali, calcium, aluminium and sulfate, and the pH is quite low, around 10.5, compared to OPC (pH 13-14). The sulfate concentration is, within the first hours after the mixing, around 30÷40 mM. After 16 hours an important change of pore solution chemistry occurs: gypsum is completely depleted, sulfate decreases down to 1÷10 mM and calcium as well, hydroxide concentration increases leading to a pH around 11.8. During hydration, the ongoing release of alkali ions and consumption of pore fluid to form hydrates lead to a pH value of 12.7 after 28 days. The same trend, but with higher concentrations of the elements, was found for CSA-2.

Table 1.6: Pore solution chemistry of two CSA cement pastes [50].

Time 0	Na mmol/l	K mmol/l	Ca mmol/l	Al mmol/l	Si mmol/l	S mmol/l	OH mmol/l	pH
CSA-1								
1 h	0.60	2.1	18	10	<0.01	19	0.50	10.7
2 h	0.77	2.8	17	9.9	<0.01	19	0.38	10.6
5 h	3.0	9.2	15	7.3	0.01	21	0.19	10.3
8 h	7.8	29	13	7.5	0.02	31	0.19	10.3
16 h	16	59	1.2	51	0.02	19	6.6	11.8
2 days	16	98	0.60	100	0.03	1.9	27	12.4
7 days	17	120	0.57	120	0.04	2.1	43	12.6
28 days	21	120	0.31	100	0.05	3.4	50	12.7
CSA-2								
1 h	11	52	11	20	<0.01	36	0.73	10.9
2 h	14	60	4.4	51	0.01	20	2.1	11.3
4 h	15	62	4.3	47	0.01	22	1.8	11.2
6 h	15	65	3.4	52	0.01	21	1.5	11.2
16 h	16	65	3.0	59	0.01	18	2.7	11.4
2 days	41	140	0.41	101	0.09	32	16	12.2
7 days	44	140	0.42	91	0.18	11	73	12.9
28 days	34	82	0.23	26	0.21	9	70	12.8
Detection limit								
	0.002	0.001	0.001	0.004	0.01	0.005	–	–

CSA-1 produced in laboratory blending 78% of CSA commercial clinker with 22% of calcium sulfate dehydrate (Fluka);

CSA-2 used as provided by the manufacturer.

Compared to an OPC pore solution chemistry, the presence of sulfates within pore solution of CSA concrete slightly greater. Vollpracht et al [63] report the measured composition of the pore solution of a cement paste manufactured with Portland cement (w/c = 0.46) hydrated for 69 days. They found stable pH values with time, about 13.6, and a sulfate concentrations ranging from 8 to 13 mM.

However, no literature focused the attention on the effect of sulfates on steel reinforcements in CSA systems, which are rich sulfates environments characterized by low pH values, compared to OPC. Huge literature has been devoted to the study of the effect of sulfates on OPC concrete durability and, rarely, also to the direct effect of sulfate ions on carbon steel behavior.

Shi Jinjie et al [64] report the effect of sulfate ions on the corrosion behavior of steel emdedded in ordinary Portland cement through the use of electrochemical tests. The electrochemical results showed that, compared to OPC concrete in contact with pure chloride solution, the presence of sulfphate ions in the chloride solution both reduced the time to corrosion initiation and led to an increase in corrosion rate of steel in OPC

specimens. Furthermore, the corrosion rate of steel exposed to chloride solution was higher to that of the sulfate solution both in OPC and HPC specimens.

Le Saoût et al [65] and Pelletier-Chaignat [66] state that the water of the pores of concretes manufactured with Portland cement and addition, in lower amounts, of sulfoaluminate cement, tends to reach rapidly pH greater than 12, which becomes stable after one day to 13, that is a suitable level for carbon steel passivation.

The review of Juenger et al [67] on concrete based on new binders, alternative to Portland cement, states that, from experimental data of laboratory, durability of calcium sulfoaluminate concretes can be compared to that of traditional ones. The authors also underline that long ageing results are necessary. Protectiveness of this binder is confirmed by Glasser and Zhang [48], which report the results of a structure exposed to environment for 14 years in China. No damaging of concrete cover and corroding reinforcements were observed. However, they do not report thr environmental conditions of exposure and the behavior of adjacent structures made of traditional OPC concretes.

The most of item of researches is devoted to the study of hydration kinetics and to the characterization of hydration products just after the mixing, during settlement and in the first phase of hardening. These works give interesting information about aqueous solution characteristics, describing the alkalinity and the phases, such as calcium hydroxide, which influence steel passivation. However, they do not focus the research on corrosion behavior of carbon steel bars in concrete using electrochemical techniques. Such techniques are able to characterize the corrosion state. In addition, the few works that face the theme of durability of sulfoaluminate concretes restrict their approach only for estimating the penetration rate of carbonation and, rarely, of chlorides.

Pastore et al. [68] [69] underlined the difficulty for mild steel rebar embedded in CSA mortars to reach potentials typical of passive conditions, due to the low amount of alkali in the pore solution. Experimental data revealed that unfavorable environmental conditions can develop, that inhibit or slow down the formation of the passive film and

expose the steel to corrosion. The great variability of raw material used for sulfoaluminate cement production and possibility to have initial excessive amount of chlorides must be considered. The presence of chlorides over the critical concentration during the first period, when alkalinity level is still too low to achieve stable passivation of carbon steel, can increase the risk of early localized corrosion. In order to define the maximum amount inside the concrete, also the pH evolution after the mixing should be considered.

Kalogridis et al [56] report that weight loss measurements evidenced higher corrosion rates in CSA mortars, particularly being 4, 5 and 7.5 times greater compared to OPC, when exposed to tap water, continuous and interrupted 3.5 % NaCl solution respectively (Figure 1.20). The evolution of the open circuit potential (OCP) was also monitored. In tap water, OPC-based samples showed stable potentials in the range of -150 to 0 mV (Ag/AgCl) for more than 1 year of exposure. The rebar embedded in CSA mortars evidenced low values (around -500 to -400 mV (Ag/AgCl)) for the first 6 months, followed by the increase of OCP till nobler potentials of -200 to -150 mV (Ag/AgCl) after 8.5 months. These results state that in the absence of chlorides, steel rebar embedded in OPC mortars are completely passive, as expected, while those embedded in CSA mortars suffer from corrosion attack at very early stages, and become later repassivated. The OCP measurements performed in 3.5 % NaCl solution indicated no steel passivation for CSA samples, while the steel in OPC mortar suffered from the corrosion only after 6 months of exposure. Kalogridis et al proposed that higher susceptibility for reinforcement corrosion in CSA systems should be provided by lower pH of the pore solution, compared to OPC mortars, estimated at the values of 6 vs. 12 respectively. However these values do not agree with the findings of other researchers that observed higher values of the pH for pure CSA cementitious materials after 2-3 days [50] [60] [61] [62] [65] [66].
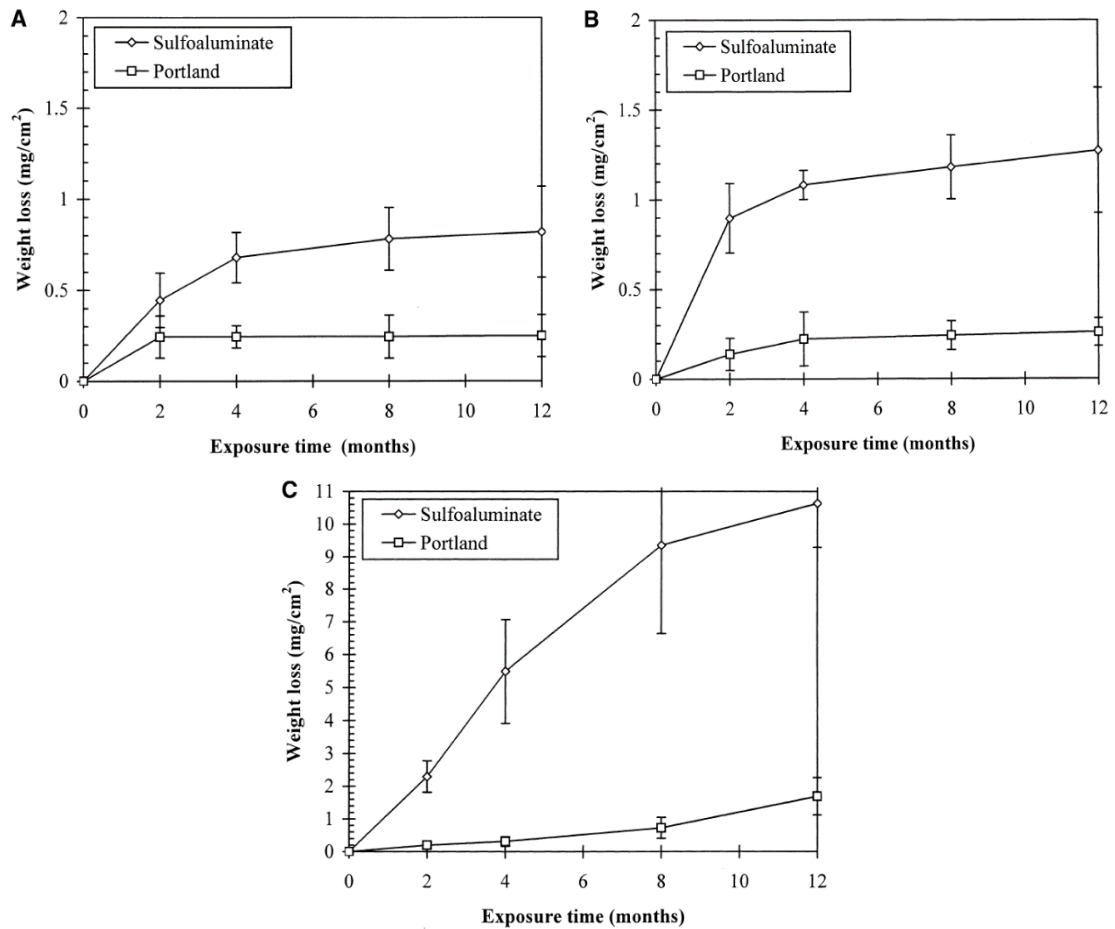
Figure 1.20: Weight loss of steel bars embedded in sulfoaluminate and Portland cement mortars as a function of time for (a) continuous exposure in tap water, (b) continuous exposure in 3.5% NaCl solution and (c) interrupted exposure in 3.5% NaCl solution [56].

Quillin [52] evaluated the carbonation resistance of a belite-based CSA concrete and of a calcium ferroaluminate concrete (FAC) with same w/c ratio of 0.56. CSA concrete carbonates more rapidly than equivalent FAC concrete. Anyway, both concretes carbonate more rapidly than OPC concretes with similar 28 days compressive strength, cement content and exposure conditions. The absence of calcium hydroxide as hydration product correspond to the inability of concrete to buffer the pH in correspondence of reinforcements, when carbonation occurs.
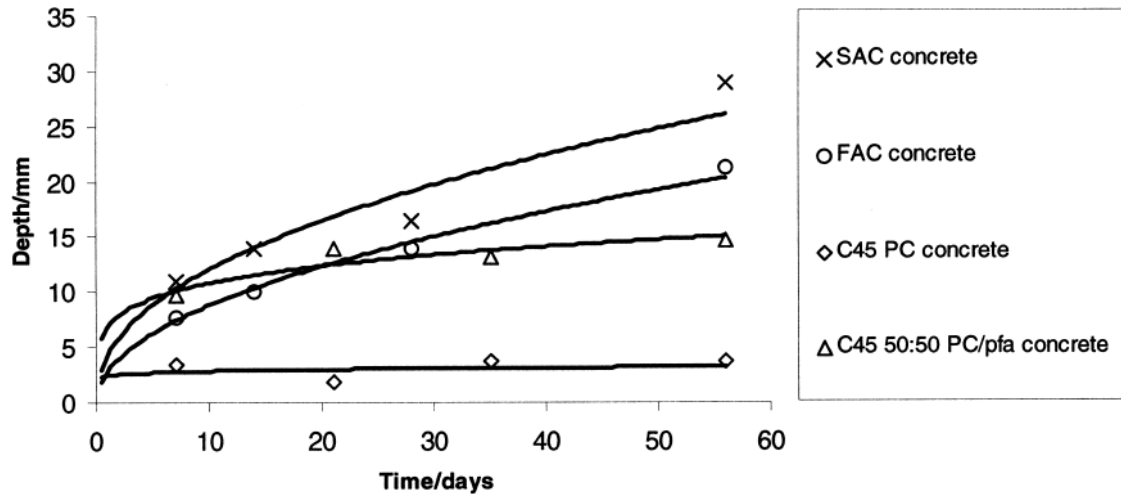
Figure 1.21: Accelerated carbonation depths against time for SAC(calcium sulfoaluminate cement), FAC (ferroaluminate cement) concrete, PC (Portland cement concrete) and a blended PC/pfa (pulverised fuel ash) concrete [52].

Janokta et al [70] manufactured blends of Portland cement (CEM I 42.5) and sulfoaluminate-belite (SAB) cement with weight ratios OPC/SAB of 100/0, 85/15, 70/30, 55/45, 15/85 and 0/100. Mortars with cement/sand ratio of 1:3 by weight, water/cement ratio of 0·5 were considered. PC-mortar showed excellent protective properties against corrosion of steel reinforcement, but carbon steel in pure SAB cement mortar was not passivated. The pH of the extract was established at 11.32. The authors reported that a 15 wt% replacement of SAB cement by OPC was sufficient to avoid corrosion of carbon steel, increasing the pH value of the mortar extract to around 11.9.

2 MATERIALS AND EXPERIMENTAL PROCEDURE

The experimental work was carried out at University of Bergamo, Department of Engineering and Applied Sciences, and at Construction Material Testing Lab of University of Bergamo.

Experimental tests in solutions were carried out at Corrosion laboratory of Instituto Supérior Tecnico (Universidade de Lisboa)

Tests were performed to study the corrosion behavior of reinforcements in concrete manufactured by CSA-based cements and OPC as reference. Both laboratory tests and field tests were carried out for evaluation passivation of carbon steel e passivating properties of CSA concretes covering:

- Electrochemical measurement and corrosion monitoring of reinforcement (including OCP / open circuit free corrosion potential and EIS / electrochemical impedance spectroscopy).
- Design, manufacturing and characterization of embeddable probes sensitive to the pH and suitable for concrete application
- Development of procedure for evaluation of pH in hardened cement past or mortar

Two different techniques were studied in order to evaluate the alkalinity of concretes. The first technique is based on observation of the concrete surface after spraying with indicators alternative to phenolphthalein. ███████████████████████████████
███████████████████████

Furthermore, tests was carried out on carbon steel immersed in sulphate simulating pore solutions for recognizing the effect of combination of sulphates concentrations and pH values lower than that tipical of OPC systems, representing different stages of hydration of CSA-based concretes/cement pastes.

2.1 Tests in concrete

A set of electrochemical tests was performed to study the corrosion behavior of reinforcements in concrete environment manufactured with CSA-based cements and OPC as reference. Both laboratory tests with controlled environmental conditions and field tests on full-scale beams were carried out. The electrochemical tests include open circuit potential (OCP) monitoring and electrochemical impedance spectroscopy (EIS) technique.

In order to support the OCP and EIS tests, the design, manufacturing and characterization of embeddable probes, suitable for concrete applications and sensitive to the pH were also carried out.

2.1.1 Tests in single electrode cubic samples

Corrosion tests were performed in cubic formworks, with length of 150 mm, using carbon steel working electrode, two carbon steel counter electrodes. A Reference Mortar Electrode (RME) probe and Titanium Mixed Metal Oxide (Ti-MMO) probe were embedded inside the concrete to be used as reference electrodes. An external standard calomel electrode (SCE) was also used. Electrochemical Impedance Spectroscopy (EIS) tests and open circuit potential (OCP) monitoring were performed since after concrete casting until long ageing.

2.1.1.1 Materials and mix design

2.1.1.1.1 Carbon steel bar

Ferritic-pearlitic carbon steel bar were used as working and counter electrodes embedded in concrete specimens for corrosion tests. Its microstructure was observed with optical microscope after polishing and etching by Nital 2% reagent. The metal surface was polished by using carbon silicon carbide emery paper up to 400 grit at 500 rpm with grinder-polisher Mekton FORCIPOL 1V. (Figure 2.1).
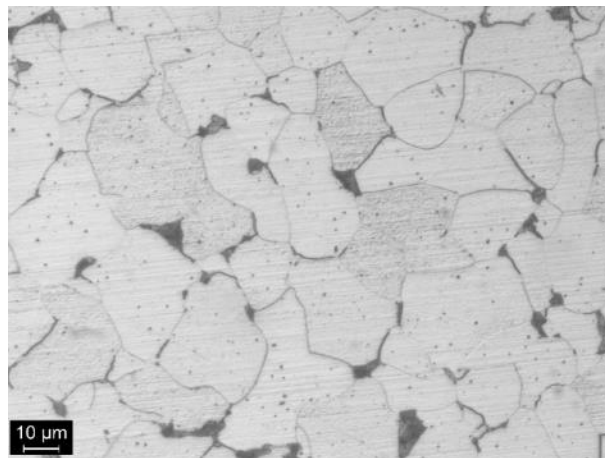
Figure 2.1: Ferrite-pearlite microstructure of carbon steel bar after etching with Nital 2%.

2.1.1.1.2 *Cements*

Four different cements were studied, one Ordinary Portland Cement (OPC), that was used as reference, and three experimental calcium sulfoaluminate-based cements (CSA), differing in content of $C_4A_3\bar{S}$ (ye'elimite).

The OPC is Limestone Portland cement CEM II/A-LL 42R, characterized by high early strength development. According to EN 197-1, the main constituents are Portland clinker (80-94%) and limestone (6-20%).

The experimental CSA cements are blend of clinker and sulfoaluminate cement, with three different amounts of ye'elimite: EXP1 binder has the greater amount of ye'elimite, which correspond to 50.4% of the mineralogical of the binder, EXP2 binder contains 25.2% of $C_4A_3\bar{S}$ and EXP3 15.1%, respectively.

2.1.1.1.3 *Aggregates*

Commercial fine and coarse aggregates, were used with 6 different gradings:
- Filler (≤ 0.063 mm)
- Fine sand (0.2-0.35 mm)
- Sand (0.6-1 mm)
- Gravel (1.5-2.5 mm)
- Coarse Gravel (3-4 mm)
- Coarse Gravel (6-10 mm)

Before mixing, aggregates were brought to dry saturated surface condition.

2.1.1.1.4 Additives

Citric acid was added to retard CSA cement hydration kinetic. Commercial superplasticizer dosage was adjusted to achieve a suitable workability at the end of the mixing procedure [71].

2.1.1.1.5 Mix design

Two concretes were manufactured by using Limestone Portland cement CEM II/A-LL 42R and water to cement ratios of 0.50 and 0.55. The concretes assumed as reference are named "OPC w/c 0.50" and "OPC w/c 0.55", respectively. CSA-based concretes were manufactured by using experimental CSA binder: EXP1, EXP2 and EXP3. EXP1 cement was used to manufacture two concretes with water to cement ratios of 0.50 and 0.55, these concretes are named "EXP1 w/c 0.50" and "EXP1 w/c 0.55", respectively. EXP 2 binder was used to manufacture concrete with water to cement ratios of 0.52, named as "EXP2", and EXP3 binder for concrete "EXP3", with water to cement ratio of 0.55.

Different additions were also considered to manufacture concretes with the experimental EXP1 binder, having the highest amount of ye'elimite, in order to study modifications regarding the corrosion behavior of carbon steel reinforcements. Calcium hydroxide was added at amounts of 2% and 4% vs. cement mass, at water to cement ratio of 0.55. The concrete with the lowest amount of calcium hydroxide is named "EXP1+Ca(OH)$_2$" and the one with twice the amount is named "EXP1+2*Ca(OH)$_2$". Lithium carbonate was also used as set accelerator, considering the amount of 0.1% vs. cement mass, to manufacture concrete named "EXP1+Li$_2$CO$_3$", with water to cement ratio of 0.55.
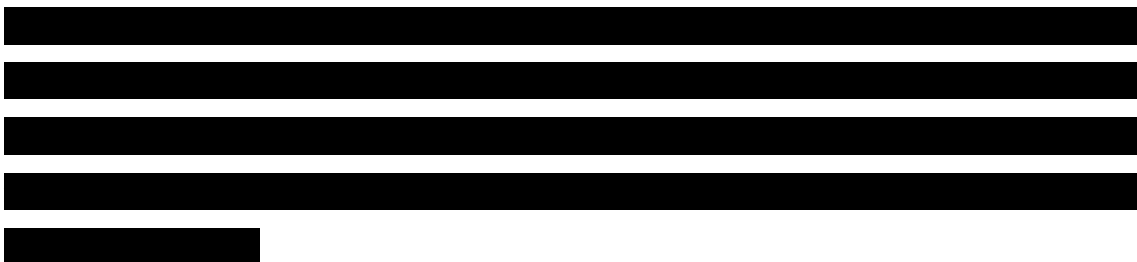
The compressive strength of concretes was measured at 1, 7 and 28 days on cubic samples (Figure 2.2). At 28 days, both two OPC concretes have about 40 MPa strength , while EXP2 and EXP3 concretes reached about 35 MPa. EXP1 concrete - having w/c = 0.55 - showed compressive strength about 27 MPa after 1 days and 70 MPa after 28 days. █████ ██ ██████████████████████████████████ while the use of calcium hydroxide, independently on the amount, slightly increased the mechanical performances of concrete EXP1 both at 1, 7 and 28 days. The set accelerator lithium carbonate strongly improved the mechanical behavior of EXP1 concrete, which developed a compressive strength of about 53 MPa even after one day.
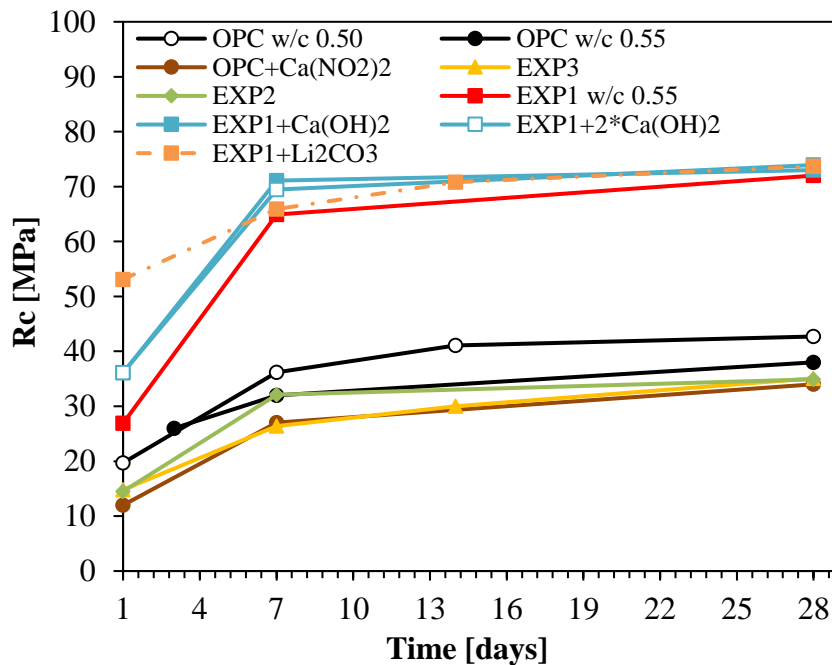
Figure 2.2: Compressive strength at 1, 7 and 28 days evaluated on cubic samples.

2.1.1.2   Preparation of the samples

Cubic samples were manufactured by using polystyrene cubical formworks with length of 15 cm. Two lateral carbon steel bar, with diameter of 10 mm, were used as counter electrodes (CE), considering a concrete cover of 40 mm, and a third carbon steel bar used as working electrode (WE), having same diameter, placed in the middle of the formwork

(Figure 2.3). In order to perform electrochemical tests, a titanium Mixed Metal Oxide (Ti-MMO) probe and a Reference Mortar Electrode were fixed to the counter electrodes for measuring corrosion potential of working electrode, as shown in Figure 2.3.
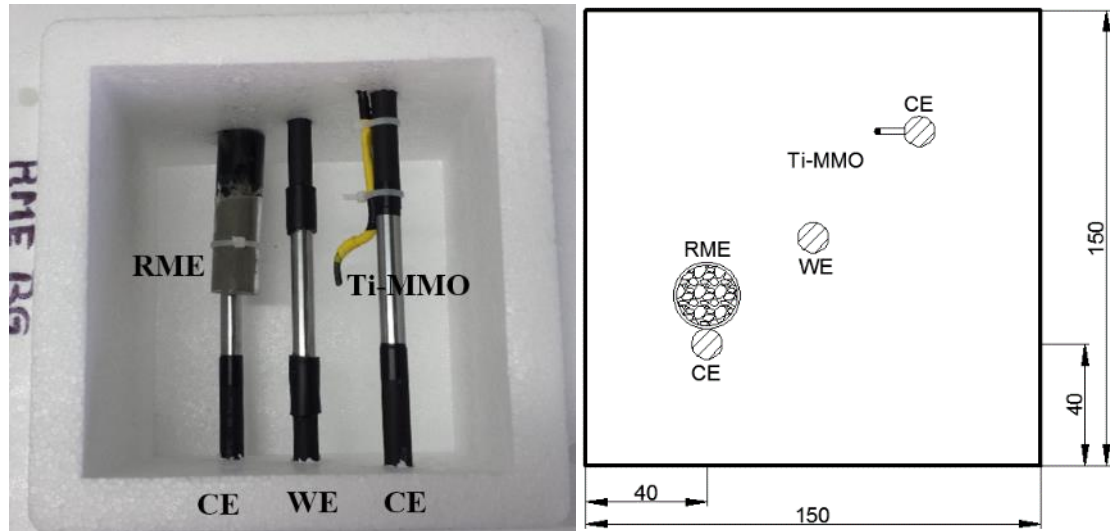
Figure 2.3: Single electrode reinforced cubic sample.

In order to prepare working and counter electrodes, carbon steel bar were cut in pieces with length of 24 cm. The lateral surface was polished with emery paper at 1200 grit, then washed with deionized water and acetone using Triton® digital heated ultrasonic machine. On one end of each bar, the electrical connection was made by welding an electrical cable or through the installation of a rivet. Finally, the extremities of the bar were isolated with a flexible heatshrink tube in order to delimit the central part for a length of 5 cm, which correspond to an exposed surface of 15.7 cm^2 (Figure 2.4).

Figure 2.4: Completed working electrode.

After casting, concrete samples were cured in the formwork with the upper surface covered with the formwork top, in a climatic chamber at 20°C.

2.1.1.3 Electrochemical Impedance Spectroscopy (EIS)

The EIS spectra were obtained by using Ivium Compactstat potentiostat-galvanostat by applying single sinusoidal potential perturbations of 10 mV (rms) amplitude versus OCP (open circuit potential) within the frequency range from 40 kHz to 5 mHz. During the tests, the embedded RME probe was used as reference electrode. Before the beginning of EIS test, free corrosion potential of carbon steel working electrode was monitored with respect to the internal RME and Ti-MMO probes and an external standard calomel electrode (SCE).

2.1.1.4 Electrochemical Impedance Spectroscopy (EIS) in wet and dry environmental conditions

EIS tests were also carried out in dry and high humidity conditions in "EXP1 w/c 0.50" and "OPC w/c 0.55" concretes. After 28 days of curing, the specimens were demolded and stored at 20°C and 95% relative humidity (R.H.). Free corrosion potential was measured before the beginning of each EIS tests. The specimens were weighted for assessing water absorption.

After 500 days of curing, further environmental conditions were studied by means of EIS tests and OCP measurements, concerning sample "EXP1 w/c 0.50", in the following order:

- Exposure to 20°C and 70% R.H. for 3 days;
- Exposure to 20°C and 40% R.H. with partial immersion of the specimens in water (2÷3 cm), for 18 days ;
- Exposure to 20°C and 70% R.H. with partial immersion of the specimens in water (2÷3 cm), for 13 days ;

- Drying at temperature of 20°C and 40% R.H. for 15 days;
- Drying at 60°C for 24 hours;
- Exposure at 20°C and 40% R.H. for 13 days.

2.1.2 Field tests in full-scale reinforced beams

Free corrosion potential of carbon steel rebar embedded in full-scale structure was monitored. Corrosion tests were performed in full-scale beams (20x20x200 cm), using as reference electrodes RME probes, placed under the upper longitudinal bar, (Figure 2.5 and Figure 2.6).

After manufacturing, the beams were placed in a climatic chamber at 20°C and R.H. above 95% for 28 days. They were then exposed to natural external environment. Corrosion potential of embedded carbon steel bar was measured since the first hours after the mixing. A standard calomel electrode (SCE) was also used for free corrosion potential monitoring.

Five concretes were manufactured, using the same mix design as reported for concretes with same name used for cubic samples: the two reference concretes, "OPC w/c 0.50" and "OPC w/c 0.55", and three CSA cement-based concretes, "EXP1", "EXP2" and "EXP3".
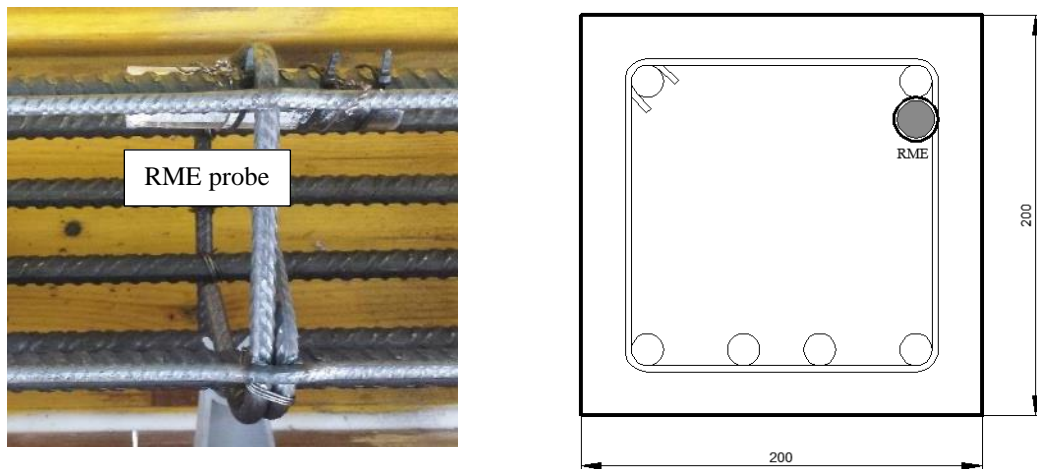
Figure 2.5: RME probe installed on steel reinforcements.

Figure 2.6: Concrete casting inside the formwork.

2.1.3 Design, manufacturing and characterization of MEP, RME and single Ti-MMO probes

In order to monitor the corrosion behavior of carbon steel reinforcements Multi Electrode Probes (MEP), single Titanium Multi Metal Oxide (Ti-MMO) probe and Reference Mortar Electrode (RME) were developed, designed and manufactured.

Two Mixed metal oxide (MMO) activated titanium wires were used to manufacture pH sensitive probes and reference electrodes, suitable for concrete applications. The atomic composition of activated layer was performed by Energy Dispersive X-Ray analysis (EDX-R) and a scanning electron microscope (SEM) Zeiss EVO 40.

Two different compositions were noticed, based on Iridium and Tantalum (IrO_x-TaO_x) oxides (Figure 2.7) and Ruthenium and Iridium (RuO_x-IrO_x) oxides (Figure 2.8).
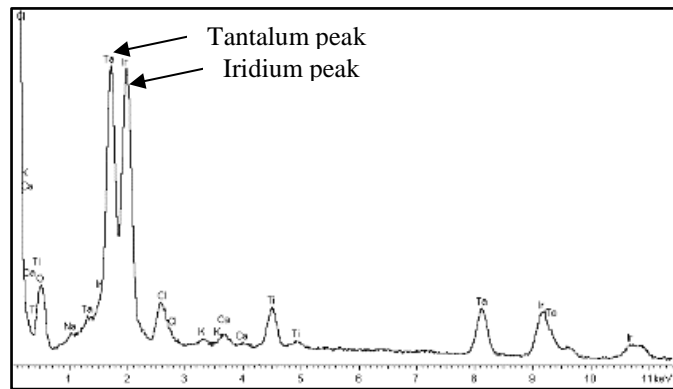
Figure 2.7: Spectrometry of IrOx-TaOx performed with EDX probe.
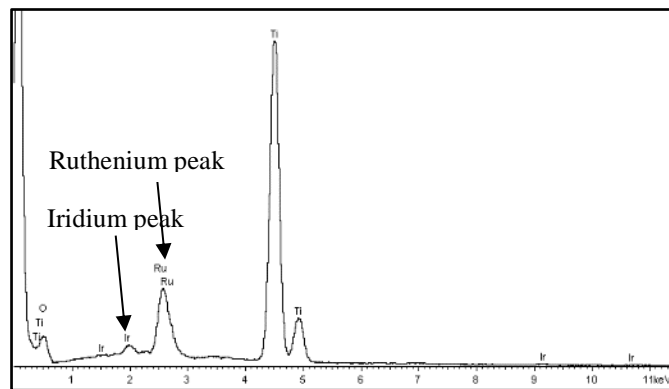
Figure 2.8: Spectrometry of RuOx-IrOx performed with EDX probe.

The MEP probe is made of 10 MMO titanium segments, with exposed length to environment around 10 mm, connected to D PCB male connector with 15 pins (Figure 2.9). The electrical multi-clip was inserted in a Plexiglas housing filled with resin in order to guarantee water sealing (Figure 2.10). The probes were manufactured by using the RuO_x-IrO_x activated wire having 0.3 mm of thickness and 1.1 mm of width. Pieces of 35 mm length were cut from a net for cathodic protection and rinsed in acetone in ultrasound for about two minutes.
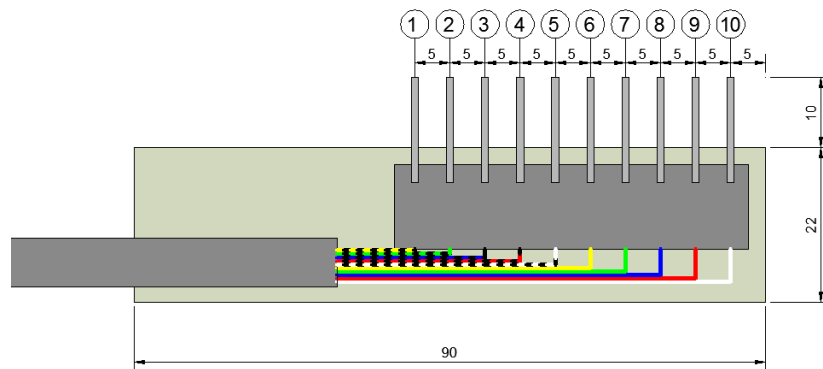
Figure 2.9: Scheme of MEP probe connection and geometry.

Figure 2.10: Completed MEP probe.

A multi-selector permits multiple measurements (Figure 2.11). Every pin of the D-PCB female connector is welded to the corresponding number on the multi-selector, following the scheme in Figure 2.9. The first pin is connected to the black jack in order to work also as reference.
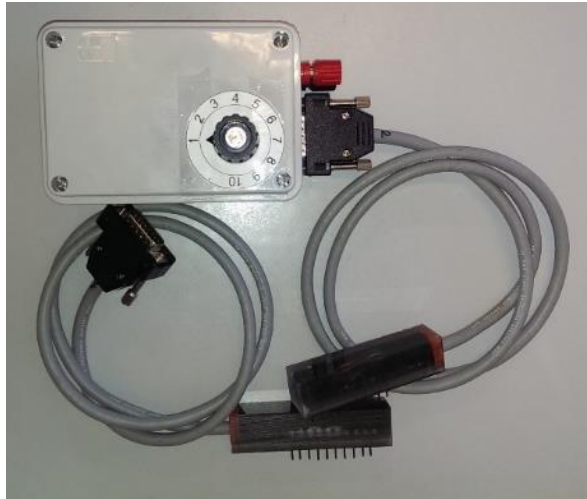
Figure 2.11: Multi-selector connected to the MEP probe.

Single titanium wire (Ti-MMO) probes were manufactured by using IrO_x-TaO_x wire, having 3 mm of diameter. A piece of 80 mm of length is cut, rinsed in acetone with ultrasound machine and welded to an electrical cable. Finally, the wire is isolated with flexible heatshrink tube in order to expose only the extremity for a length of 10 mm (Figure 2.12).

Figure 2.12: Completed single Ti-MMO probe.

Reference Mortar Electrode (RME) were designed and manufactured by using RuO_x-IrO_x net segments embedded in alkaline OPC mortar in a Plexiglas housing (22 mm diameter, 2 mm thickness, and 100 mm length). Portland cement mortar (CEM II/A 42.5R-LL) with w/c ratio of 0.47 and a sand/cement ratio of 0.8 was mixed. The titanium segment was immersed for half of its length in the fresh mortar; the other end was connected to a screened cable (Figure 2.13 a)). The upper section of the Plexiglas housing - with the electrical connection - was filled with bi-component resin (Resin Scotchcast™ n° 40) in order to guarantee electrical insulation and water sealing (Figure 2.13 b)). Once the resin

was hardened, RME probes were soaked in a solution of water and cement for 7 days, in order guarantee a correct curing of the mortar.
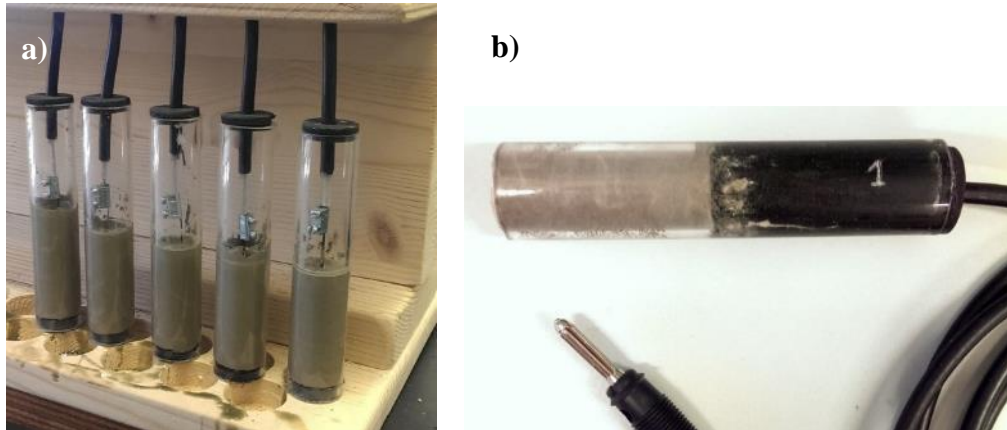
Figure 2.13: a) RME probes after pouring of the mortar; b) RME probe after sealing with resin.

Before embedding in concrete structures/samples, the probes were tested in order to evaluate their stability tests.

2.1.3.1 Tests at different pH, oxygen concentration and temperature

In order to evaluate the effect of the pH, the potential of Ti-MMO and RME electrodes were measured versus a SCE reference electrode in alkaline solutions at different concentration of sodium hydroxide, from 0.1 M up to 1 M. The tests were performed in one liter of deionized water, by progressive additions of sodium hydroxide through a 25mL ±0.05mL burette. Waiting time of at least 20 minutes was considered after each additions to achieve a stable potential. The tests were carried out at room temperature (20 ± 3 °C) and at 40°C, both in aerated and deaerated solutions. The oxygen concentration (mg/l) and the temperature (°C) were measured using a WTW Multi 3410 instrument with a SC-FDO 925 probe. An AMEL model 2335-pH METER was used to assess the pH.

The potential of IrO_x-TaO_x elements was also monitored in six different solutions, at room temperature, with pH values ranging from 9 to 14:

- 100 mL of $Na_2B_4O_7 \cdot 10H_2O$ 0.025M, 9.2 mL of HCl 0.1M, bringing the volume of solution up to 200 mL by deionized water – pH 9.1;
- 100 mL of $NaHCO_3$ 0.05M with 21.4 mL of NaOH 0.1M, bringing the volume of solution up to 200 mL by deionized water – pH 10;
- 100 mL of Na_2HPO_4 0.05M with 8.2 mL of NaOH 0.1M, bringing the volume of solution up to 200 mL by deionized water – pH 11;
- 50 mL of KCl 0.2M with 12 mL of NaOH 0.2M, bringing the volume of solution up to 200 mL by deionized water – pH 12.2;
- 50 mL of KCl 0.2M with 132 mL of NaOH 0.2M, bringing the volume of solution up to 200 mL by deionized water – pH 13.1;
- NaOH 1M, pH 14.

The potential probes was monitored to assess their stability. The evolution of potential was monitored for 7 days by placing the probes in 1 L cell containing two different solutions: deionized water saturated with $Ca(OH)_2$ (pH 12.6) and 0.001 M of NaOH (pH 11).

2.2 Development of pH-sensitive indicators alternative to phenolphthalein

The evaluation of alkalinity of hard concretes made with sulfoaluminate cement, and on reference OPC concretes as well, was carried out through spraying tests by means of suitable indicators, alternative to phenolphthalein.

Phenolphthalein is the well-recognized pH indicator to assess concrete carbonation depth. It turns pink in solution with pH included from 8.3-9 to 13 and it is colorless under or beyond these values (Figure 2.14). However, as reported in Figure 1.3, the pH value necessary to passivate carbon steel, in absence of chlorides, is 11.5. Therefore, it would not be convenient to use phenolphthalein indicator to assess if conditions to promote carbon steel passivation are present or not, because the response of this indicator would be positive (colour transition to pink) also for pH values much lower than 11.5.
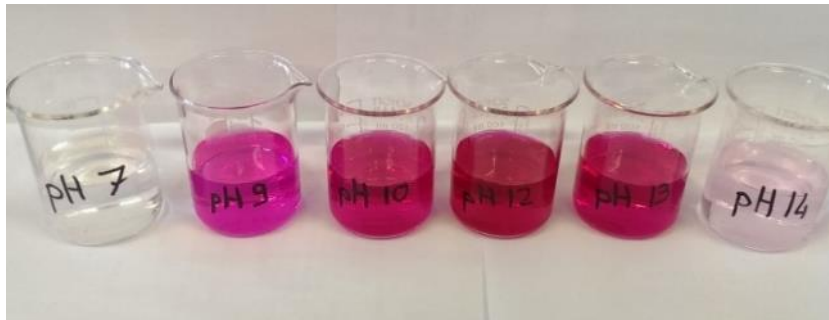
Figure 2.14: Phenolphthalein color transition at pH values of 7, 9, 10, 12, 13 and 14.

Thus, alternative pH sensitive indicators able to give a more detailed response in the range of pH values close to those of carbon steel passivation should be usefull.

Indigo Carmine is the first alternative pH indicator that may be selected for concrete application. Its color is blue at pH below 11.4, green above 11.5 and yellow above 13 (Figure 2.15). Generally, Indigo Carmine is dissolved in water and its maximum solubility is about 10 g/l. However, water solutions are not indicated to assess the pH of concrete due to pore solution dilution. Non aqueous solutions Indigo Carmine has been developed by the University of Bergamo research group in order to mitigate such effect.

The second pH indicator is Alizarin Yellow R, which has an approximate pH range for color change from 10.2 to 12.0. The color is yellow below pH 10, orange between pH 10 and 12, red for pH over 12 (Figure 2.16). Generally, this indicator is soluble in water and ethanol, slightly soluble in acetone, insoluble in other organic solvents. Also for Alizarin Yellow R, the University of Bergamo research group developed a composition suitable for concrete applications.
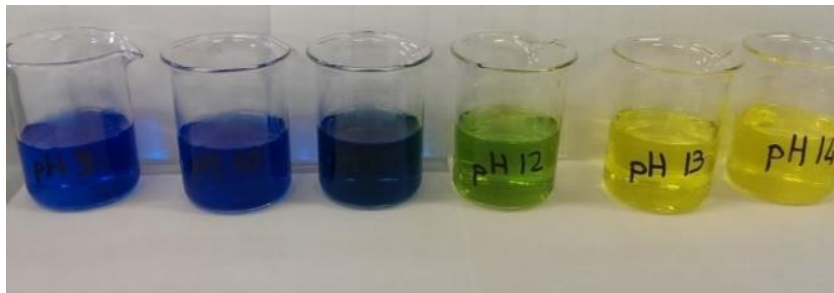
Figure 2.15: Indigo Carmine color transition at pH values of 9, 10, 11, 12, 13 and 14.
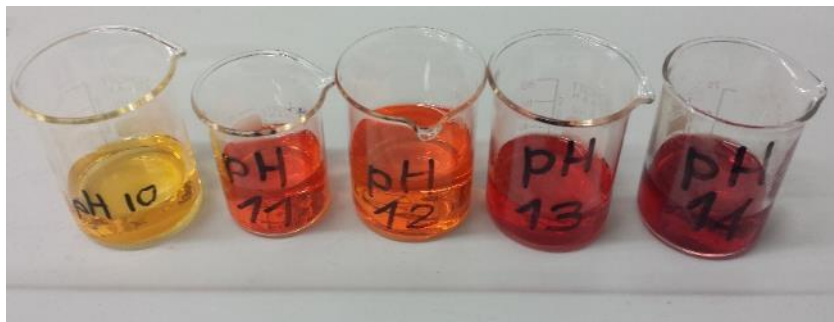
Figure 2.16: Alizarin Yellow R color transition at pH values of 10, 11, 12, 13 and 14.

██

██

██████████████ Alizarin Yellow R modified indicator was prepared by using ethanol absolute saturated with Alizarin Yellow R powder.

Among the two alternative indicators, Indigo Carmine modified indicator was the one that gave the best response in terms of colour transition and pH discrimination. Therefore, it was the one selected to be sprayed on the concrete surface, at different ageing

The spraying tests were performed at different ageing, just after splitting of a cubic sample with length of 10 cm in two half. Compressed air was used to remove incoherent particles or aggregates on fracture surface and then, the pH indicator was sprayed on the surface. After spraying and waiting for the colour transition, pictures of the surface were taken. Phenolphthalein indicator was also used, following the same procedure, as reference.
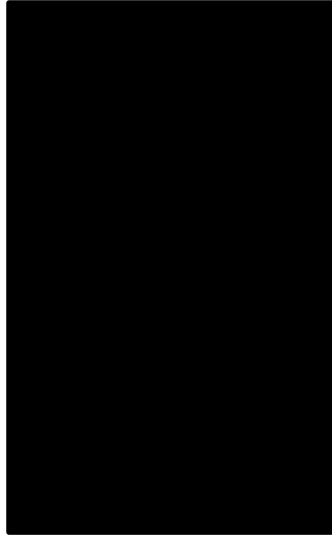
Figure 2.17: pH measurement on Agar-based gelatin applied on cement paste.

2.4 Tests in simulating solutions

A set of electrochemical and non-electrochemical tests were performed in Corrosion laboratory of Instituto Supérior Tecnico (Universidade de Lisboa) to study the corrosion behavior of common reinforcing steel in simulating solutions that correspond to different stages of hydration and service life of CSA-based cementitious systems. This paragraph wants to study the combined effect of pH and sulfate content that, according to the literature [48], simulates CSA-based systems. The electrochemical tests include open circuit potential (OCP) monitoring and electrochemical impedance spectroscopy (EIS) technique. The tests were carried out at room temperature (25±3°C) in a Faraday cage. A conventional three-electrode arrangement was used, consisting of a Pt wire as counter electrode, a saturated calomel reference electrode (SCE), and carbon steel sample as working electrode. The results of electrochemical studies are supported by the visual and microscopic (Leica DMS 300 microscope with Achro 1.6 lens) observation of the corroding surfaces.

Test in simulating solution have been carried out on low carbon steel, having the following composition in wt.%: C (0.35-0.45), Mn (0.6-0.9), Si (0.1-0.3), S (max. 0.05), P (max. 0.05).

Three different pH in combination with four concentrations of sulfates were tested. The pH was achieved by addition of sodium hydroxide to deionized water in order to get the values of 10.5, 11.5 and 12.5. The pH of the solutions has been verified using pH-meter PC 700 (Eutech Instruments) before the beginning of the test and at the end of the tests. For each pH value, four concentrations of SO_4^{2-} were studied by addition of potassium sulfate salt: 0, 1, 10 and 200 mM.

In order to prepare the samples, plain reinforcement steel of 1.2 cm in diameter was cut perpendicularly to the rebar axis in pieces of 0.5±0.2 cm with a water-cooled circular sand saw, using 01014 resinoid cut-off wheel from Presi-Métallographie and C180H cut-off machine from MetaServ, operating at 3000 rpm. The cut pieces were embedded into

epoxy resin SP 106 (Gurit Ltd., UK), using PMMA-tube of 2 mm wall thickness as a permanent mould, to form cylindrical samples of 2.0 cm in diameter. To prepare the samples for the electrochemical tests, a copper wire, attached to the sample with a silver paint (SPI 5002, Structure probe Inc.), was used for electrical connection. The quality of connection was checked before measurements using a multimeter (3478A, Hewlett-Packard company). After complete epoxy hardening, the metal side was abraded and polished under water using silicon carbide papers up to 1000 grit size at 500 rpm (LaboPol-25, Struers Inc.), rinsed afterwards with deionized water and ethanol and dried with compressed air. To prevent the development of the crevice corrosion at the steel-epoxy interface, 3M™ Scotchrap™ 50 all-weather corrosion protection tape was applied over polished sample to define the exposed area (0.6 cm in diameter, 0.24 cm^2). For each experimental condition, at least two samples were prepared and tested.

The EIS spectra were obtained using Autolab PGSTAT302N potentiostat-galvanostat by applying single sinusoidal potential perturbations of 10 mV (rms) amplitude versus OCP within the frequency range from 50 kHz to 5 mHz. Corrosion potential values were collected before the beginning of each EIS tests. Electrochemical tests were carried out at different time, since immersion of the sample until one month of exposure. When corrosion occurred, tests were stopped.

In order to support electrochemical data, visual observation was carried out by using Leica DMS 300 microscope with Achro 1.6 lens on carbon steel samples immersed in simulating solutions with same composition as those used for EIS tests.

CHAPTER **3**

---

3   EXPERIMENTAL RESULTS

3.1   Tests in concrete

The paragraphs report the experimental results of free corrosion potential evolution and EIS spectra of reinforcements embedded in cubic concrete samples and in full-scale beams, exposed to controlled environmental conditions (laboratory tests) or to natural climatic conditions (field tests).

Furthermore, the experimental results regarding the characterization at different temperature, oxygen concentrations and pH of embeddable probes, suitable for concrete application, are reported.

3.1.1 Single electrode cubic samples

3.1.1.1 Free Corrosion Potential (OCP) monitoring

Figure 3.1 and Figure 3.2 shows the evolution of free corrosion potential of carbon steel rebar in OPC concretes with respect to internal RME probes and an external standard calomel reference electrode (SCE), respectively. Just after concrete pouring, the free corrosion potential of OPCs decreases significantly, meaning that carbon steel is initially behaving as an active material. Then, it increases after cement setting and rapidly reaches stable values of about -200 mV vs. SCE, meaning that passive film forms due to alkaline of pore solution. As reported in paragraphs 3.2.2, cement pastes manufactured with Portland cements develop pH values around 13.3.
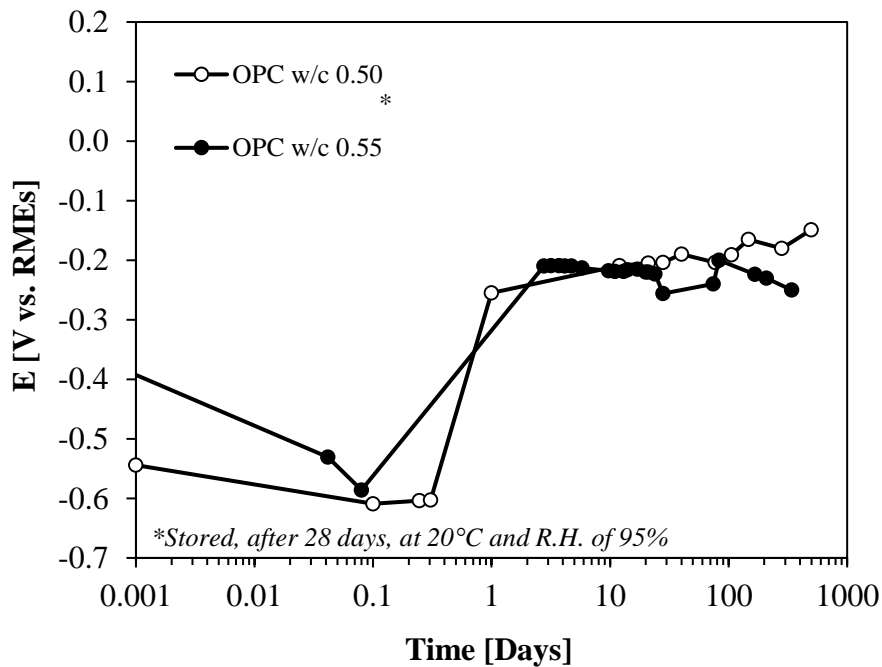
Figure 3.1: Potential evolution of carbon steel working electrode (WE) vs. RME probe in OPC concretes.

75
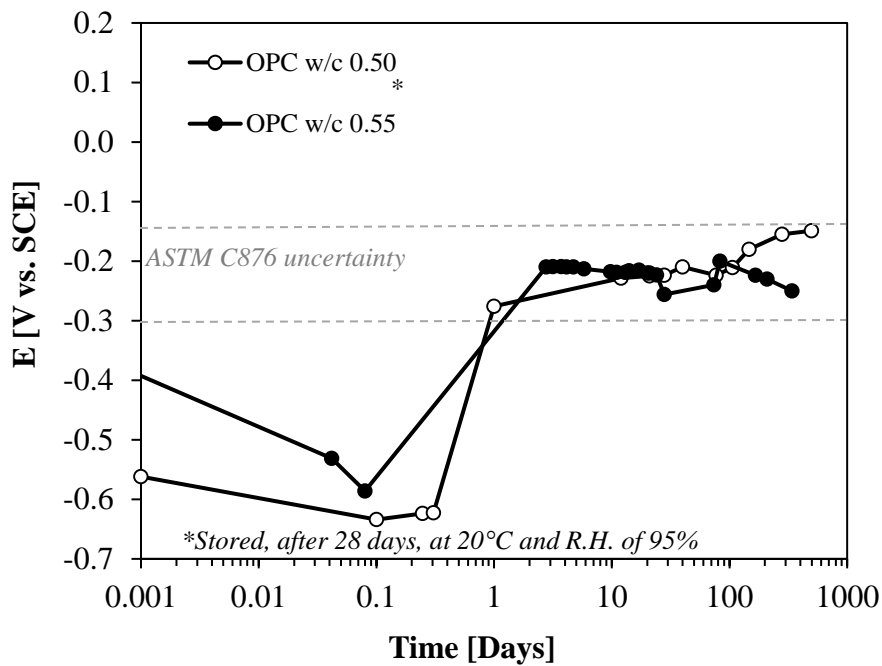
Figure 3.2: Potential evolution of carbon steel working electrode (WE) vs. standard calomel electrode (SCE) in OPC concretes.

Figure 3.3 and Figure 3.4 report the free corrosion potential in CSA-based concretes. The corrosion potential of rebar in concretes "EXP1 w/c 0.50" and "EXP1 w/c 0.55" – having the highest ye'elimite content - initial was in the range of about -400÷-500 vs. SCE, with a further decrease to -580÷-700 mV vs SCE after one day. Then, the specimen with w/c ratio 0.55 shows stable potentials at about -450 mV vs. SCE, which only increased above -300 mV vs. SCE after 8 months. However, the free corrosion potential in "EXP1 w/c 0.50" concrete placed at 95% R.H since one month remains stable at low values in the range -560÷-600 mV vs. SCE.

Concrete "EXP2" - having a ye'elimite amount of 25% - only shows low initial potential, of about -580 mV vs. SCE at 1 day, and a marked subsequent increase after 20 days, approaching -200 mV vs SCE after about 30 days. Such potential values indicate that the corrosion behavior of carbon steel only remains active during the first 2-3 weeks after manufacturing.

76

Carbon steel rebar embedded in concrete "EXP3", which contains 15% of ye'elimite, reveals a noticeable increase of the corrosion potential from -500 mV vs. SCE to -300 mV vs. SCE since one day, reaching -200 mV after 12 days.

The additions of calcium hydroxide do not modify the behavior in CSA-based concretes manufactured with EXP1 binder, even if the amount was doubled from 2% vs. cement mass to 4%.

███
███
███
███
██
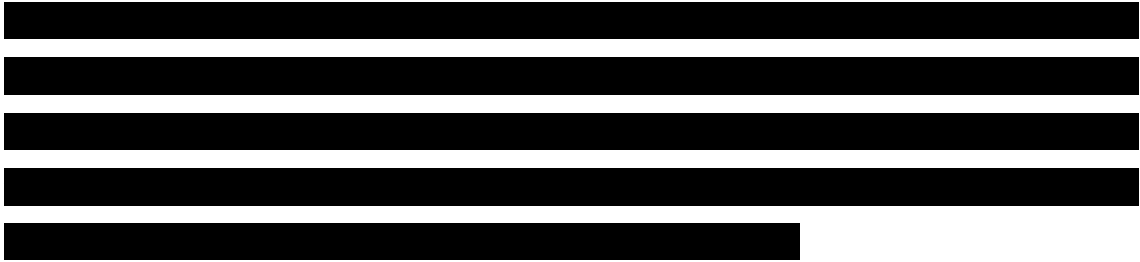
Lithium carbonate, used as set accelerator with EXP1 binder, does not modify the free corrosion potential evolution, compared to concretes manufactured with the same binder without any other addition.
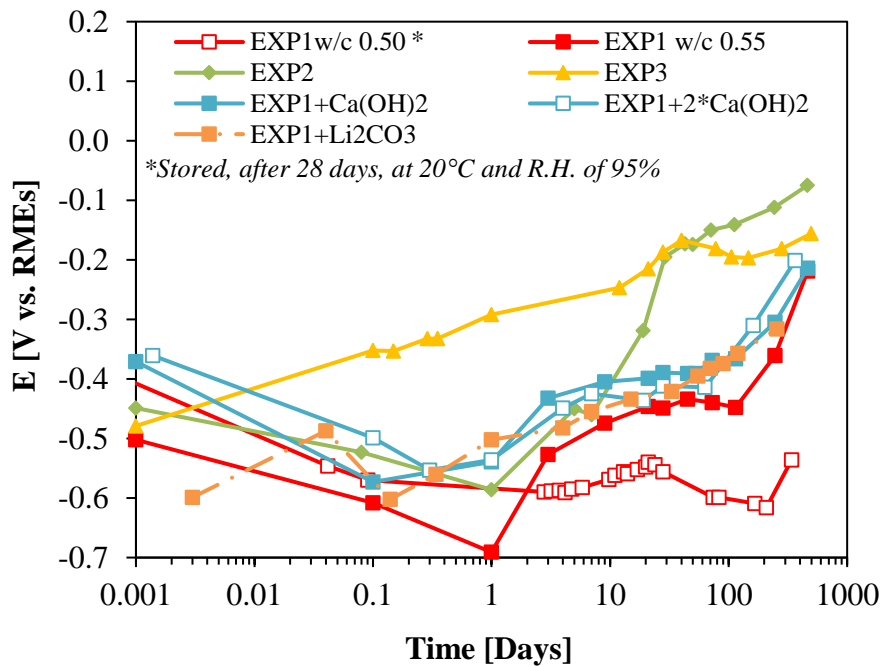
Figure 3.3: Potential evolution of carbon steel working electrode (WE) vs. RME probe in CSA-based concretes.
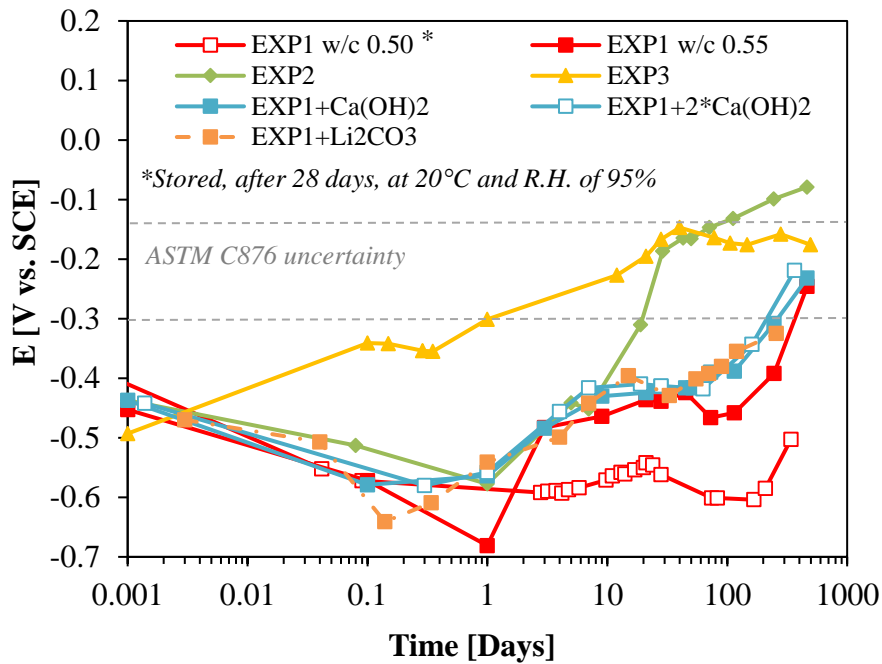
Figure 3.4: Potential evolution of carbon steel working electrode (WE) vs. standard calomel electrode (SCE) in CSA-based concretes.

3.1.1.2 Potential monitoring during dry and wet exposure

In Figure 3.5 shows the variation of corrosion potential in concrete "EXP1 w/c 0.50" exposed to different humid environmental conditions. The tests were performed after 500 days of curing of the sample.

The corrosion potential was almost constant, around -475 mV vs. SCE in concrete exposed to 70% relative humidity. It decreased to -515 mV vs. SCE after 18 days of partial immersion exposure in water, for a depth of about 2÷3 cm, in a climatic chamber at 20°C temperature and 40% R.H. A further decrease, down to -530 mV vs. SCE, was observed after increasing to 70% R.H. in the chamber. During successive drying at 40% R.H. without any immersion of the specimens, the free corrosion potential slowly increased up to -466 mV vs. SCE. Finally, after the specimens was dried in an oven at 60°C for 24 hours and then placed at 20°C and R.H. of 40%, the corrosion potential reached values around -390 mV vs. SCE.
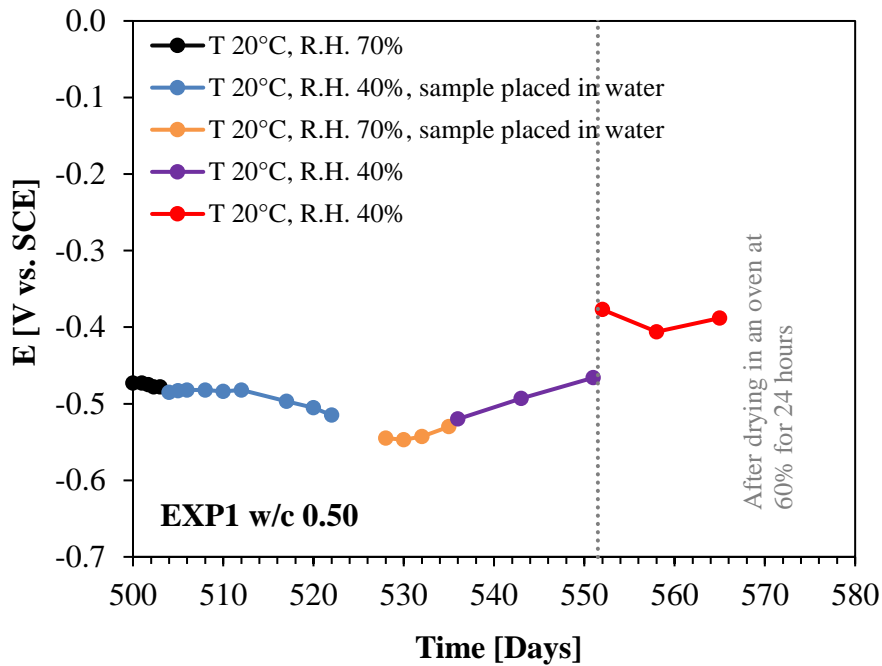
Figure 3.5: Potential evolution of carbon steel working electrode (WE) vs. standard calomel electrode (SCE) in concrete cubic sample "EXP1 w/c 0.50" exposed to wet and dry environmental conditions.

3.1.1.3 Electrochemical Impedance Spectroscopy (EIS) spectra

Figure 3.7 to Figure 3.17 describes the evolution of EIS spectra at different curing time. All concretes show a shift to lower frequencies of the phase and a marked increase of Z modulus at high frequency over the time. The impedance at the frequency of 1 kHz ($|Z|_{1 kHz}$), that can be assumed representative of ohmic resistance of concrete (R_Ω), increases significantly due to the reduction of porosity caused by hydration of cement.

The ohmic resistance (R_Ω) of OPCs varies in function of the w/c ratio. As far as the lowest w/c ratio is concerned ("OPC w/c 0.50 - Figure 3.7) the impedance at high frequencies varies from 100 Ω at 1 day up to 700 Ω at 280 days while, concretes "OPC w/c 0.55" ██ ███████████ (Figure 3.8 and Figure 3.9), develop values from 50 Ω at 1 day up to 360÷370 Ω after 260÷340 days.

The ohmic drop, (R_Ω), is strongly dependent on the quality of the matrix of the concrete, which depends upon the nature of the binder. Generally, CSA-based concretes showed higher R_Ω compared to OPCs, at the same ageing. Concretes manufactured with EXP1 binder - which has the greatest amount of ye'elemite in its composition - show the higher values of ohmic drop, around 1000 Ω at 12 days and around 30000 Ω after 1 year from casting (Figure 3.10 and Figure 3.11). By decreasing the amount of ye'elemite in the binder, from binder EXP2 to EXP3, is possible to see that the ohmic drop decreases from 60 Ω to 47 Ω at 1 day and from 5000 Ω to 850 Ω after 250 days of curing, respectively (Figure 3.12 and Figure 3.13).

The addition of calcium hydroxide to EXP1 binder strongly increases the ohmic drop of the concrete both at low (150÷350 Ω at 1 day) and at long ageing (100000 Ω after one year) (Figure 3.15 and Figure 3.16). The use of lithium carbonate seems to increase the ohmic drop but only at short ageing (Figure 3.17) ███████████████████████ ████████████████████████████████████

A correlation between the ohmic drop and the compressive strength over time can be seen in Figure 3.6.

CSA concretes (with and without additions of calcium hydroxide and calcium nitrite) show the highest ohmic drop (about 1000÷1800 Ω) and the highest compressive strength (about 70 MPa) at 28 days. OPCs and concretes manufactured with binder EXP2 and EXP3 have ohmic resistance of about 200÷350 Ω and compressive strength about 35÷42 MPa.
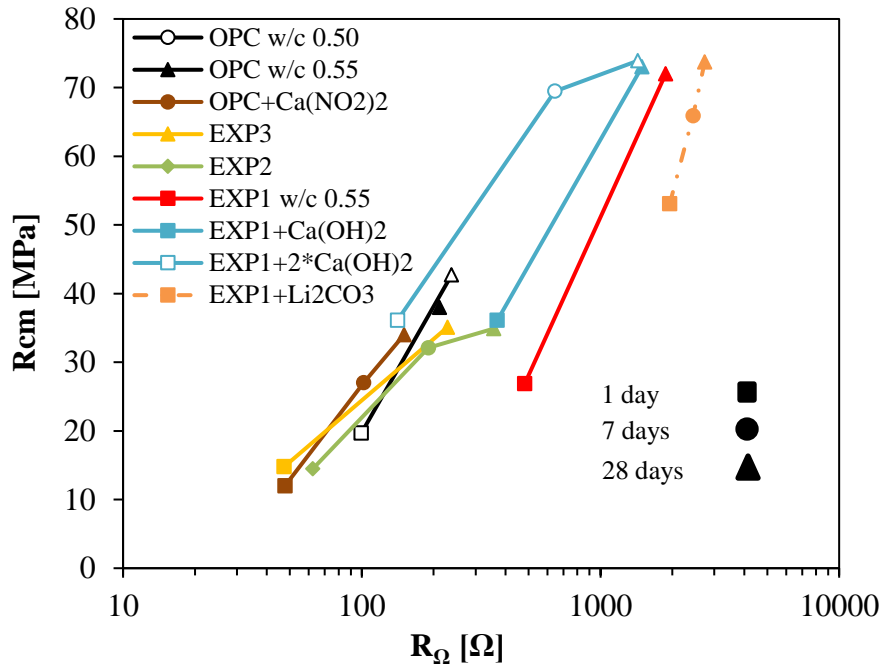
Figure 3.6: Correlation between the compressive strength (MPa) and the ohmic drop R_Ω (Ω).

OPCs concrete show rapid increase of the impedance that reach values of about 30000÷40000 Ω at the lowest frequency of 0.005 Hz. For this admixtures is not possible to observe, at the lowest frequencies used during EIS tests, the presence of a clear plateau and therefore, it is not possible to determine the polarization resistance value.

All spectra related with concretes manufactured with Portland cement shows phase angle of about -80° that tend to shift to low frequencies with prolonged exposure. The shape of EIS spectra supports free corrosion potential monitoring previously described. It outlines a rapid formation of stable protective film on the steel surface.

CSA-based concretes manufactured with binder EXP1 (Figure 3.10 and Figure 3.11) exhibit behaviors that can be interpreted by Randles equivalent circuit (see Chapter 1) with low polarization resistance R_P, meaning that the corrosion rate should be higher compared to OPCs, confirming the low free corrosion potentials measured over time.

For active material, R_p can be obtained, according to Randles equivalent circuit, by subtracting from the value of impedance at 5 mHz ($|Z|_{5\ mHz}$) the impedance at 1000 Hz ($|Z|_{1\ kHz}$). However, the phase shift to lower frequencies and the decrease of amplitude over time suggest that pseudo-passivation conditions could occur due to active corrosion of steel in a cement matrix characterized by low porosity and very low water content.

Concretes "EXP3" (Figure 3.13) and ███████████████████████ show Bode spectra similar to those of OPCs, likewise corrosion potential evolution over time.

The use of calcium hydroxide with EXP1 binder increased the R_P values and the phase displacements; in these mixes, the phase angle displacement shifted to the left for time increasing and the steady state tend to disappear (Figure 3.15 and Figure 3.16).

The use of lithium carbonate as set accelerator (Figure 3.17) increased the R_Ω values, after 1 day of curing, from 471 Ω up to 1900 Ω while, for longer ageing, the Bode spectra were similar to those of concretes manufactured with binder EXP1.
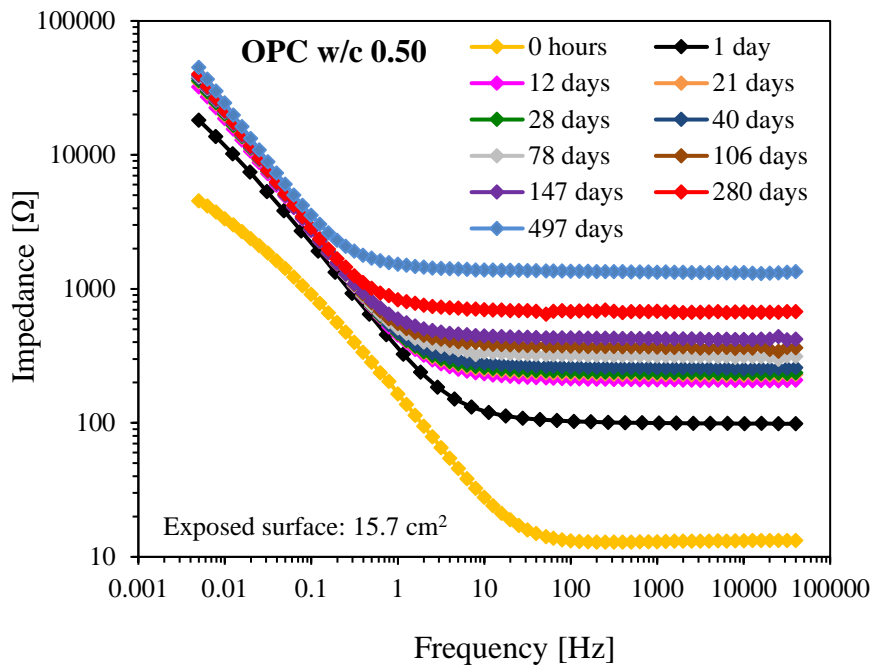
Figure 3.7: Bode spectra for modulus of Z (upper) and Phase angle (lower) - OPC w/c 0.50 concrete.
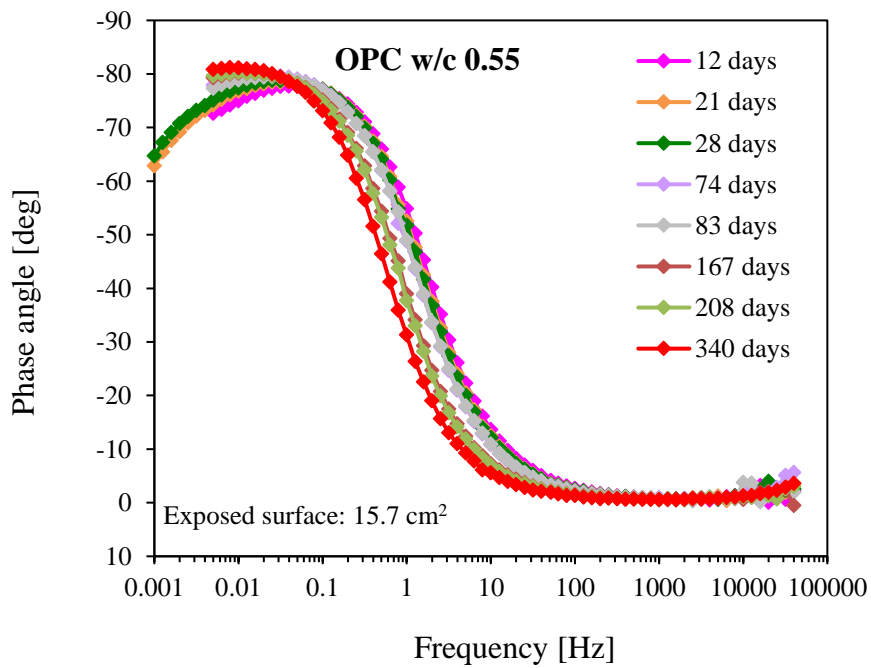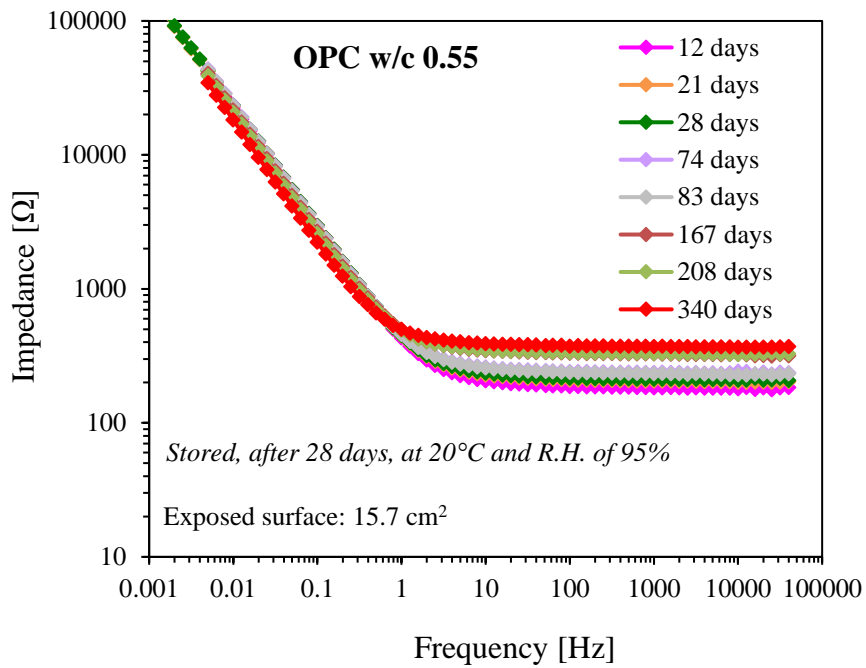
Figure 3.8: Bode spectra for modulus of Z (upper) and Phase angle (lower) - OPC w/c 0.55 concrete.
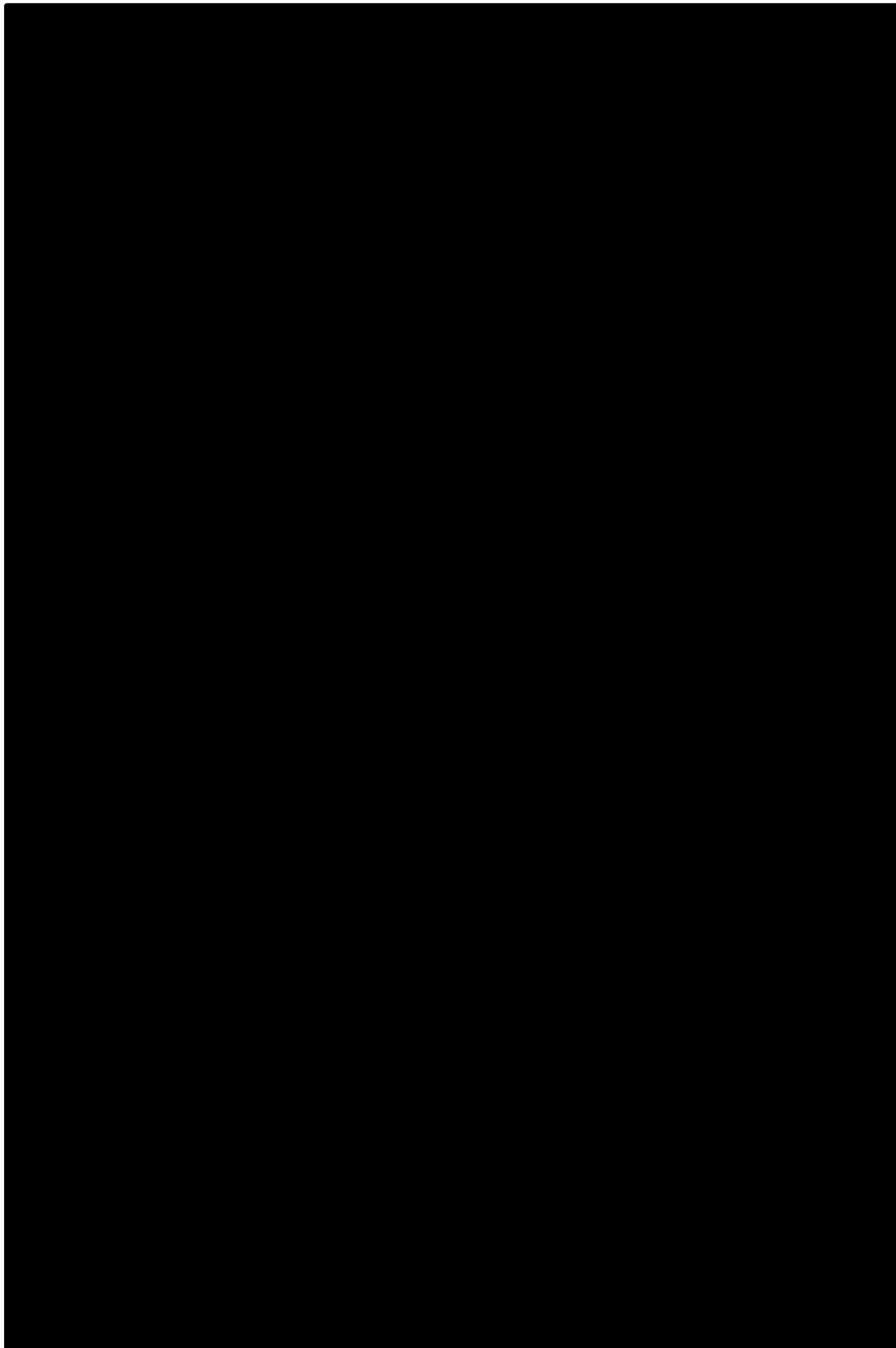
Figure 3.9: ██
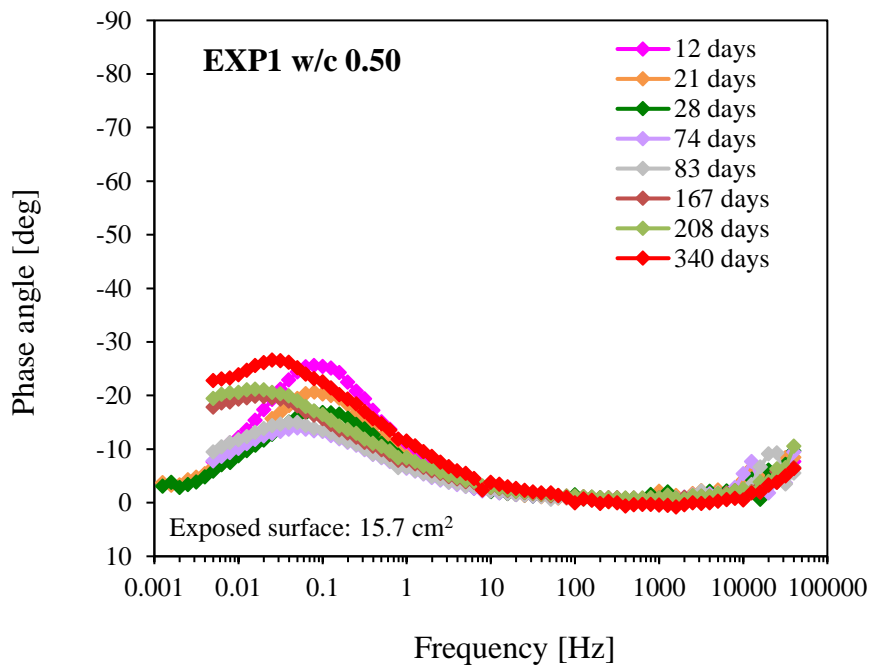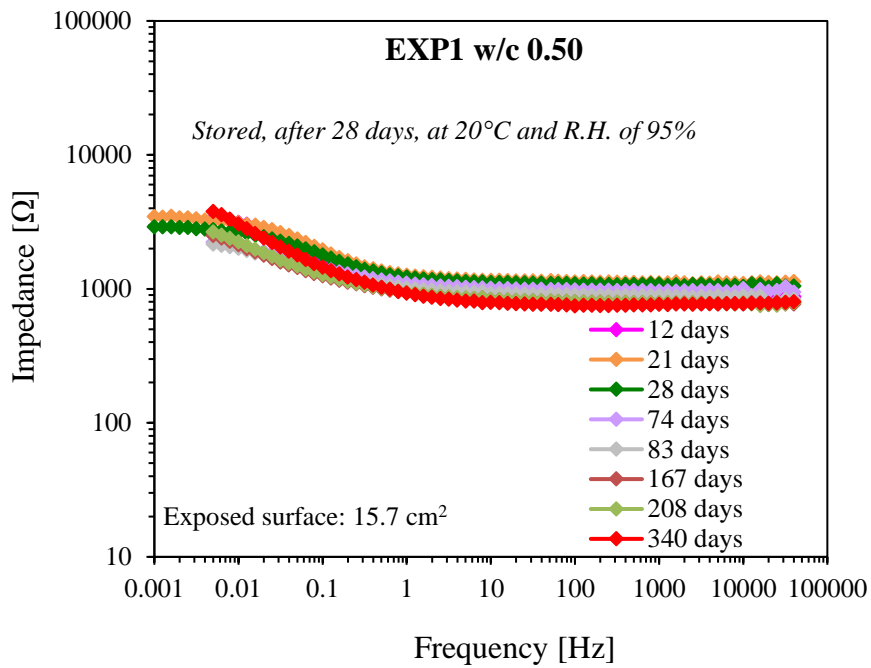
Figure 3.10: Bode spectra for modulus of Z (upper) and Phase angle (lower) – EXP1 w/c 0.50 concrete.
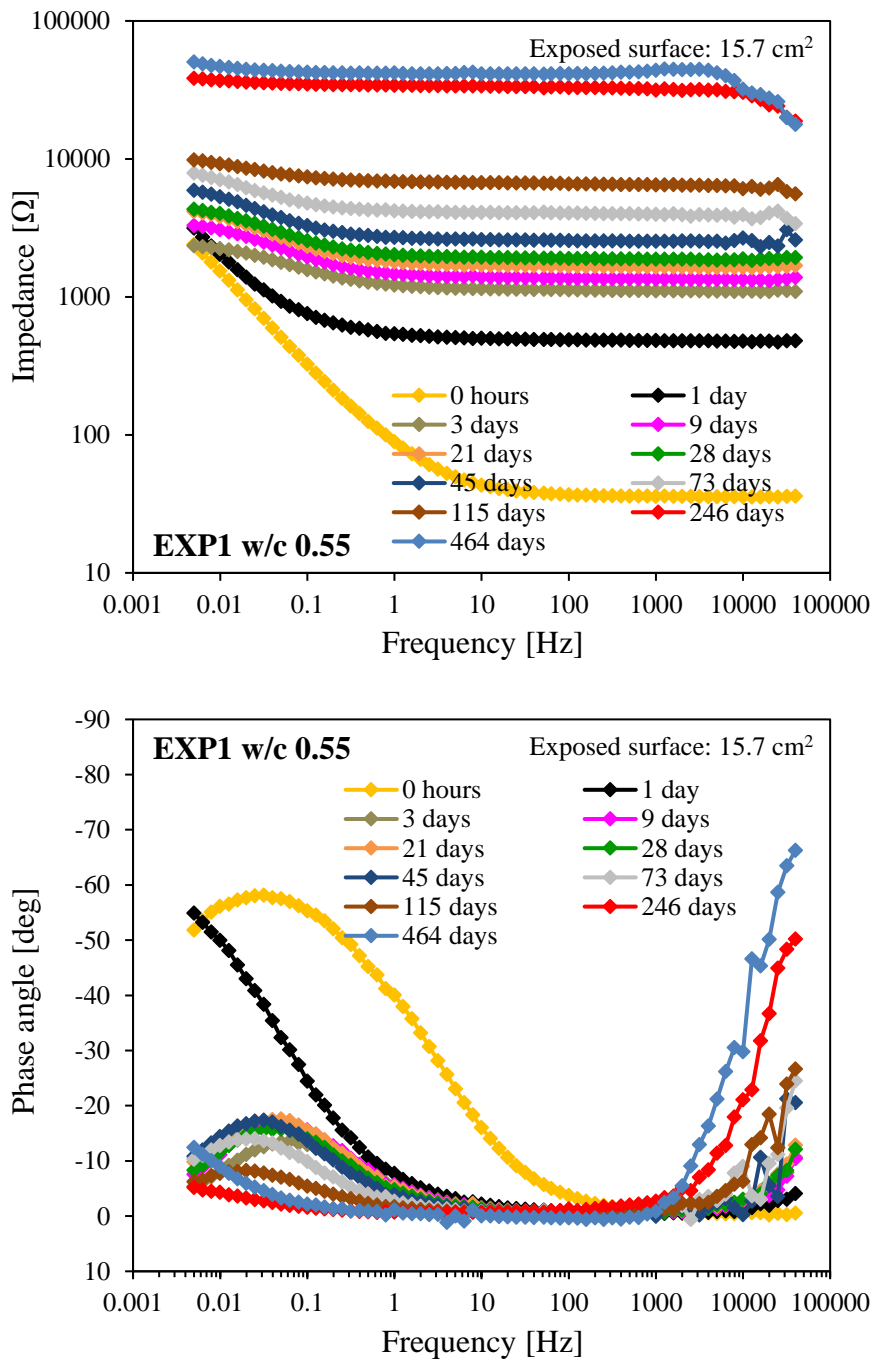
Figure 3.11: Bode spectra for modulus of Z (upper) and Phase angle (lower) - EXP1 w/c 0.55 concrete.
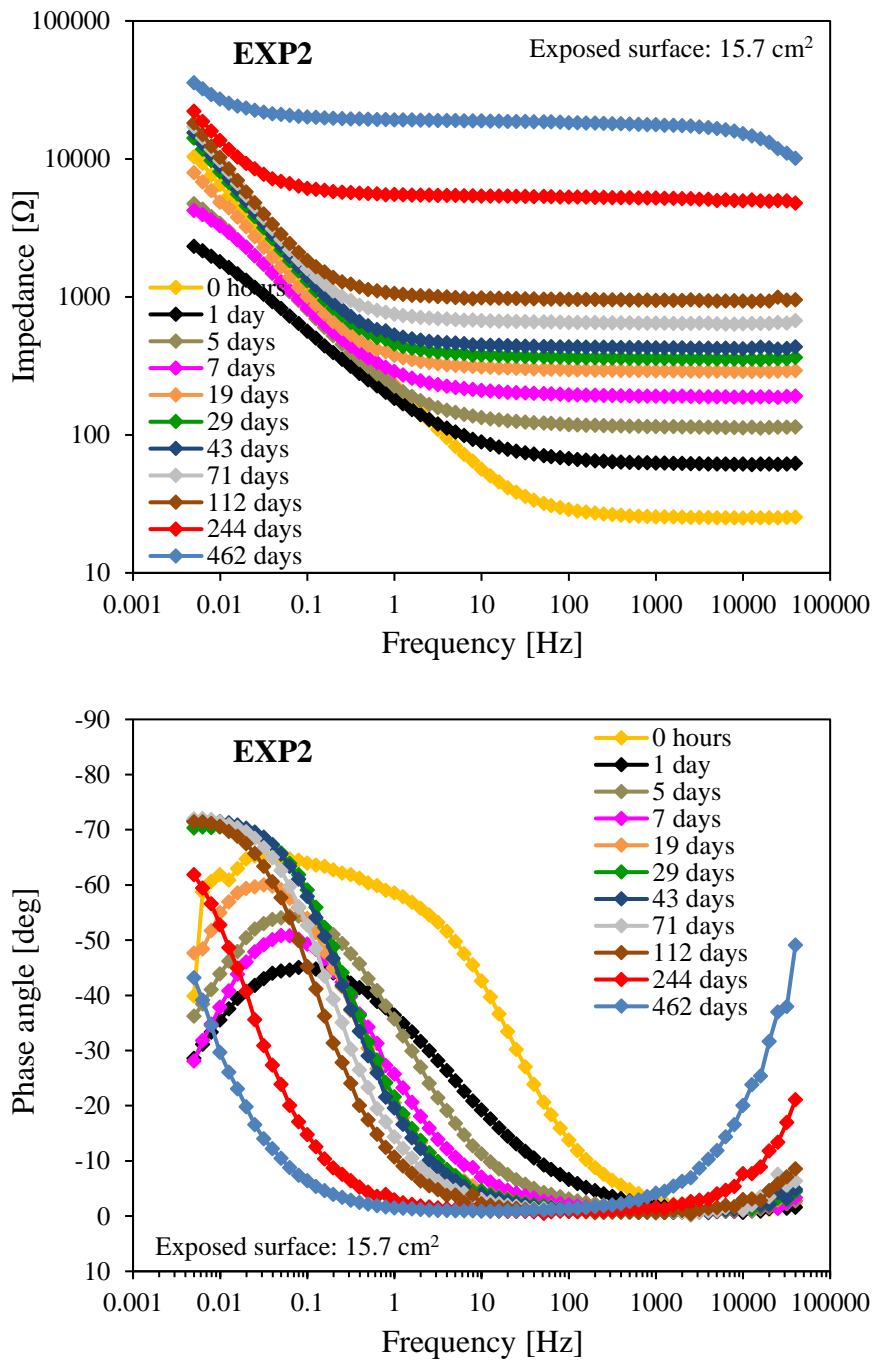
Figure 3.12: Bode spectra for modulus of Z (upper) and Phase angle (lower) – EXP2 concrete.
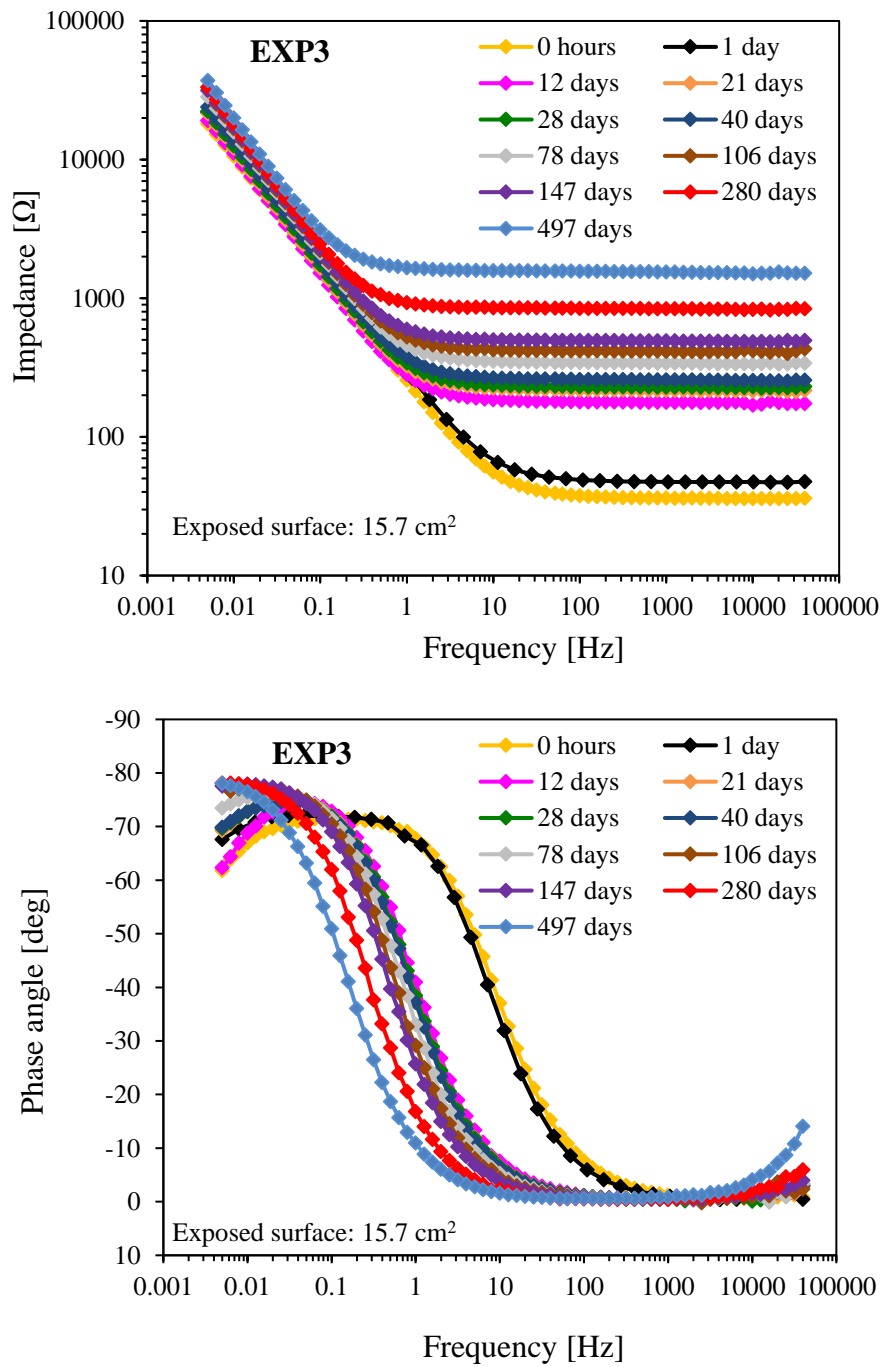
Figure 3.13: Bode spectra for modulus of Z (upper) and Phase angle (lower) - EXP3 concrete.
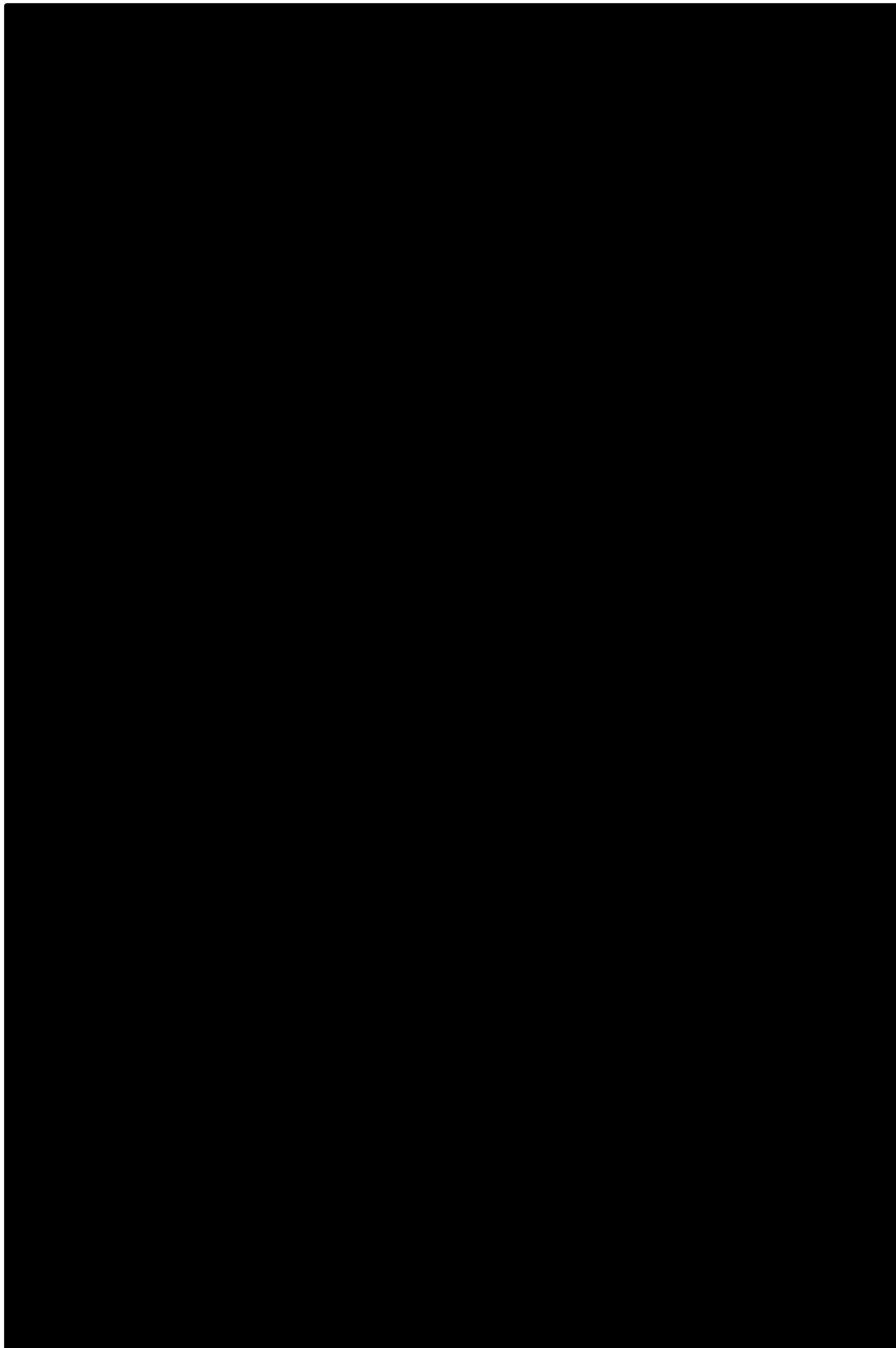
Figure 3.14: ███
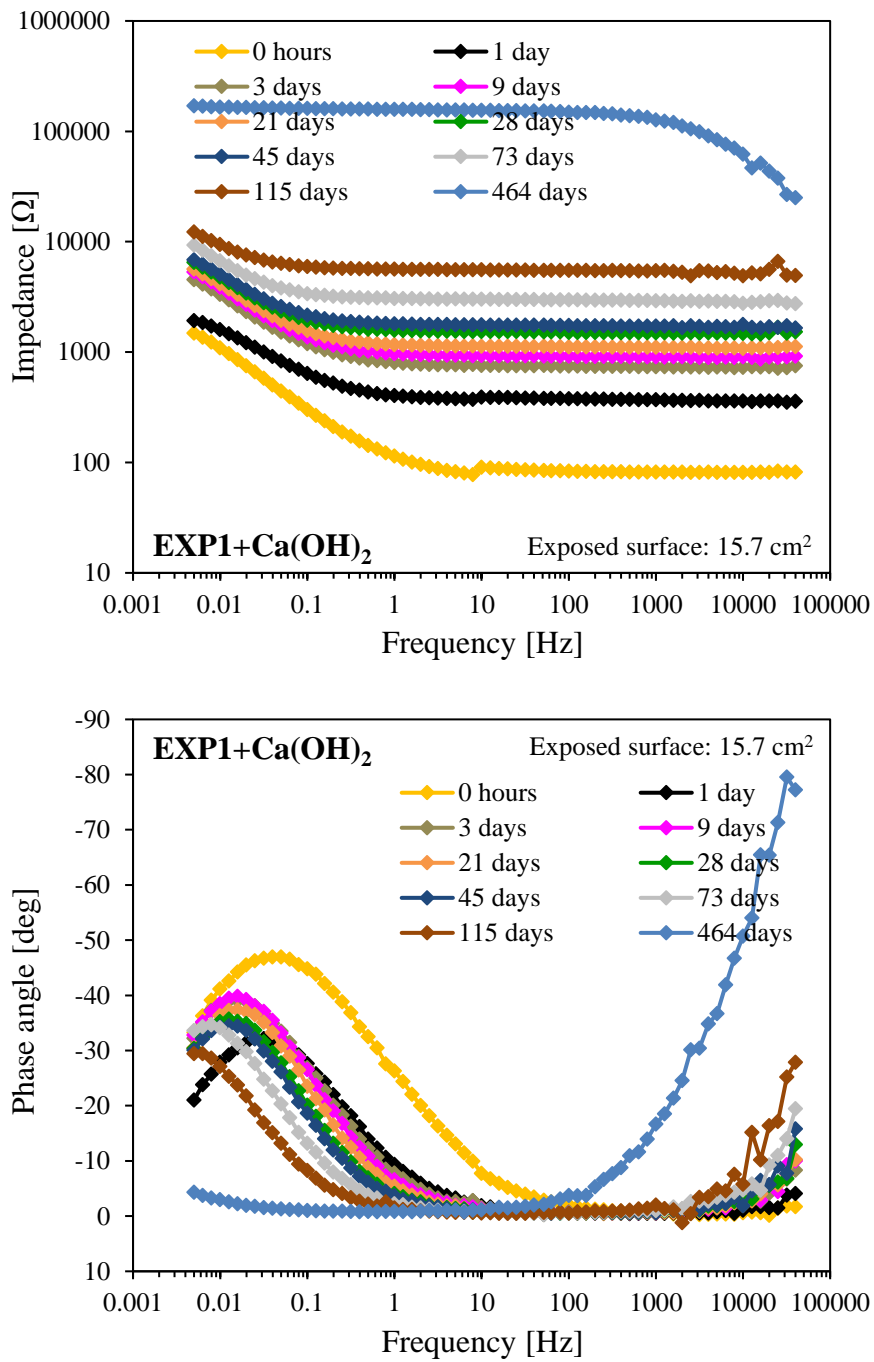
Figure 3.15: Bode spectra for modulus of Z (upper) and Phase angle (lower) - EXP1+Ca(OH)₂ concrete.
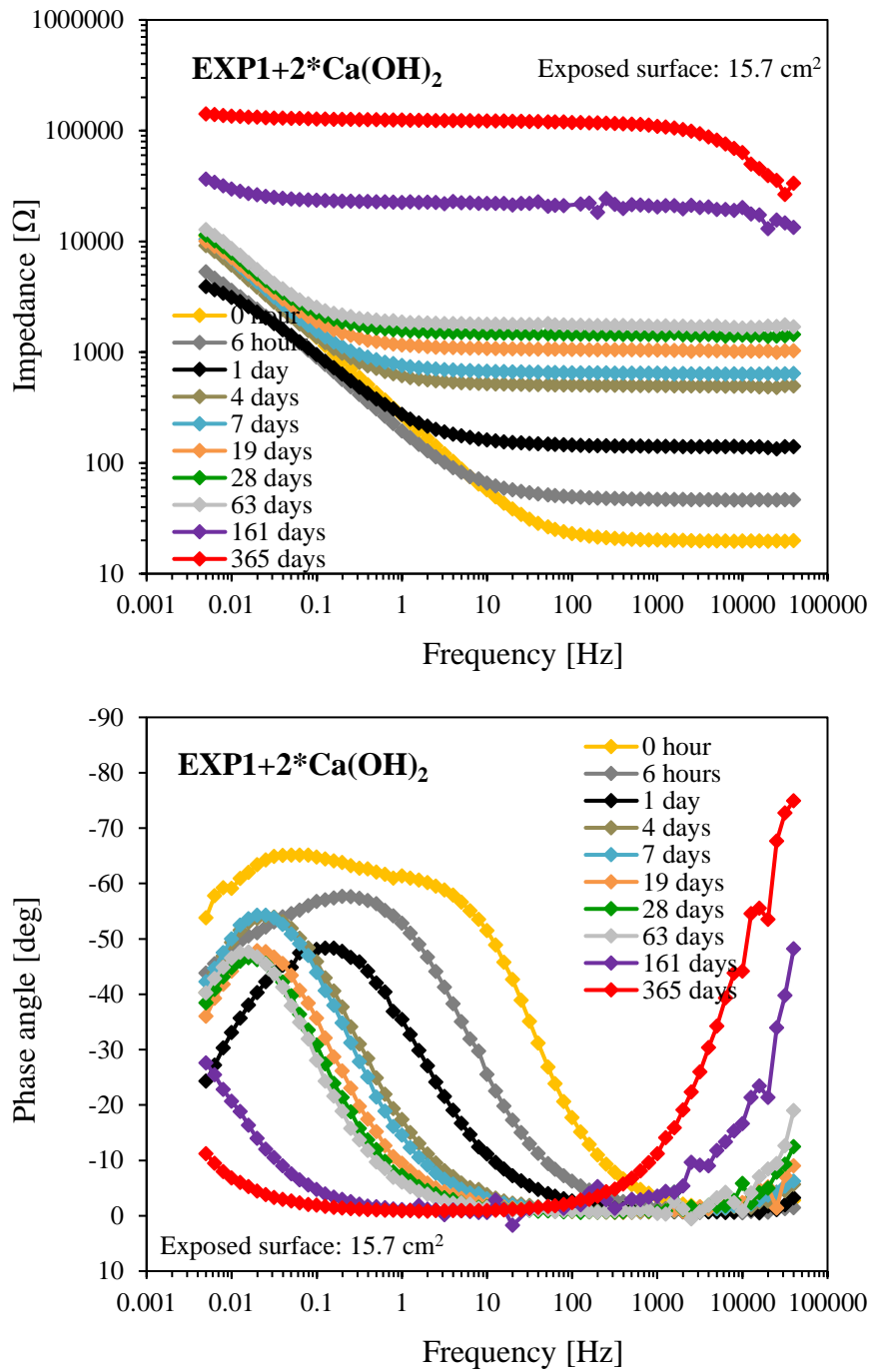
*Figure 3.16: Bode spectra for modulus of Z (upper) and Phase angle (lower) - EXP1+2*Ca(OH)₂ concrete.*
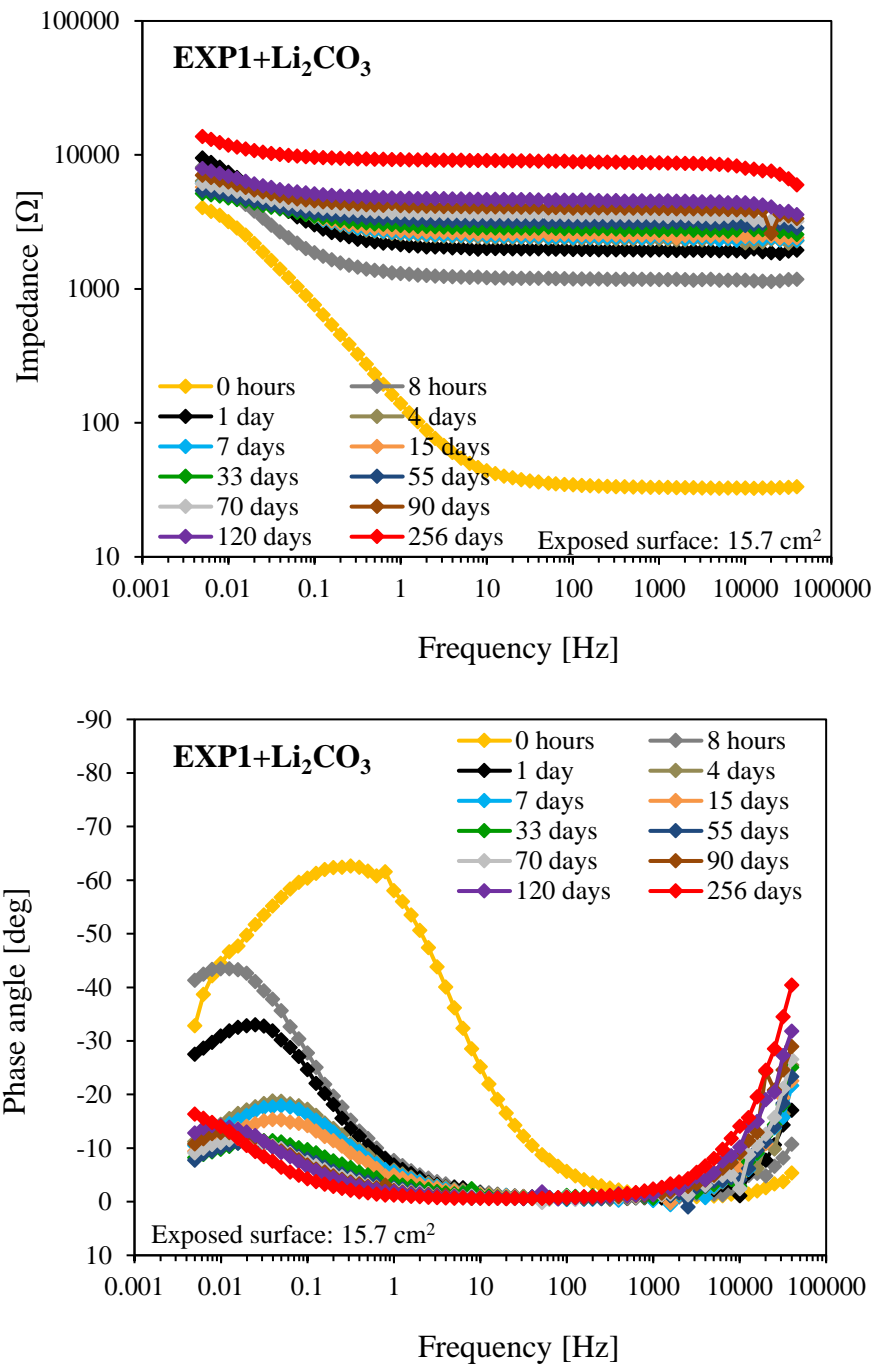
Figure 3.17: Bode spectra for modulus of Z (upper) and Phase angle (lower) - EXP1+Li₂CO₃ concrete.

Figure 3.18 and Figure 3.19 report a comparison between the Bode spectra, at short and long ageing (28÷33 and 250÷280 days, respectively). After 28 days of exposure, it is possible to identify two groups of concrete with different behavior. OPC and CSA-based concretes manufactured with experimental binder EXP2 (25% of ye'elimite) and EXP3

(15% of ye'elimite) showed similar R_Ω values and high impedance values at low frequencies ███). Their phase angle displacement showed peaks around -80° within the frequency range of 0.02÷0.05 Hz. Concretes manufactured with binder EXP1 (50% of ye'elimite) revealed high ohmic drops, but low impedance values at low frequencies; the sample stored in a climatic room at 20°C and R.H. of 95% showed lower values of the impedance compared to that stored in its formwork. ██████████████████████████████████

██

██

██████████████████████████████████

At long ageing, it is possible to observe that only concrete "EXP3" had almost the same R_Ω of OPCs while, "EXP2" shifted to higher values close to concretes manufactured with binder EXP1. The phase angle, for all concretes, shifted to low frequencies: EXP1 concretes showed again low displacements, OPCs ██████████████████ values around -75÷-80° and concrete "EXP2" an intermediate behavior.
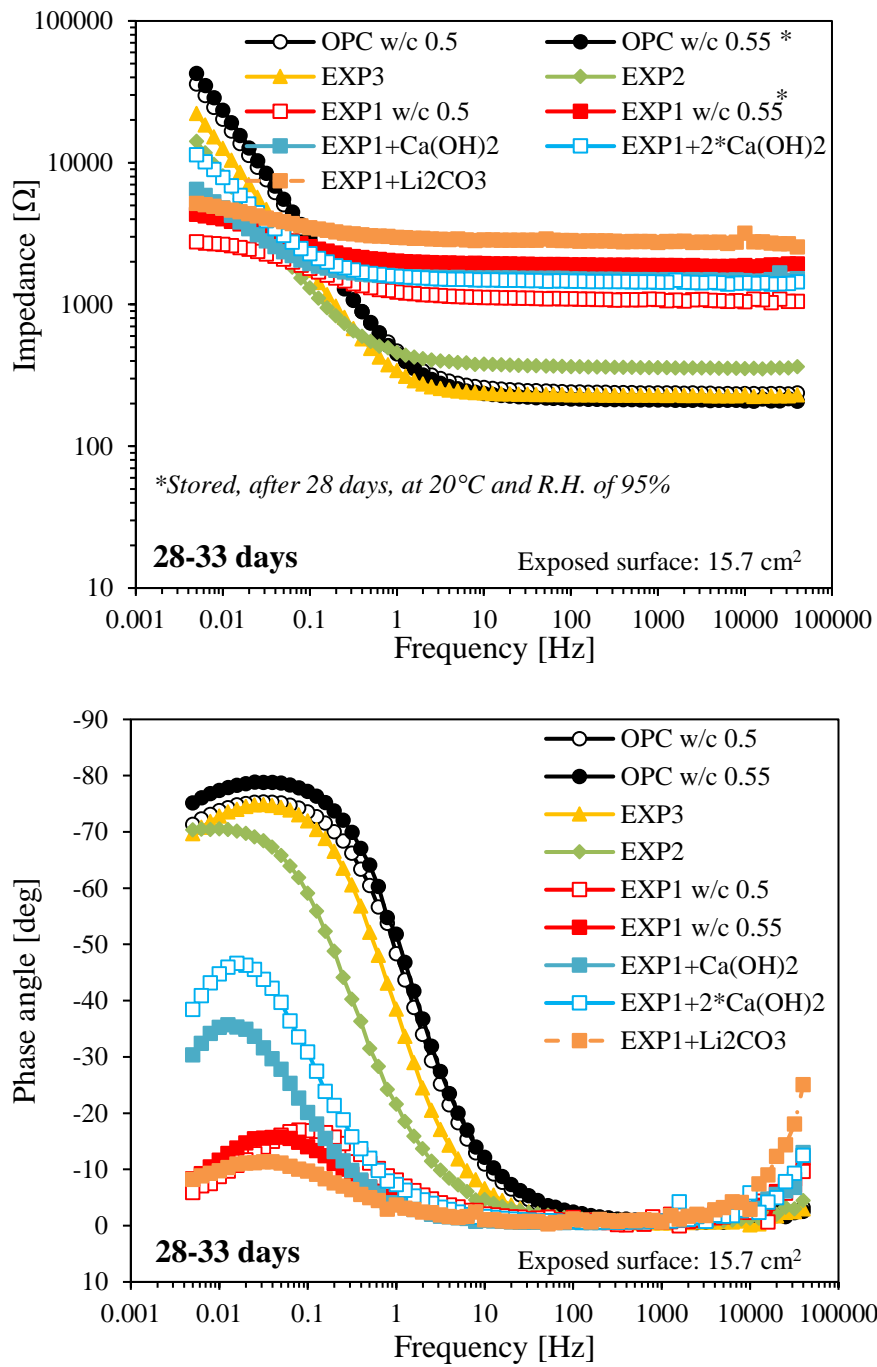
Figure 3.18: Bode spectra for modulus of Z (upper) and Phase angle (lower) after 28-33 days of curing.
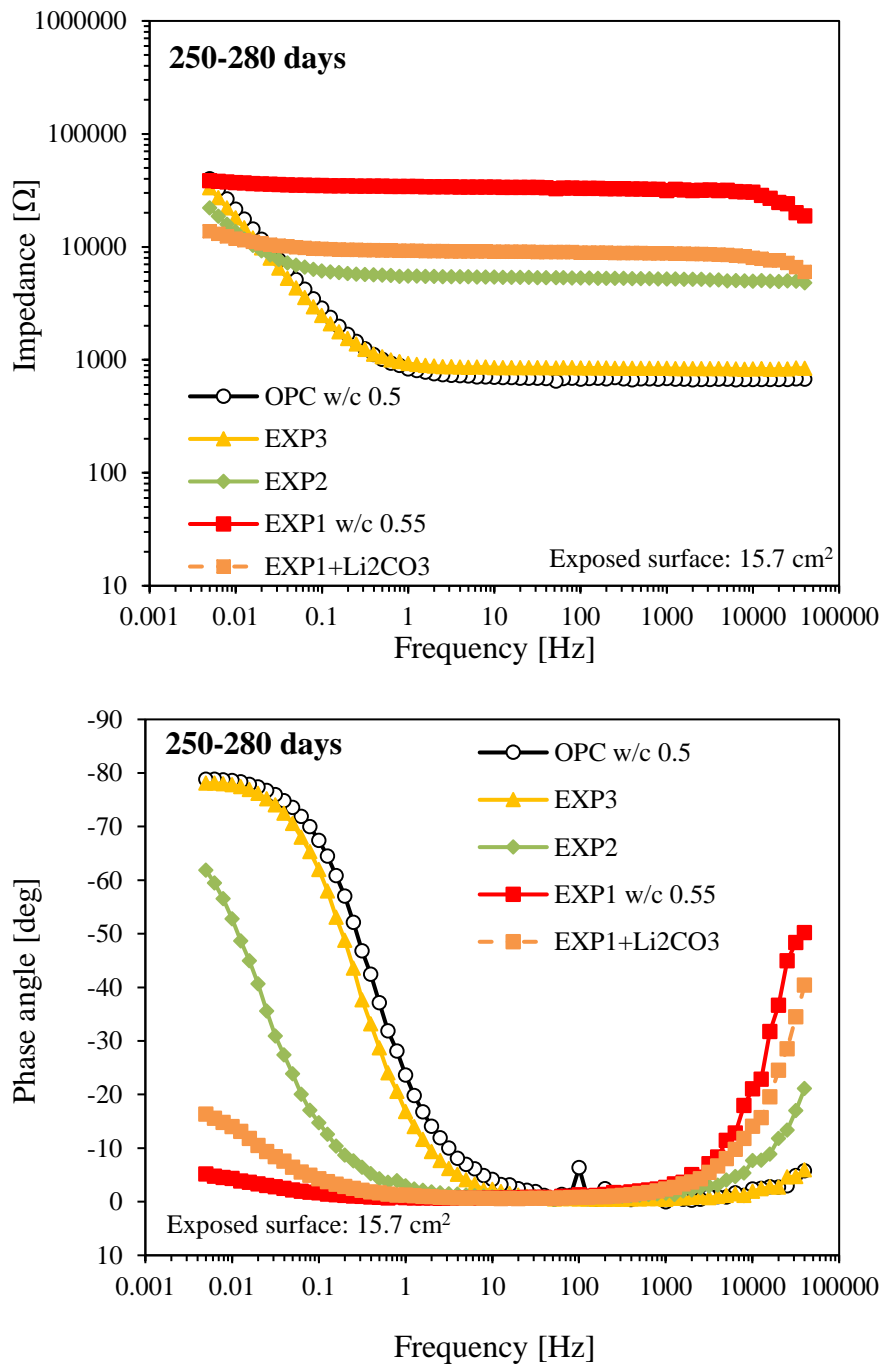
Figure 3.19: Bode spectra for modulus of Z (upper) and Phase angle (lower) after 250-280 days of curing.

3.1.1.4 EIS spectra at different dry and wet exposure

Figure 3.20 reports the modifications of EIS spectra in "EXP1 w/c 0.50" concrete exposed, after 500 days, to wet and dry environmental conditions. After exposure for 500 days at 20°C and R.H. of 95%, the specimen was stored in a climatic chamber with temperature of 20°C and relative humidity of 70%. The Bode spectra showed a strong increase of the impedance at the low frequencies, which correspond to the ohmic resistance R_Ω, from 800 Ω (grey curve) up to 2400 Ω (black curves) and a less marked increase at the low frequencies. A clear variation of the phase angle displacement from -28° to -12° can also be noticed. Then, the specimen was placed in a chamber with temperature of 20°C and R.H. of 40%, with the bottom part of the specimen immersed in water for a depth of about 2÷3 cm. The impedance at high frequencies decreased and after 18 days under these conditions it reached a value of 990 Ω; at low frequencies, slightly modifications were visible. The phase angle displacement slightly shifted to more negative values of -18 degrees. A shift of the impedance to lower values was achieved, for all the frequency range, increasing the R.H. up to 70% while, the phase angle was almost the same. Then, the sample was dried. First at 20°C and R.H. of 40%, later in an oven at 60°C for 24 hours. The impedance at high frequencies showed a strong increase up to values around 4000 Ω while, that at low frequencies, developed a lower increase; in dry conditions the phase angle reached values close to -6°.

All curves, contrary to those collected until 340 days for concretes manufactured with binder EXP1 (also with the use of lithium carbonate as set accelerator) cured in their formworks or in dry environment at R.H. of 95%, didn't show the presence, at the lowest frequencies, of a well defined plateau.

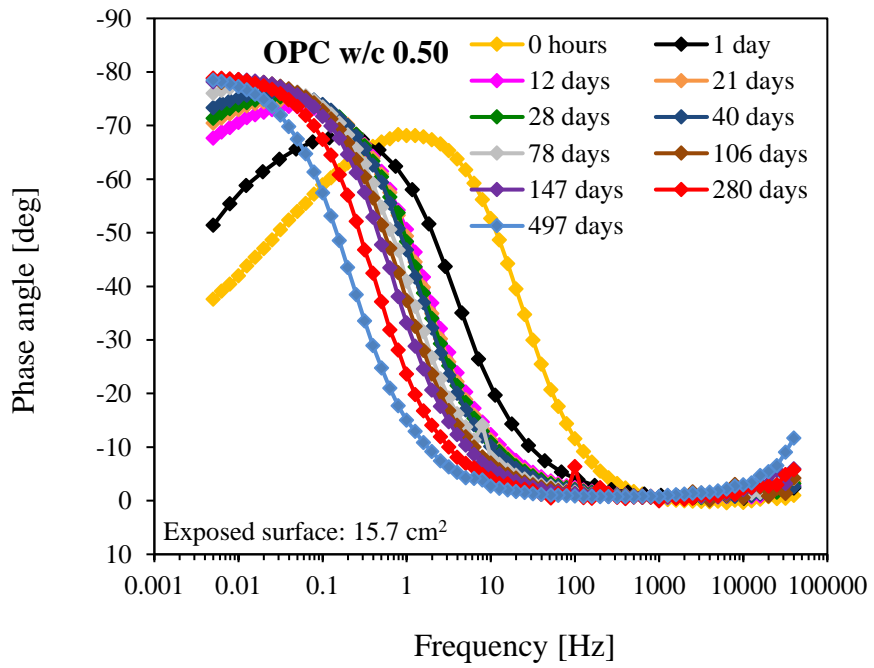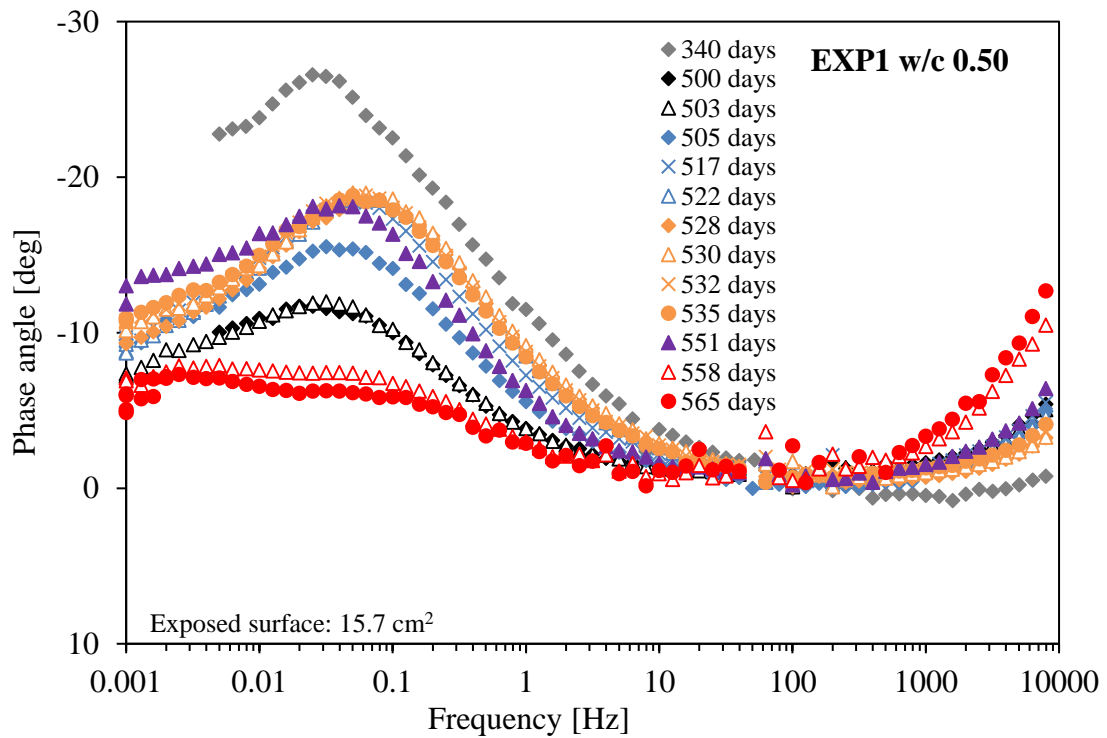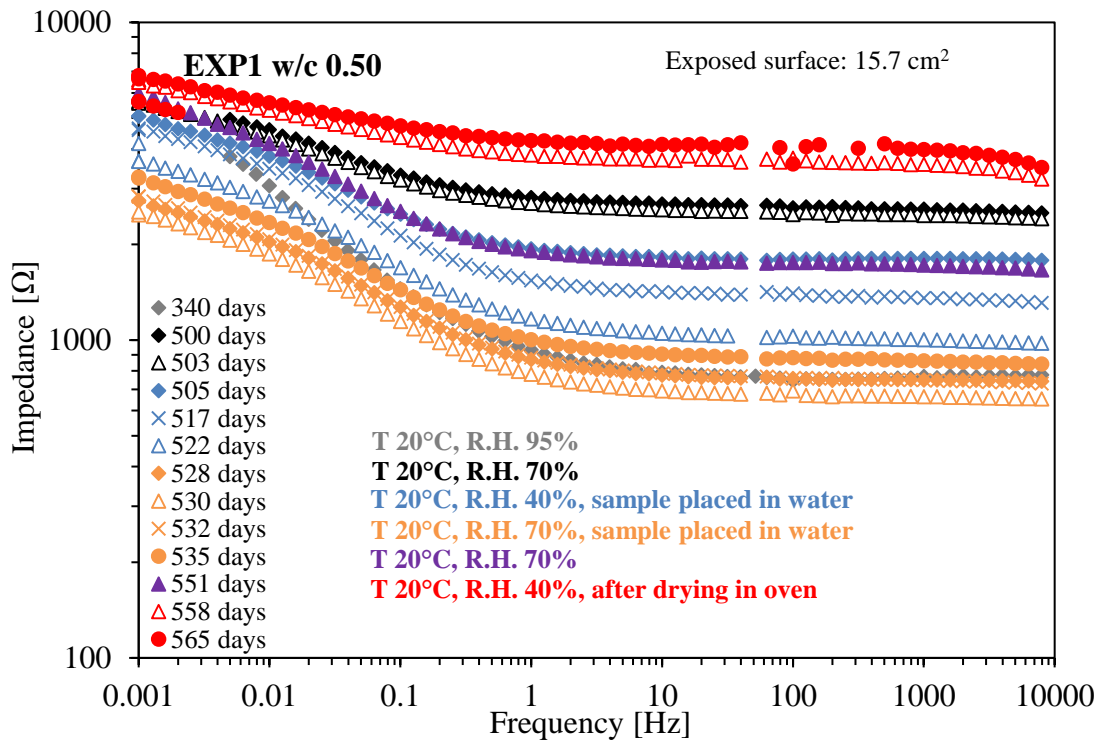*Figure 3.20: Bode spectra for modulus of Z (upper) and Phase angle (lower) of cubic sample "EXP1 w/c 0.50", exposed to wet and dry environmental conditions.*

3.1.1.5   Weight measurements at 20°C and R.H. of 95%

Figure 3.21 reports the weight evolution and the weight variations over time of concretes "EXP1 w/c 0.50" and "OPC w/c 0.55", exposed to wet environment characterized by R:H of 95% and temperature of 20°C after 28 days of curing inside their formwork. Concrete manufactured with Portland cement showed a stable weight and very little variations over time when exposed to an environment characterized by R.H. of 95%. Concrete manufactured with CSA-based concrete shows an increase of its weight over time around 70 grams after 6 months of exposure. Therefore it is possible to observe that concrete manufactured with CSA binder adsorbed more water, compared to OPC concrete.
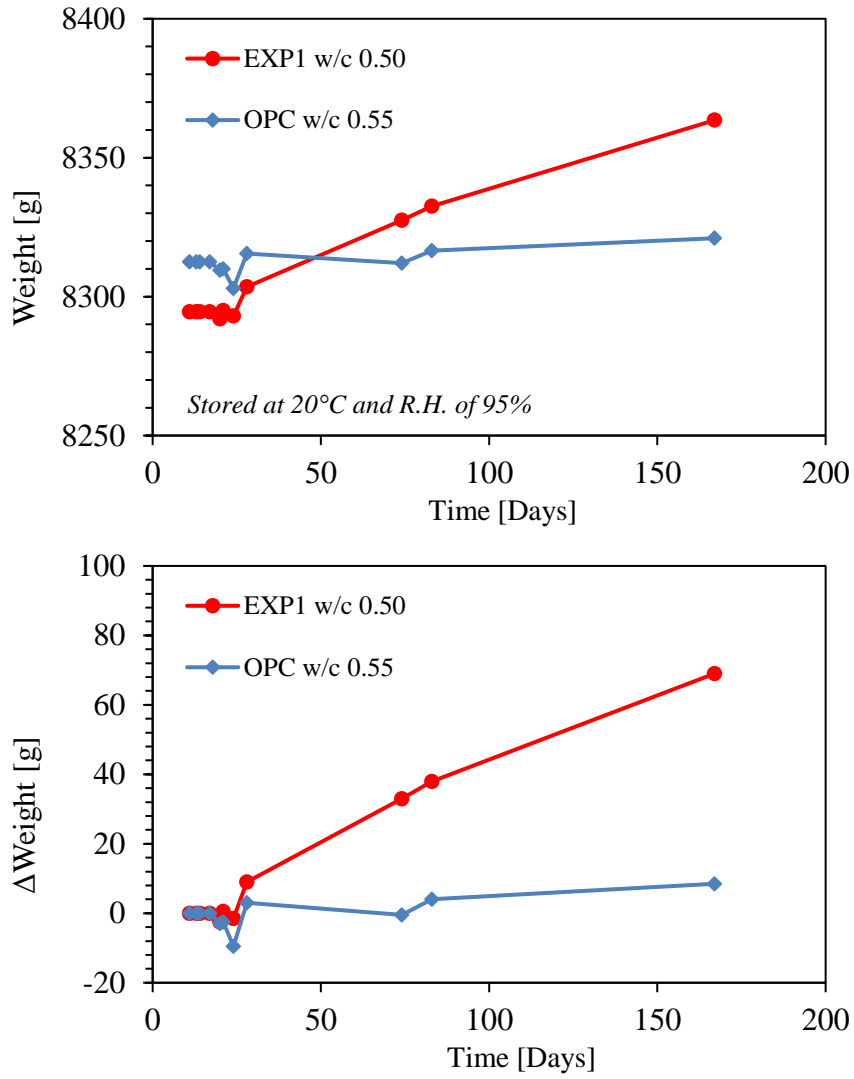
Figure 3.21: Weight evolution (upper) and variation (bottom) of demolded cubic samples stored at 20°C and R.H. of 95%.

3.1.2 Field tests in full-scale reinforced beams

3.1.2.1 Free Corrosion Potential (OCP) monitoring

Figure 3.22 reports the evolution of free corrosion potential of carbon steel reinforcement of full-scale beams. OPC concretes show an initial decrease of the corrosion potential. After few hours from manufacturing, free corrosion potential increases again reaching -100÷0 mV vs. SCE after 7÷9 days. Afterwards, it remains at the passive range established in the ASTM standard. Likewise, the evolution of OPC concretes in single electrode cubic specimens (Figure 3.2), the initial decrease of potential is related to the active behaviour of the steel, which is forming the passive film among its surface. Concretes "EXP2" and "EXP3" showed initial corrosion potential lower to those of OPCs, around -570 mV vs. SCE. Reinforcement of concrete "EXP3" showed potential values that, after 1 day, increased up to -200mV vs. SCE and stayed for 2 weeks within the uncertainty interval; after 10 months corrosion potential was close to that of concretes manufactured with Portland cement. Also concrete "EXP2" showed an increase of the corrosion potential, but in this case it occurred at longer ageing and stayed within the uncertainty interval until 3 months of exposure.

Concrete "EXP1 w/c 0.55" – having the highest amount of ye'elimite - developed very low corrosion potentials, just after casting, that increased up to -400 mV vs. SCE after 1 day and stayed stable for one month. Only after 4 months the potential reached the uncertainty interval and after almost 1 year of exposure its value was -300 mV vs. SCE.

For all beams, a good correlation between the corrosion potential measured using as reference the embedded RME probe and that measured using an external standard calomel electrode was found.

Corrosion potential values collected for reinforcement in full-scale beams generally were higher compared to those of cubic sample: the exposure conditions of cubic sample were stable and fixed while, for field tests, the environmental conditions of temperature and R.H. depended on climatic changes. However, a good reproducibility, for the same concrete, was found between laboratory tests and field tests.
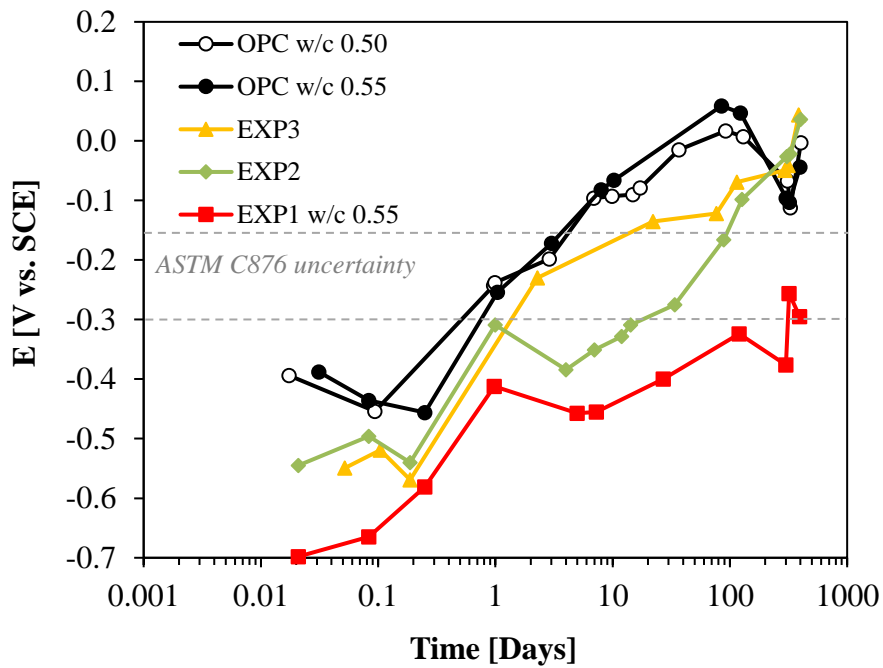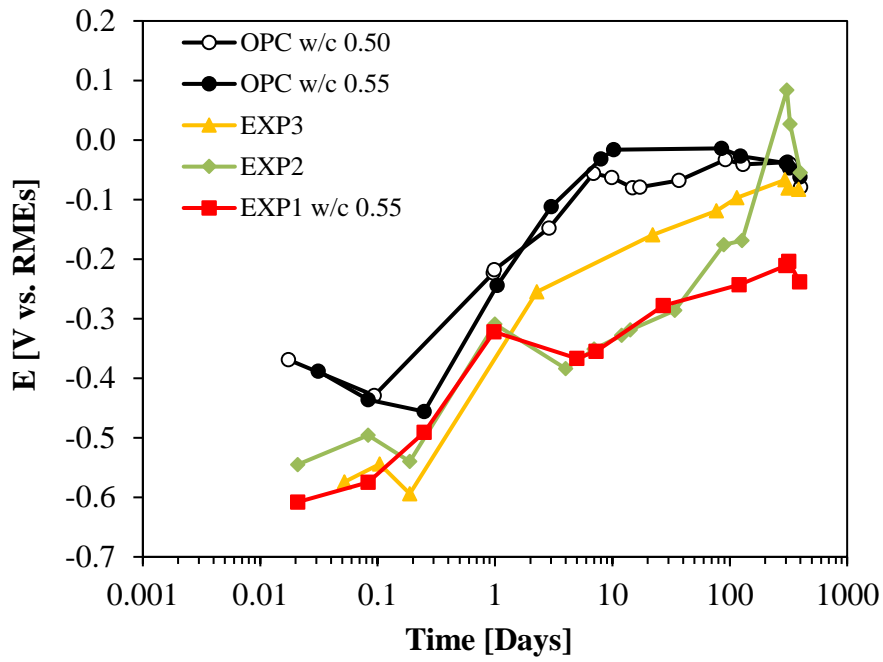
Figure 3.22: Potential evolution of carbon steel reinforcement vs. RME probe (upper) and vs. SCE (bottom) in full-scale beams.

3.1.3 Characterization of MEP, RME probes and Ti-MMO elements

3.1.3.1 Effect of pH

Figure 3.23 reports the potential evolution (mV vs. SCE) of a MEP probe, named as "Probe 2", and of IrOx-TaOx titanium electrodes (two wires with diameter of 3 and 1.5 mm, and a segment obtained from a net), in function of the pH. The MEP "Probe 2" is manufactured as reported in paragraph 2.1.3.

The curves of IrO_x-TaO_x electrodes showed good stability and reproducibility, the two wires overlap perfectly showing the same potential in function of pH. All the three elements reached a slope of about -44 mV/pH while, MEP "Probe 2", which is manufactured using 10 RuOx-IrOx segments, showed a mean value of the slope close to -40 mV/pH.
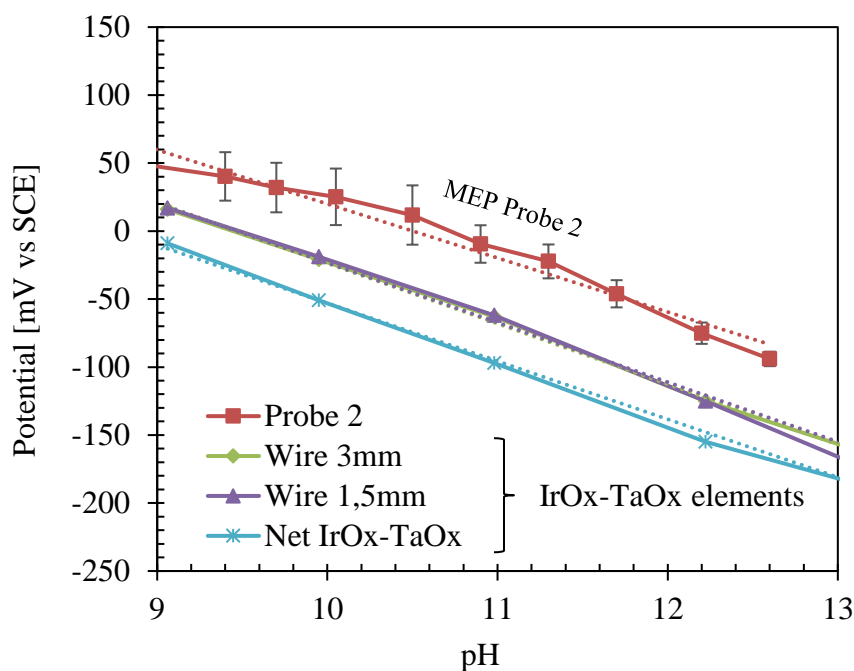
Figure 3.23: Potential evolution vs. pH of MEP probe and IrOx-TaOx elements.

Table 3.1 to Table 3.3 report the potential evolution in function of the solution's pH, the slope and the standard deviation of the tested electrodes.

Table 3.1: Potential evolution vs. pH of MEP probe.

MEP Probe 2							
pH	9.4	9.7	10.5	11.3	11.7	12.2	12.6
Average potential [mV vs. SCE]	40	32	12	-22	-46	-75	-94
STD	17.8	18.2	21.8	12.5	10	7.8	5.3
Slope	-39.7 mV/pH						

Table 3.2: Potential evolution vs. pH of IrOx-TaOx wires..

IrO_x-TaO_x Wires						
pH	9.1	10	11	12.2	13.1	14
Wire 3mm [mV vs. SCE]	16	-21	-63	-125	-159	-202
Wire 1.5mm [mV vs. SCE]	17	-19	-62	-125	-169	-189
Slope	-43.9 mV/pH					

Table 3.3: Potential evolution vs. pH of IrOx-TaOx net.

IrO_x-TaO_x Net						
pH	9.1	10	11	12.2	13.1	14
Potential [mV vs. SCE]	-9	-51	-97	-155	-184	-218
Slope	-42.7 mV/pH					

The general mechanism that describe the response of metal oxides in function of pH involves a potentiometric pH response caused by either an equilibrium between two solid phase of the oxide [72]. The potential evolution in function of the environment's pH can be described by Equation 3.1:

Equation 3.1: Potential evolution in function of the pH.

$$MO_x + 2\delta H^+ + 2\delta e^- \rightleftarrows MO_{x-\delta} + \delta H_2O$$
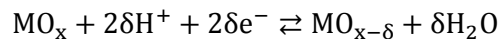
With $0 < \delta < x$ [72] [73].

The electrode potential is then given by Nernst Equation 3.2:

Equation 3.2: Nernst equation.

$$E = \frac{RT}{F} \ln a_{H^+}^l + \frac{RT}{F} \ln a_O^s + c$$

Where $a_{H^+}^l$ is the proton activity of the liquid phase and the a_O^s is the oxygen activity of the solid phase [72].

Thus, such kind of electrodes can be used both as useful embeddable reference electrodes in concrete and as pH sensors. In order to use the probes as sensitive Hydrogen ion-selective electrodes, the RedOx reaction must be reversible in aqueous solution, the electrodes must possess excellent corrosion resistance and stable potential response.

The materials, which can be used for this purpose, are oxides of Ir, Pt, Pd, Rh, Ti, Sn, Al, Os, Ta, Mo, W, Co and Ru.

Other studies used activated titanium with ruthenium oxide, as reported from J.K. Atkinson et al [72], but with slightly different results. Actually, the sensitivity of the MEP probe in natural environment is close to -39 mV/pH while Atkinson et al found a sensitivity of about -57 mV/pH. The difference can be determined by different fabrication conditions, which could lead to different oxidation states. In fact, the higher is the oxidation state, the greater is the slope [74].

3.1.3.2 Effect of Oxygen concentration and temperature on MEP potential

Figure 3.24 reports the mean value of the potential evolution measured for the 10 electrodes of the MEP Probe 2 in different environments, in order to determinate the sensitivity of the electrode to oxygen partial pressure variations and temperature, at different pH values. Potential monitoring was carried out in solution, at different pH values, bubbling air or nitrogen gas, at the temperature of 20°C or 40°C.

The potential of MEP probe showed slight differences between aerated and deaerated solution, at 20°C, and a clear increase of the slope, about 6 mV/pH.

However, increasing the temperature of the solution up to 40°C, the behavior of MEP probe, in aerated and deaerated solutions, is almost the same.
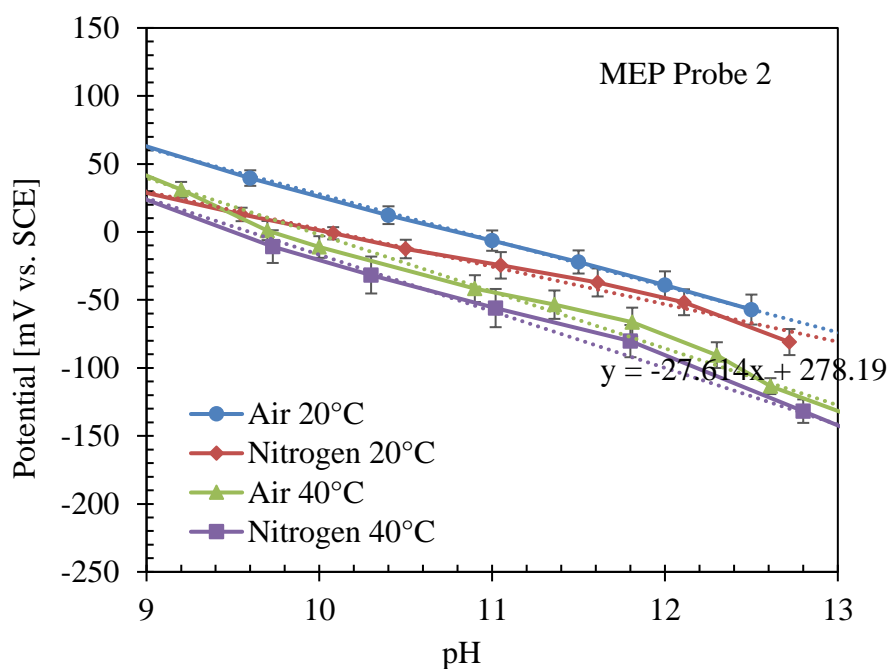
Figure 3.24: Potential evolution vs. pH of MEP probe at 20°c or 40°C, in presence of air or nitrogen bubbling.

Table 3.4 to Table 3.7 report the evolution of MEP potential in function of pH at different temperature and oxygen concentrations.

Table 3.4 Potential evolution vs. pH of MEP probe at 20°C with air bubbling.

MEP Probe 2, 20°C, Air bubbling							
pH	8.8	9.6	104	11	11.5	12	12.5
Temperature [°C]	21.5	21.6	21.7	21.8	21.9	22	22.1
Ox concentration [mg/L]	8.43	8.41	8.39	8.36	8.39	8.36	8.34
Average [mV vs. SCE]	71	40	12	-6	-22	-39	-57
STD	4.4	5.7	6.5	7.5	8.5	10	11
Slope	-33.9 mV/pH						

Table 3.5: Potential evolution vs. pH of MEP probe at 20°C with Nitrogen bubbling.

MEP Probe 2, 20°C, Nitrogen bubbling							
pH	8.9	9.6	10.5	11.1	11.6	12.1	12.7
Temperature [°C]	21.5	21.7	22.1	21.7	21.8	22.2	22.7
Ox concentration [mg/L]	0.1	0.1	0.1	0.1	0.1	0.1	0.1
Average [mV vs. SCE]	32	13	-1	-13	-25	-37	-81
STD	7.5	6.1	9	13.8	15.9	17	16.7
Slope	-27.6 mV/pH						

Table 3.6: Potential evolution vs. pH of MEP probe at 40°C with air bubbling.

MEP Probe 2, 40°C, Air bubbling							
pH	9.2	10.0	10.9	11.4	12.3	12.6	13.8
Temperature [°C]	40.4	40.5	40.2	40.2	39.8	39.3	44
Ox concentration [mg/L]	6.28	6.28	6.28	6.28	6.32	6.38	6.08
Average [mV vs. SCE]	31	-11	-42	-54	-91	-113	-170
STD	3.2	3.9	5.6	6.8	6.0	4.1	4.7
Slope	-41.8 mV/pH						

Table 3.7: Potential evolution vs. pH of MEP probe at 40°C with Nitrogen bubbling.

MEP Probe 2, 40°C, Nitrogen bubbling							
pH	8.9	9.7	10.3	11.0	11.8	12.8	13.7
Temperature [°C]	40.2	40.3	40.1	40.3	40.3	39.1	41.3
Ox concentration [mg/L]	0.1	0.1	0.1	0.1	0.1	0.1	0.1
Average [mV vs. SCE]	29	-11	-32	-56	-80	-132	-179
STD	10.6	12.0	13.6	14.0	11.8	8.6	6.0
Slope	-41.6 mV/pH						

3.1.3.3   Long term exposure tests

Two MEP probes were soaked in two different solutions for 1 week. Probe 1 was soaked in limewater (pH 12.6) while, Probe 2 in NaOH 0.0001 M (pH 11). Stable potential values

of about -58 mV vs. SCE and around 10 mV vs. SCE were noticed for limewater solution and NaOH 0.0001 M respectively (Figure 3.25 and Figure 3.26).
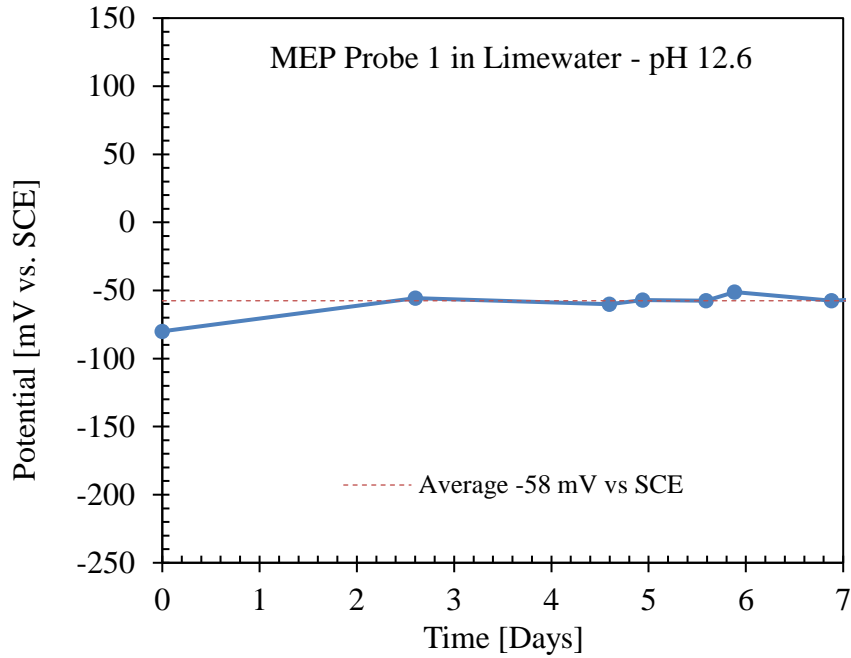
Figure 3.25: Potential evolution of MEP Probe 1 in Limewater.
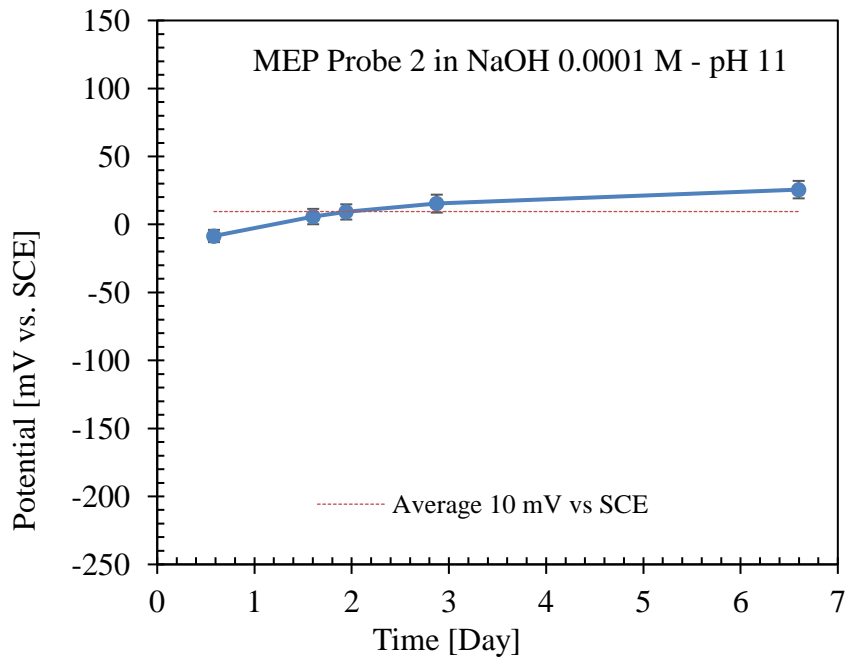
Figure 3.26: Potential evolution of MEP Probe 2 in NaOH 0.0001 M.

Four Reference Mortar Electrodes (RME) were tested at long term exposures in different solutions, monitoring their potential evolution (Figure 3.27). After manufacturing, the probes were immersed in a solution of deionized water and Portland cement for one week, in order to guarantee a proper curing of the mortar. After one week, they were immersed in deionized water for one month, then in saturated KCl solution for a short period of time and finally in alkaline solution at pH 13.2 (132 mL of NaOH 0.2M added to 50 mL of KCl 0.2M and 200 mL of deionized water).

RME probes showe stable potential values in each different environment and good reproducibility.
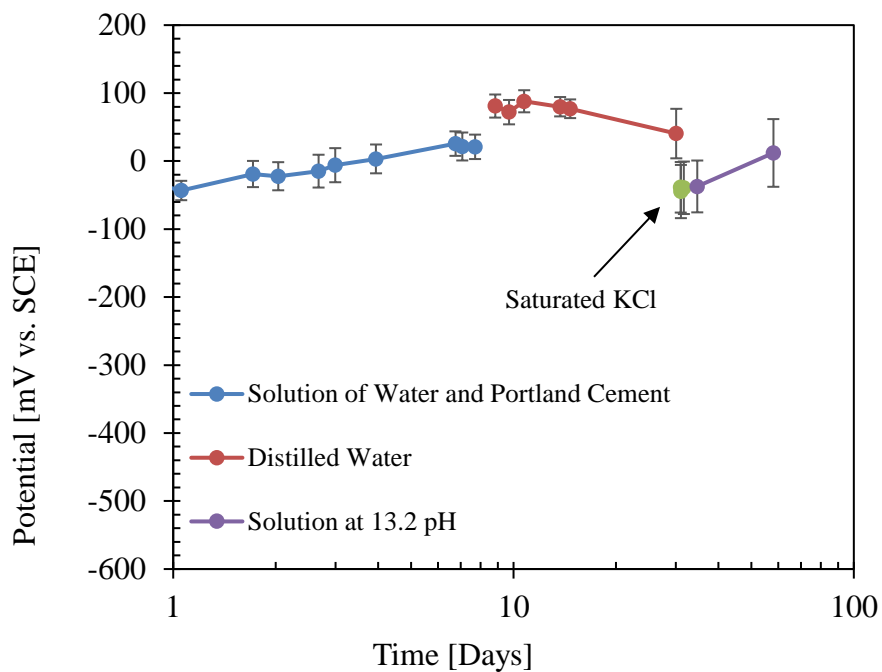
Figure 3.27: Average potential evolution of RME probes in different environments.

3.2 Evaluation of concrete alkalinity

This paragraph reports the visual analysis of concretes sprayed with an alternative indicator to the phenolphthalein, ███████████████████████████████████ ███████████████████████████████

Phenolphthalein indicator was used as reference for visual observation tests.

3.2.1 Visual analysis of concrete surface after spraying with pH sensitive indicators

Because Alizarin Yellow revealed colour variations from dark orange to light orange, which are not easy to distinguish, only modified Indigo Carmine was used to estimate the pH of concretes. Phenolphthalein indicator was also used for comparison purposes.

The results of visual analysis are shown from Figure 3.28 to Figure 3.33. OPC specimen promptly turned yellow after spraying modified Indigo Carmine indicator, confirming literature data, which fix the pore solution pH between 13.4-13.6. As expected, Phenolphthalein indicator turned pink (Figure 3.28).
CSA-based concretes show different results. EXP1 and EXP2 concretes - which are manufactured with the experimental binders characterized by the highest and medium ye'elimite content - turn on blue, thus confirming a lower pH compared to OCP, that can be estimated to be lower than 12; also in this case Phenolphthalein indicator turned pink (Figure 3.29 and Figure 3.30). EXP3 concrete, manufactured with the experimental binder characterized by the lowest amount of ye'elimite, revealed a yellow response in the core of the cubic sample, where pH value should be higher than 12.5, while, at the border, the color was light blue; on all the surface the color was pink after spraying Phenolphthalein (Figure 3.31). The concretes manufactured with ████████████████ ███ calcium hydroxide (4% vs. cement mass) revealed a light blue color tending to yellow, meaning that pH values should be around 11.5, but lower than 12, while, pink color with Phenolphthalein was observed (Figure 3.32 and Figure 3.33).

It is evident that the use of Phenolphthalein indicator cannot discriminate if the alkalinity level of the concrete is able to passivate or not carbon steel; in fact, for all concretes tested, its response was positive (the indicator turned to pink) meaning that the pH was greater than 9.
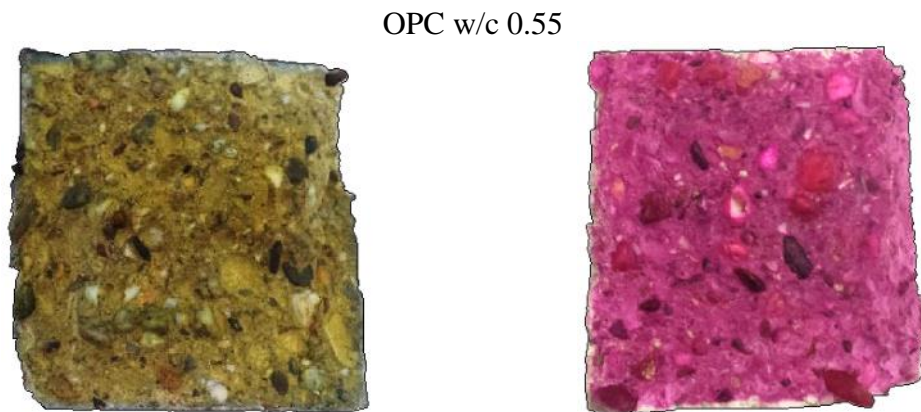
OPC w/c 0.55

Figure 3.28:Visual analysis of "OPC w/c 0.55" concrete surface after spraying with modified Indigo Carmine (left) and phenolphthalein (right) pH indicators, at 28 days of ageing.
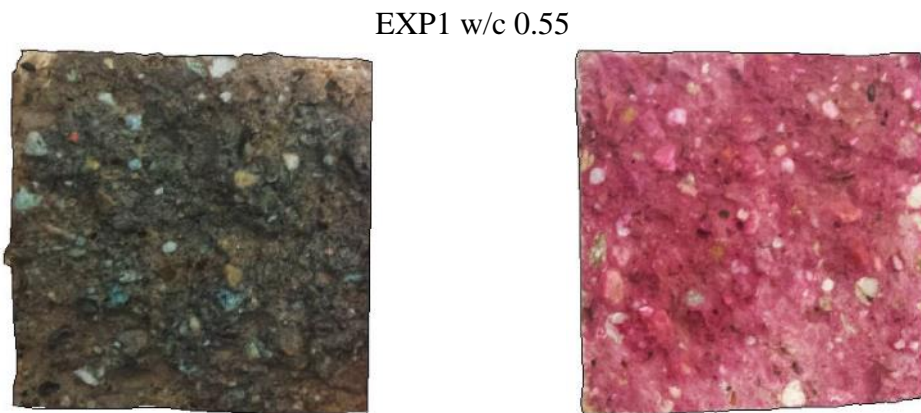
EXP1 w/c 0.55

Figure 3.29: Visual analysis of "EXP1 w/c 0.55" concrete surface after spraying with modified Indigo Carmine (left) and phenolphthalein (right) pH indicators, at 28 days of ageing.

EXP2

Figure 3.30: Visual analysis of "EXP2" concrete surface after spraying with modified Indigo Carmine (left) and phenolphthalein (right) pH indicators, at 28 days of ageing.

EXP3

Figure 3.31: Visual analysis of "EXP3" concrete surface after spraying with modified Indigo Carmine (left) and phenolphthalein (right) pH indicators, at 28 days of ageing.

Figure 3.32:

EXP1+2*Ca(OH)$_2$
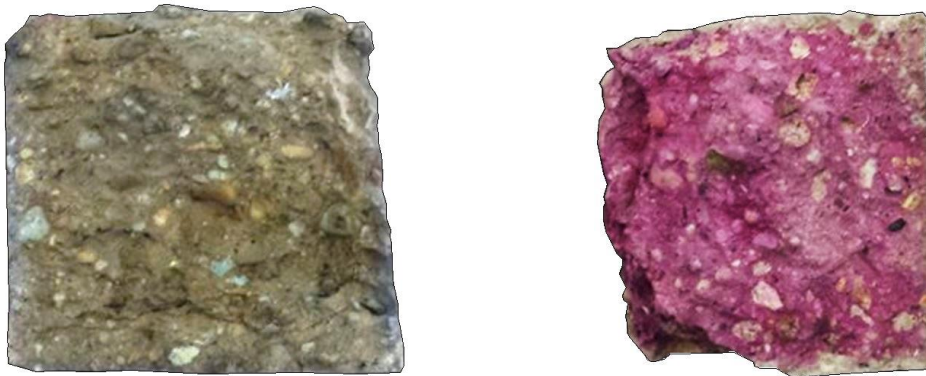
Figure 3.33: Visual analysis of "EXP1+2*Ca(OH)$_2$" concrete surface after spraying with modified Indigo Carmine (left) and phenolphthalein (right)pH indicators, at 28 days of ageing.

██

Figure 3.34 reports the pH values, evaluated within 6 days of curing ████████████ ██ The graph reports the mean value of the pH measured for at least two cement pastes with identical composition, within 6 days after the mixing; the error bars report the differences between the mean value and the maximum and minimum values measured within 6 days of curing.

██

██

The cement paste manufacture with Portland cement confirms the data reported in the literature, showing a pH value, after the first days of curing, very close to 13.3, confirming also the color transition observed on the corresponding concrete sprayed with modified Indigo Carmine indicator (Figure 3.28). "EXP3" cement paste shows high pH values of about 13.3 while, "EXP2" a value close to 12.5. Cement paste manufactured with cement EXP1 (characterized by the highest amount of ye'elimite in the binder) develops the lowest pH value, around 11.7.

According to Figure 1.3, the pH achieved correspond to a value very close to that necessary to form the passive film, in absence of chlorides, on the reinforcement surface. It is clear that also little variations of pH, for example in occurrence of carbonation, could bring the alkalinity level of the concrete to conditions that are not sufficient to guarantee the stability of the passive film.
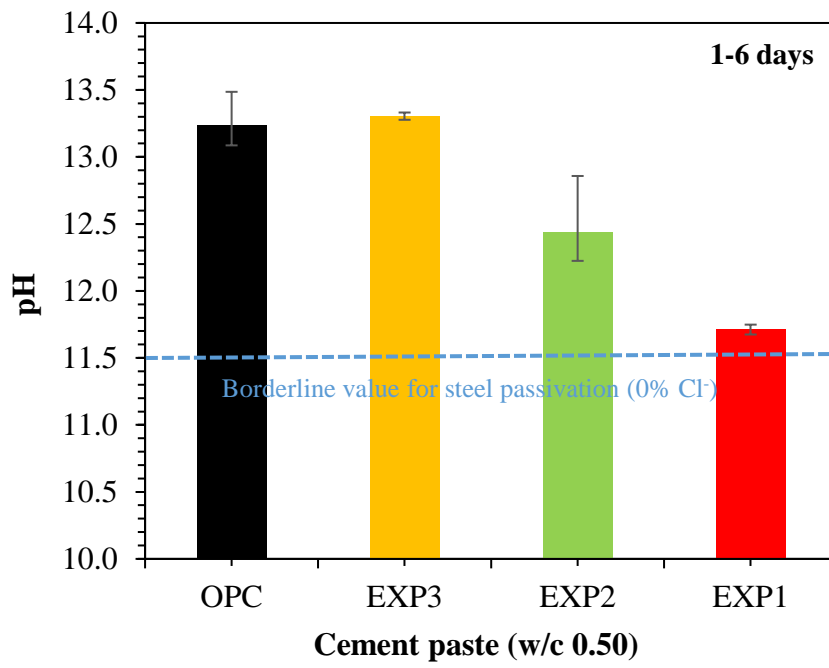
Figure 3.34: pH of cement paste (w/c 0.50) ████████████████████████

3.3 Tests in simulating solutions

CSA materials are sulfate rich environments, which are potentially dangerous, since sulfates ions can act similarly to chloride ions in the depassivation of steel. Additionally low pH values of fresh mixtures and lower alkalinity can adversely contribute to the reinforcing rebar corrosion.

This paragraph reports the experimental results of free corrosion potential monitoring and EIS spectra ofcarbon steel in simulating solutions. In order to support the electrochemical results, visual observation with microscope of the corroding surfaces are reported as well.

Before the beginning of each test, the pH of the solution was verified and corrected, if necessary, by addition of drops of NaOH 1M. At the end of each test, the pH of the solution was verified and a decrease of around 0.2÷0.3 points of pH was found for all solutions.

3.3.1.1 Free Corrosion Potential (OCP) monitoring

Figure 3.35 reports the evolution of free corrosion potential of carbon steel in solutions at pH 10.5, with increasing concentration of sulfates from 0mM (blank solution) up to 200mM solutions. In blank solution, the corrosion potential initially increases up to -300 mV vs. SCE but after few hours of immersion it drops to low potential around -600÷-700 mV vs. SCE. In presence of sulfates, independently on the amount, at pH 10.5 carbon steel shows low corrosion potential since after immersion in solution, and no passivation was observed at all.
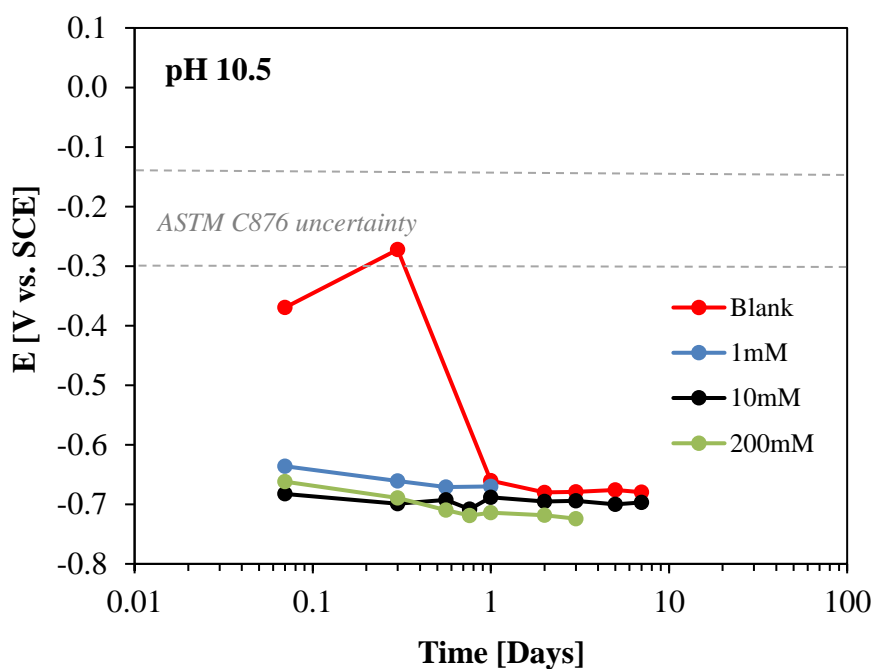
Figure 3.35: Potential evolution of carbon steel working electrode (WE) vs. standard calomel electrode (SCE) in solutions at pH 10.5.

At pH 11.5 (Figure 3.36), corrosion potential rapidly increases in blank solution up to noble potential, meaning that passive film is forming on the steel surface, but after 3 days corrosion occurs (confirmed also by visual tests) and potential values drop to -600÷-700 mV vs. SCE. With sulfates concentration of 1mM, potential initially increases up to -300 mV vs. SCE but drops after one day of immersion while, for concentrations of 10mM and 200mM no passivation was observed, and potential of about -670 mv vs. SCE were monitored since the first moments after the immersion of the sample.
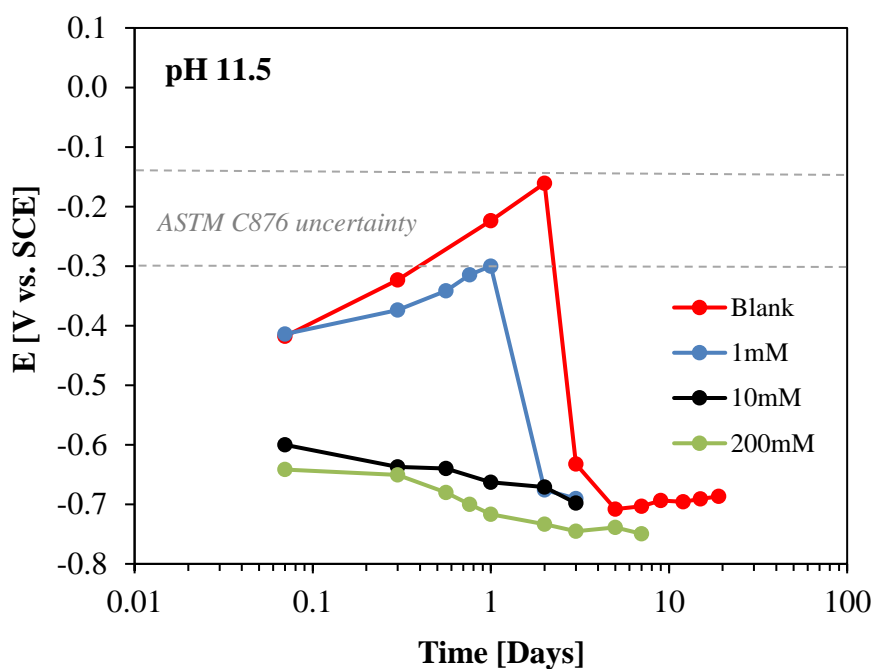
Figure 3.36: Potential evolution of carbon steel working electrode (WE) vs. standard calomel electrode (SCE) in solutions at pH 11.5.

Carbon steel samples in blank solution and 1mM SO_4^{2-} solution at pH 12.5 (Figure 3.37) show a rapid increase of the corrosion potential up -100 mV after 3 days of immersion, which increases to 0mV at 12 days and remain at noble values for all the duration of the tests. At sulfates concentration of 10mM, potential reaches noble values and stays around -200÷-300 mV vs. SCE for 12 days, before decreasing to very low values due to localized corrosion initiation. At the maximum concentration of sulfates of 200mM, passivation s observed only at until 5 days of immersion, and then free corrosion potential reaches low values of -700mV vs. SCE.
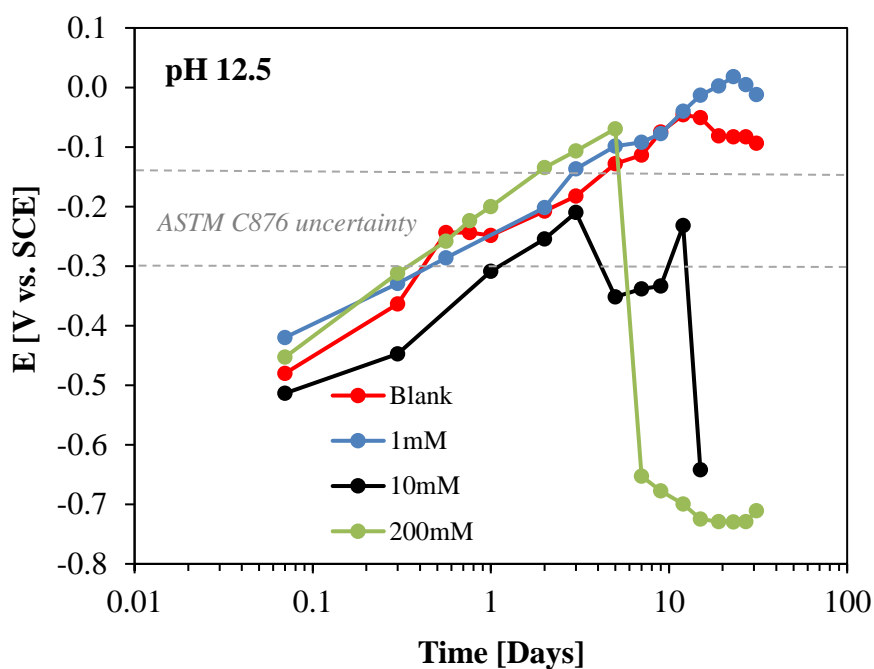
Figure 3.37: Potential evolution of carbon steel working electrode (WE) vs. standard calomel electrode (SCE) in solutions at pH 12.5.

3.3.1.2 Electrochemical Impedance Spectroscopy (EIS) spectra

The impedance values at high frequencies, according to Randles equivalent circuit (Figure 1.8), represent the ohmic drop of the solution between the reference electrode and the sample (working electrode). For all the different conditions it was possible to observe that, increasing the concentration of salts dissolved in the solution, the ohmic drop decreases from 1500 Ωcm^2 to 6÷7 Ωcm^2 at the maximum concentration of sulfates.

Figure 3.38 to Figure 3.41 report the Bode plots (Impedance and Phase angle) of the EIS spectra obtained for samples immersed in solutions with pH 10.5 and sulfates concentration increasing from 0mM (blank solution) up to 200mM. Only for the blank solution, carbon steel sample shows, during the first hours of immersion, an increase of the impedance values to 1000000 Ωcm^2 and phase angle displacement close to -80°. After 5 hours of immersion in blank solution and for all the three concentrations of SO_4^{2-}, corrosion occurs. EIS spectra show a behavior typical of an active material, with low R_p values (that for active material, according to Randles circuit, can be calculated as

119

the Impedance at low frequencies minus the ohmic drop of the solution) and phase angle displacement tending to 0° at low frequencies.
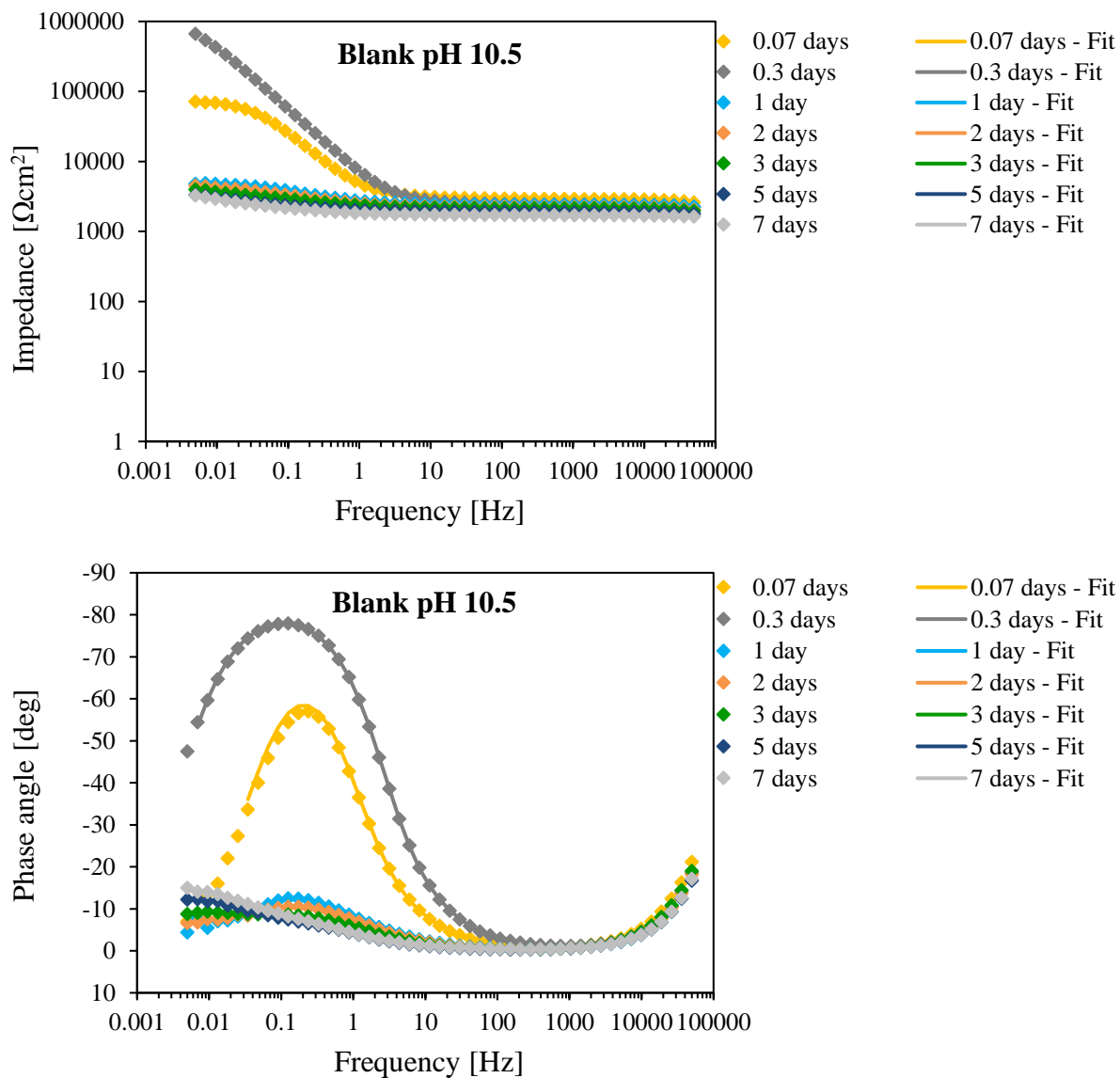
Figure 3.38: Bode spectra for modulus of Z (upper) and Phase angle (lower) – blank solution at pH 10.5.
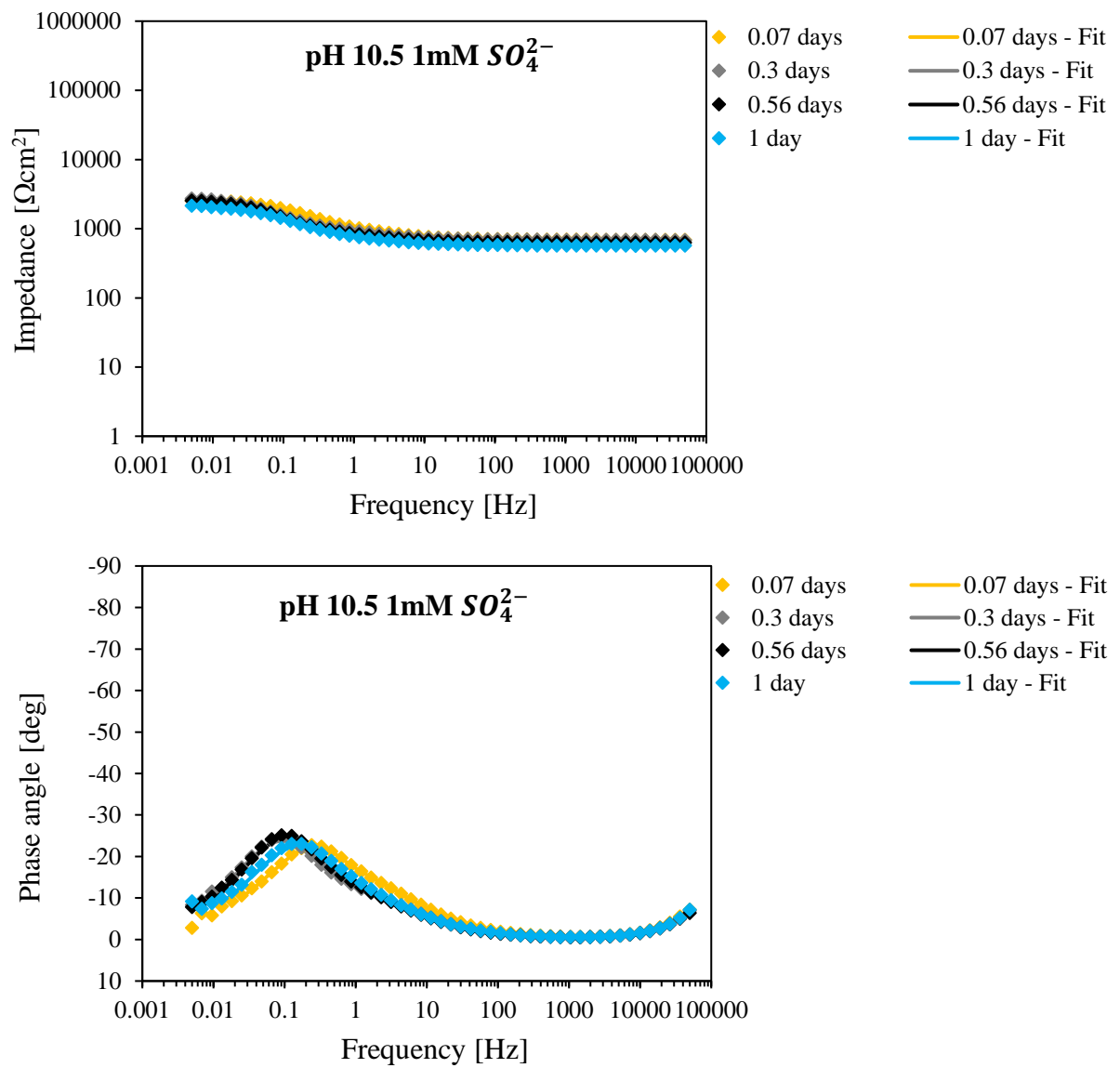
Figure 3.39: Bode spectra for modulus of Z (upper) and Phase angle (lower) – 1mM SO_4^{2-} solution at pH 10.5.
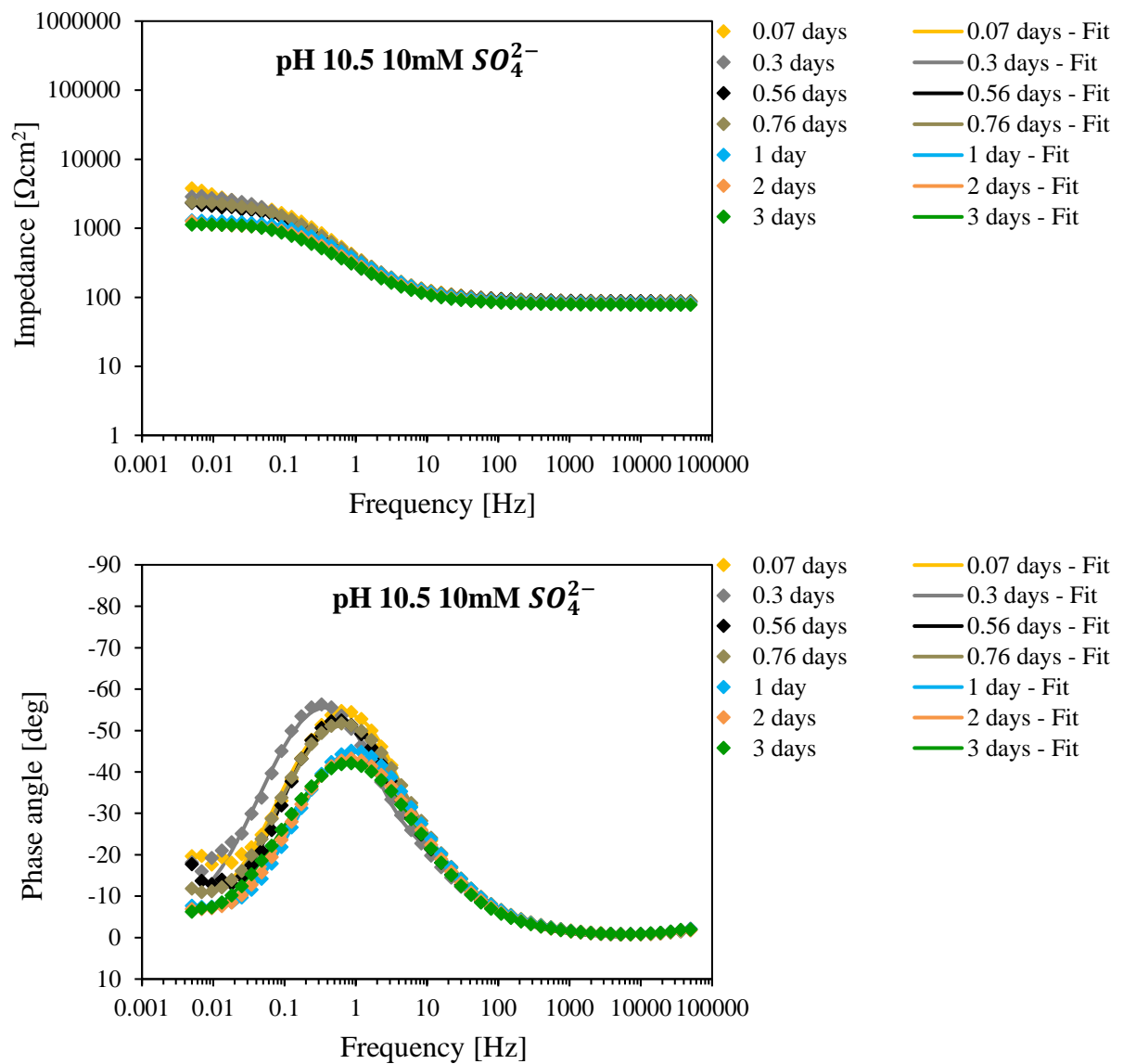
Figure 3.40: Bode spectra for modulus of Z (upper) and Phase angle (lower) – 10mM SO_4^{2-} solution at pH 10.5.
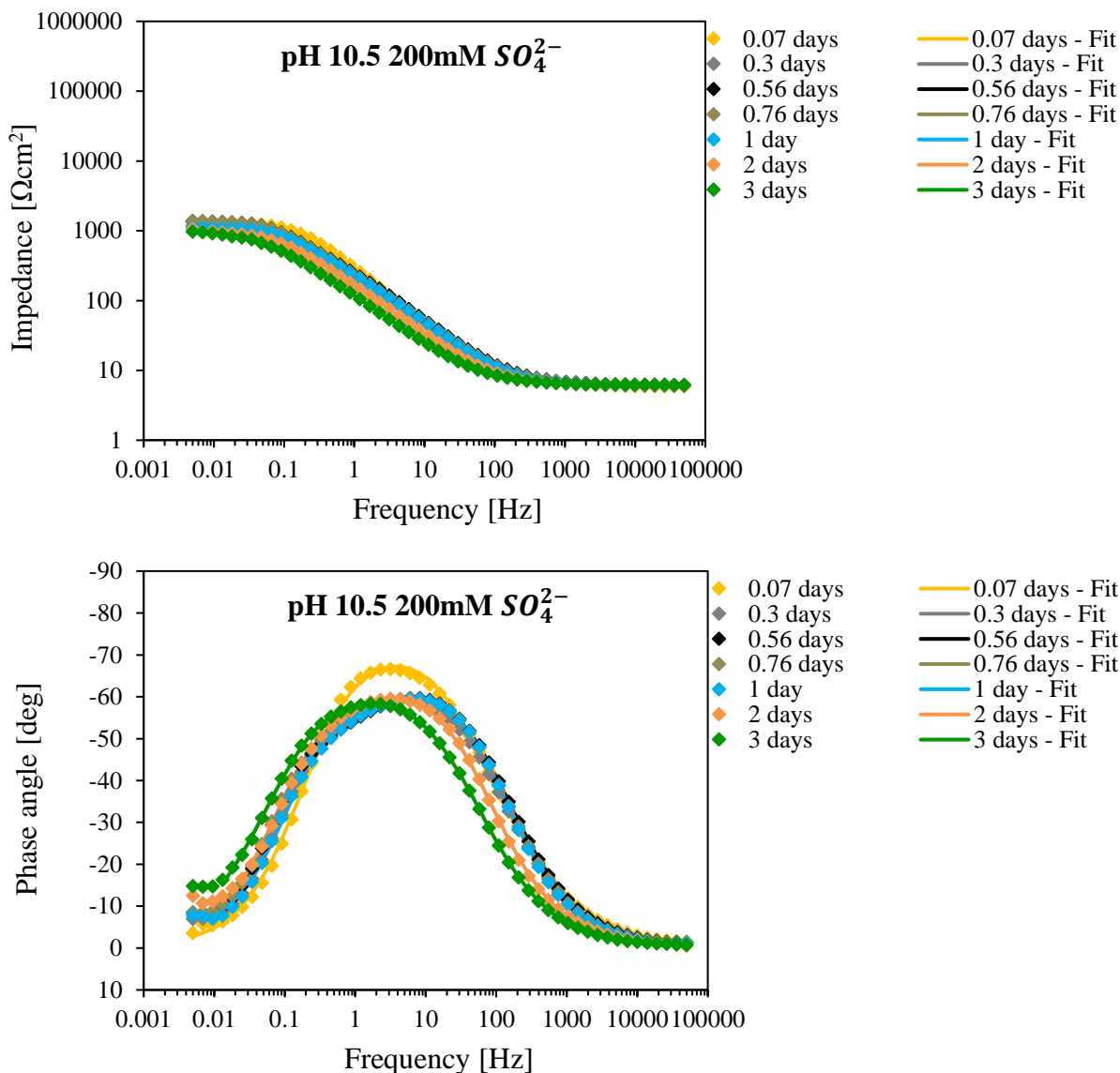
Figure 3.41: Bode spectra for modulus of Z (upper) and Phase angle (lower) – 200mM SO_4^{2-} solution at pH 10.5.

EIS spectra obtained in solutions at pH 11.5 are reported from Figure 3.42 to Figure 3.45. These solutions are characterized by the pH value that, in absence of chloride or other aggressive species, promote the formation of the protective oxide film (Figure 1.3). In blank solution, an increase of the impedance up to 1000000 Ωcm^2 and of the phase angle is visible at 2 days. After this period, corrosion occurs and impedance decreases to low values (1000 Ωcm^2) such as the phase angle. It is important to underline that the pH of the solutions decreased over time down to values around 11.2÷11.3; such conditions are

critical for passive steel formation, especially in presence of an aggressive specie. With sulfates concentration of 1mM, passivation was observed only until the first day of immersion while, for concentrations of 10mM and 200mM, Bode spectra showed trends typical of active materials.
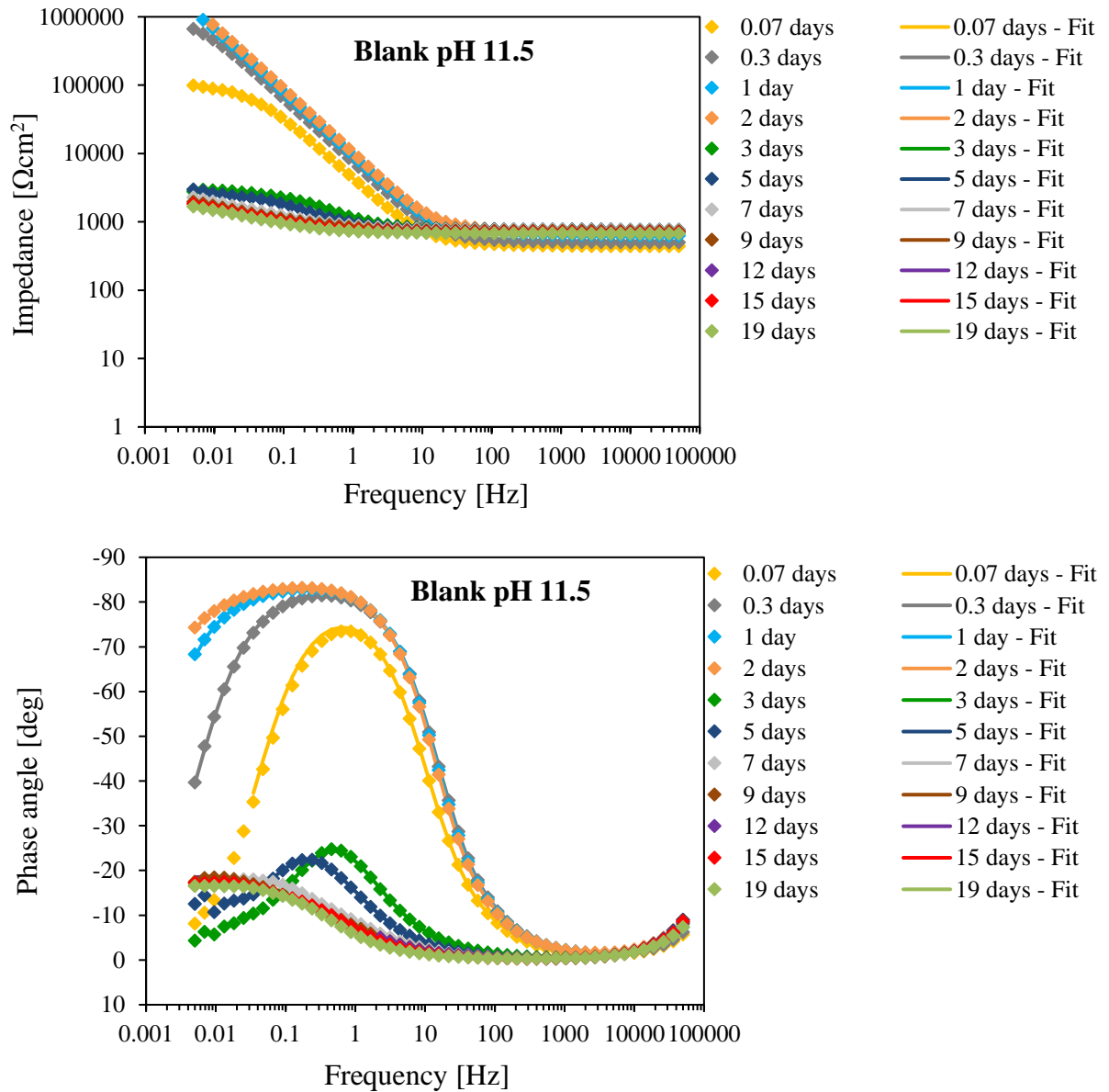
Figure 3.42: Bode spectra for modulus of Z (upper) and Phase angle (lower) – blank solution at pH 11.5.
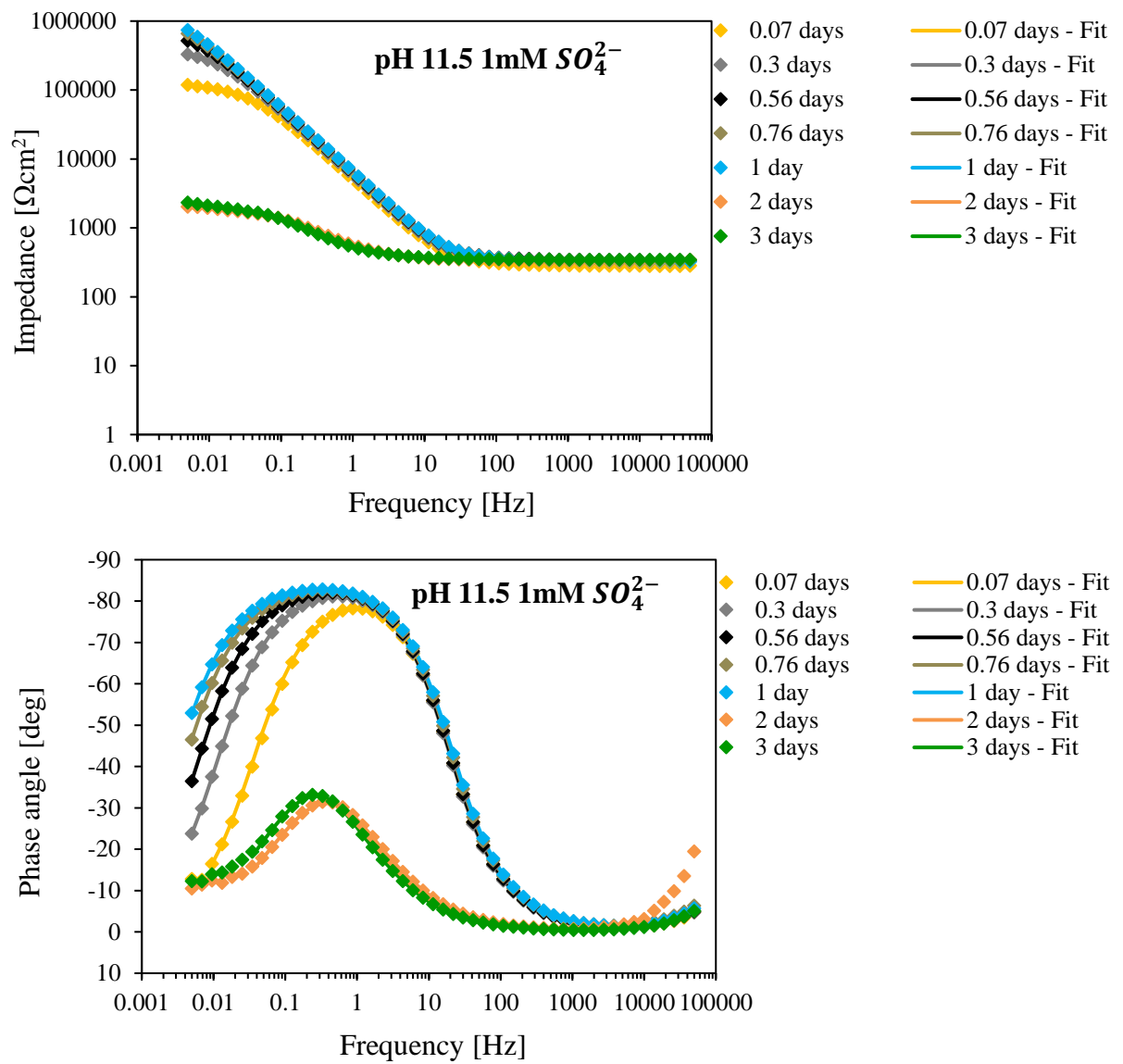
Figure 3.43: Bode spectra for modulus of Z (upper) and Phase angle (lower) – 1mM SO_4^{2-} solution at pH 11.5.
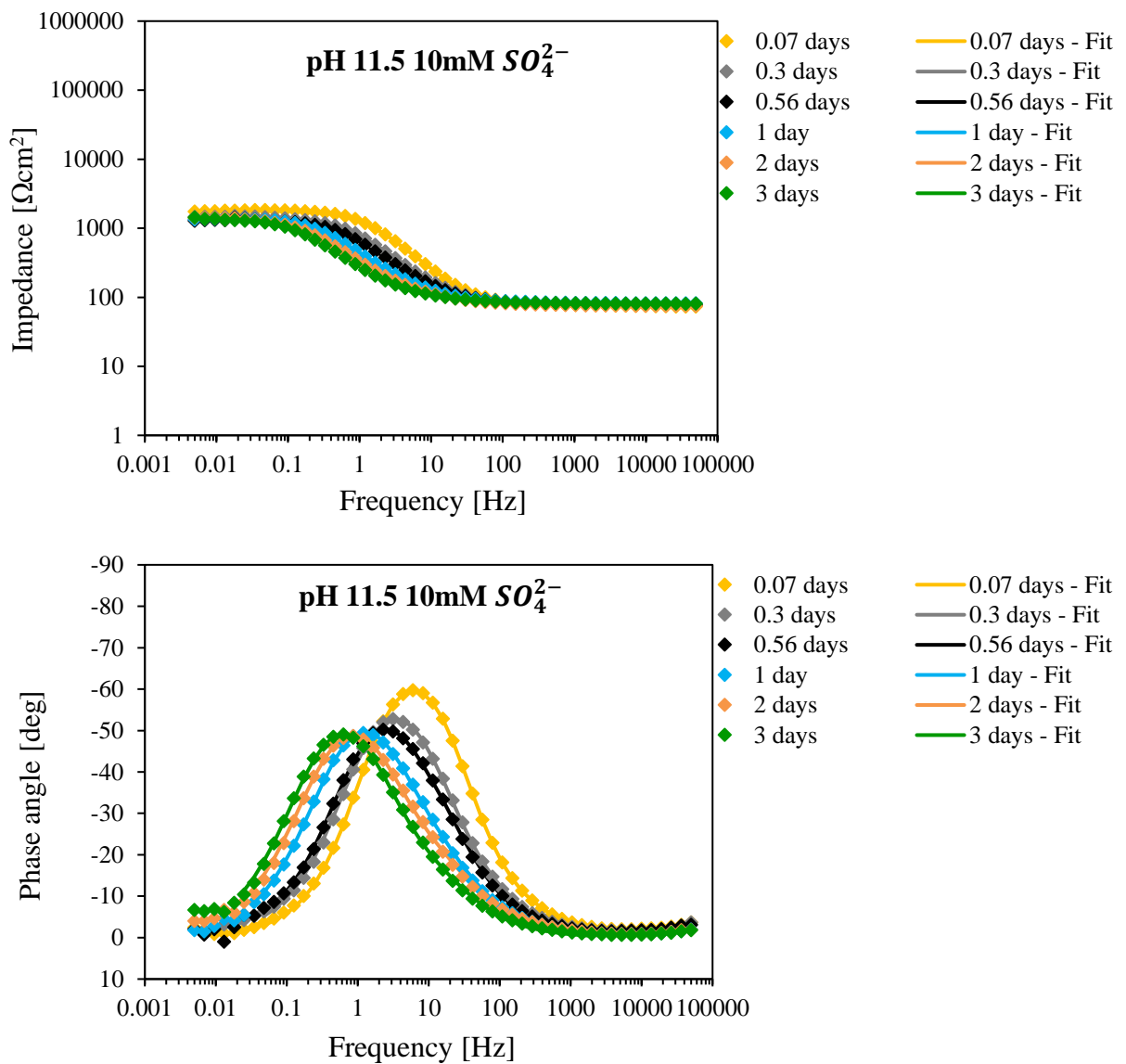
Figure 3.44: Bode spectra for modulus of Z (upper) and Phase angle (lower) – 10mM SO_4^{2-} solution at pH 11.5.
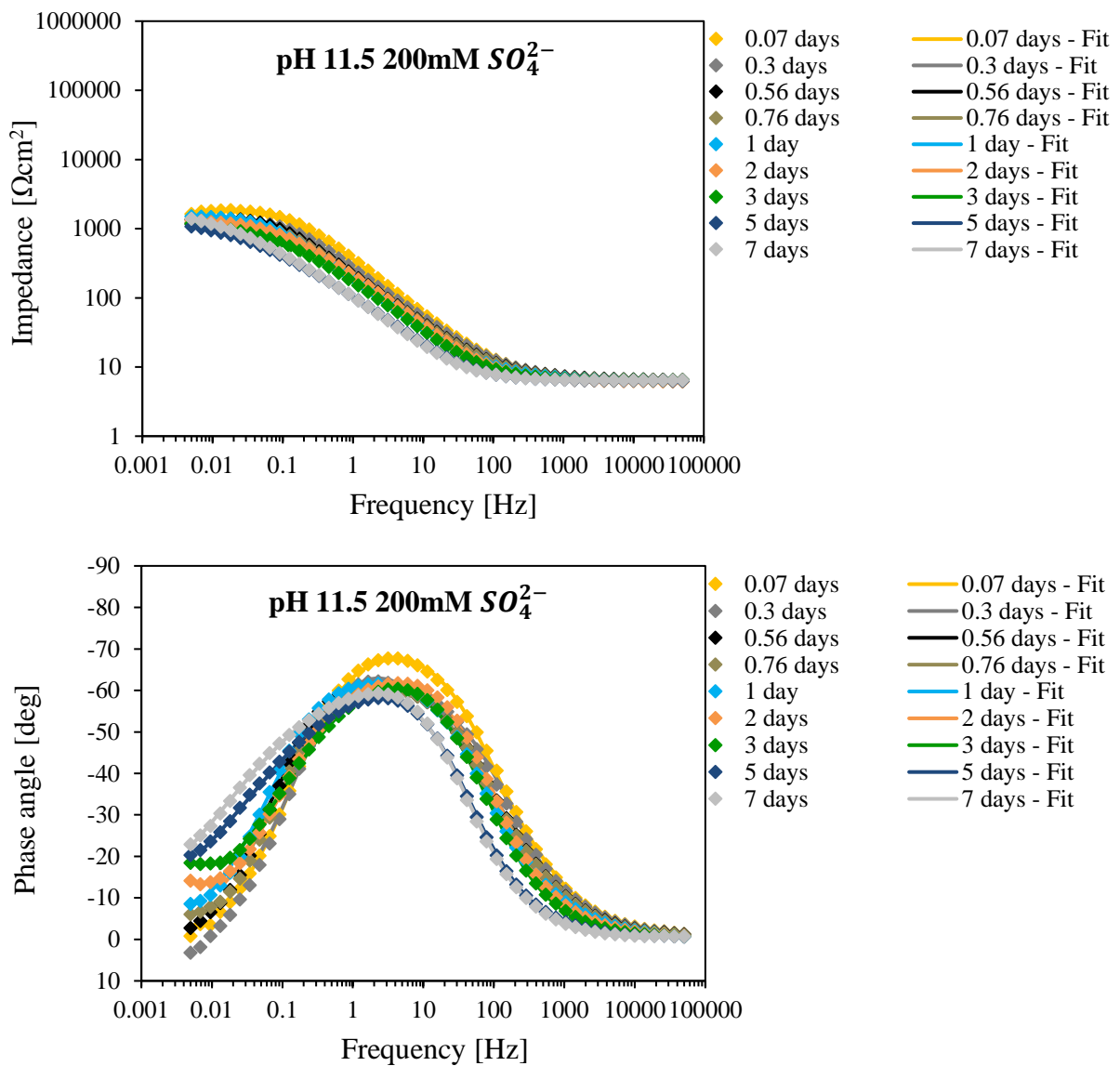
Figure 3.45: Bode spectra for modulus of Z (upper) and Phase angle (lower) – 200mM SO_4^{2-} solution at pH 11.5.

Figure 3.46 to Figure 3.49 report the EIS spectra of carbon steel in solutions at pH 12.5. For sulfates concentration of 0mM (blank solution) and 1mM, steel samples show a behavior typical of passive metal, and no corrosion phenomena were observed: the impedance values rapidly increases up to 1000000 Ωcm^2 together with the phase angle. As reported in literature, pH 12.5 is more than enough in order to form a stable passive film on the steel surface therefore, little decrease of the pH during the tests did not promote the breakdown of the oxide film even in presence of little amount of sulfates.

Increasing the SO_4^{2-} concentration to 10mM and 200mM, the impedance drops to values around 1000 Ωcm^2 and the phase angle reaches 0° at low frequencies, after 12 and 5 days of immersion, respectively, meaning that the breakdown of the passive film occurred.
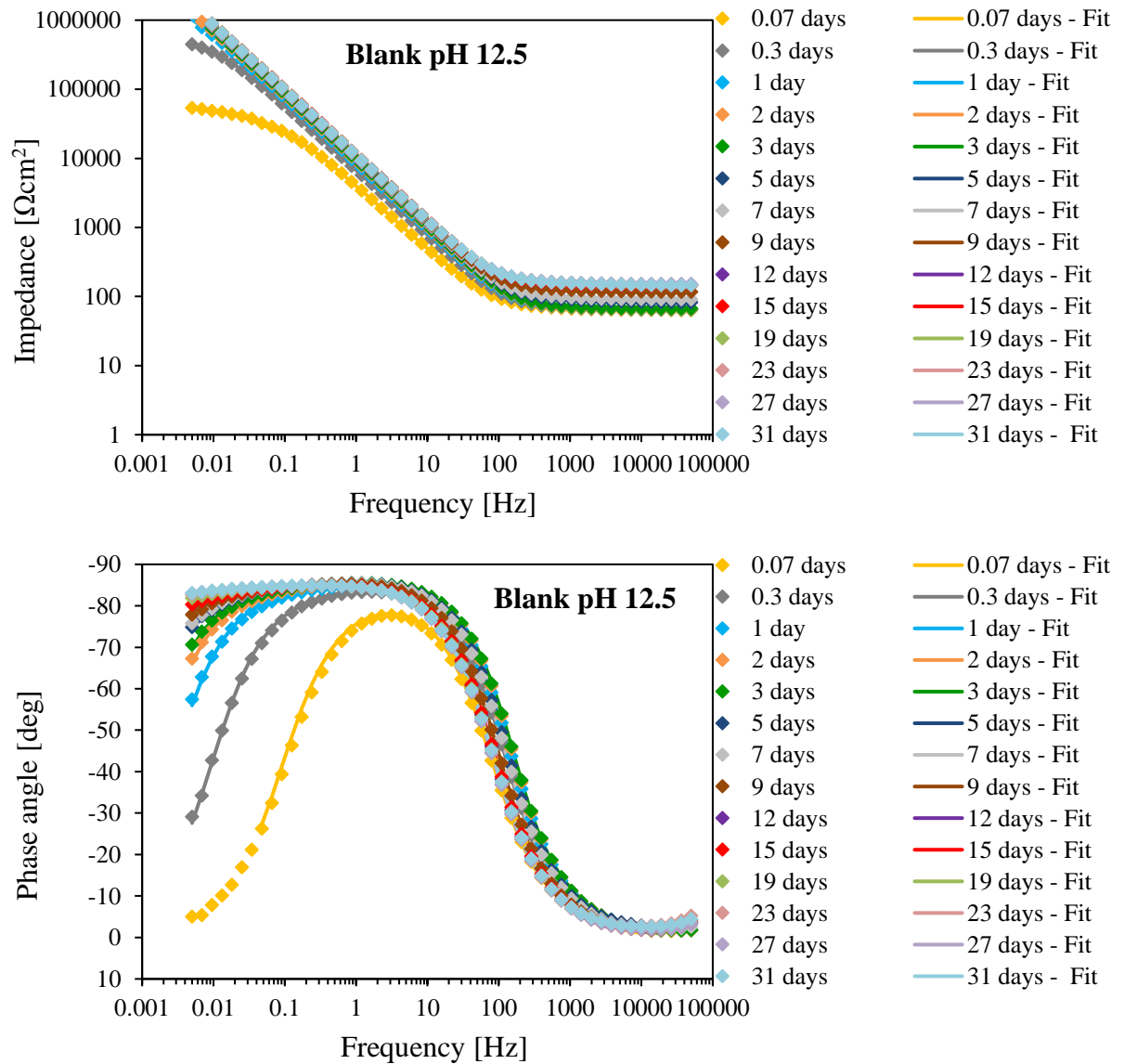
Figure 3.46: Bode spectra for modulus of Z (upper) and Phase angle (lower) – blank solution at pH 12.5.
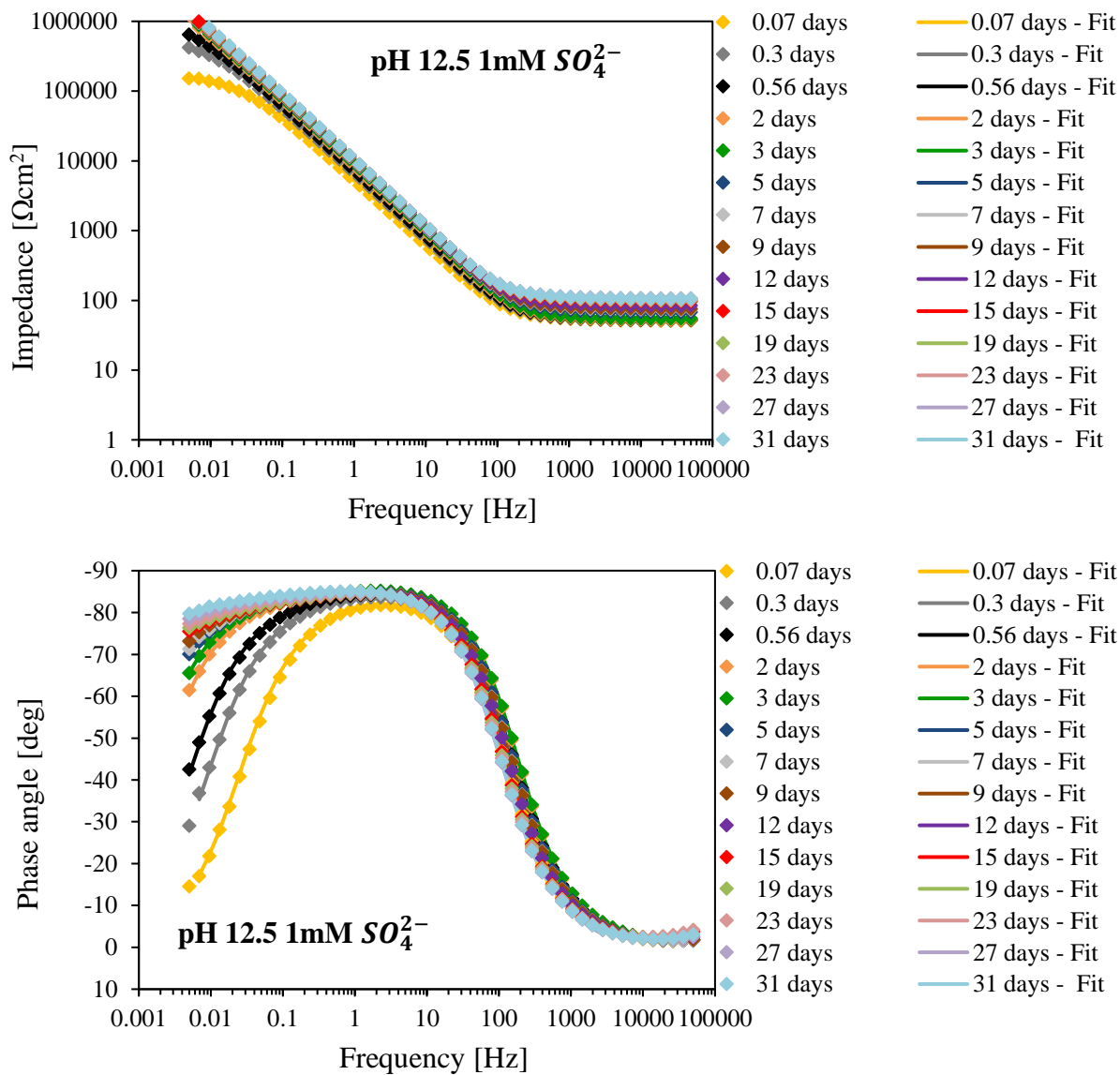
Figure 3.47: Bode spectra for modulus of Z (upper) and Phase angle (lower) – 1mM SO_4^{2-} solution at pH 12.5.
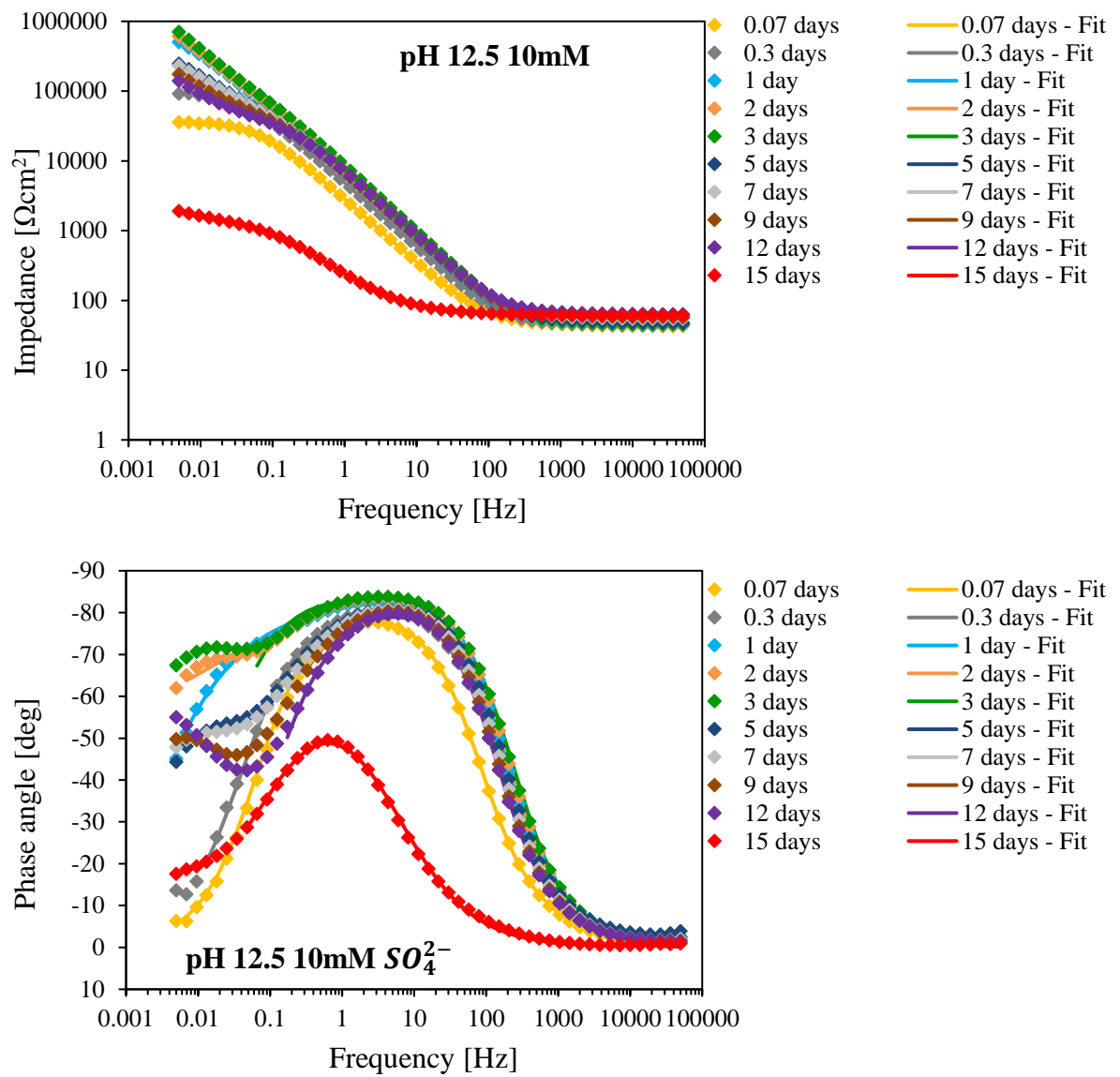
Figure 3.48: Bode spectra for modulus of Z (upper) and Phase angle (lower) – 10mM SO_4^{2-} solution at pH 12.5.
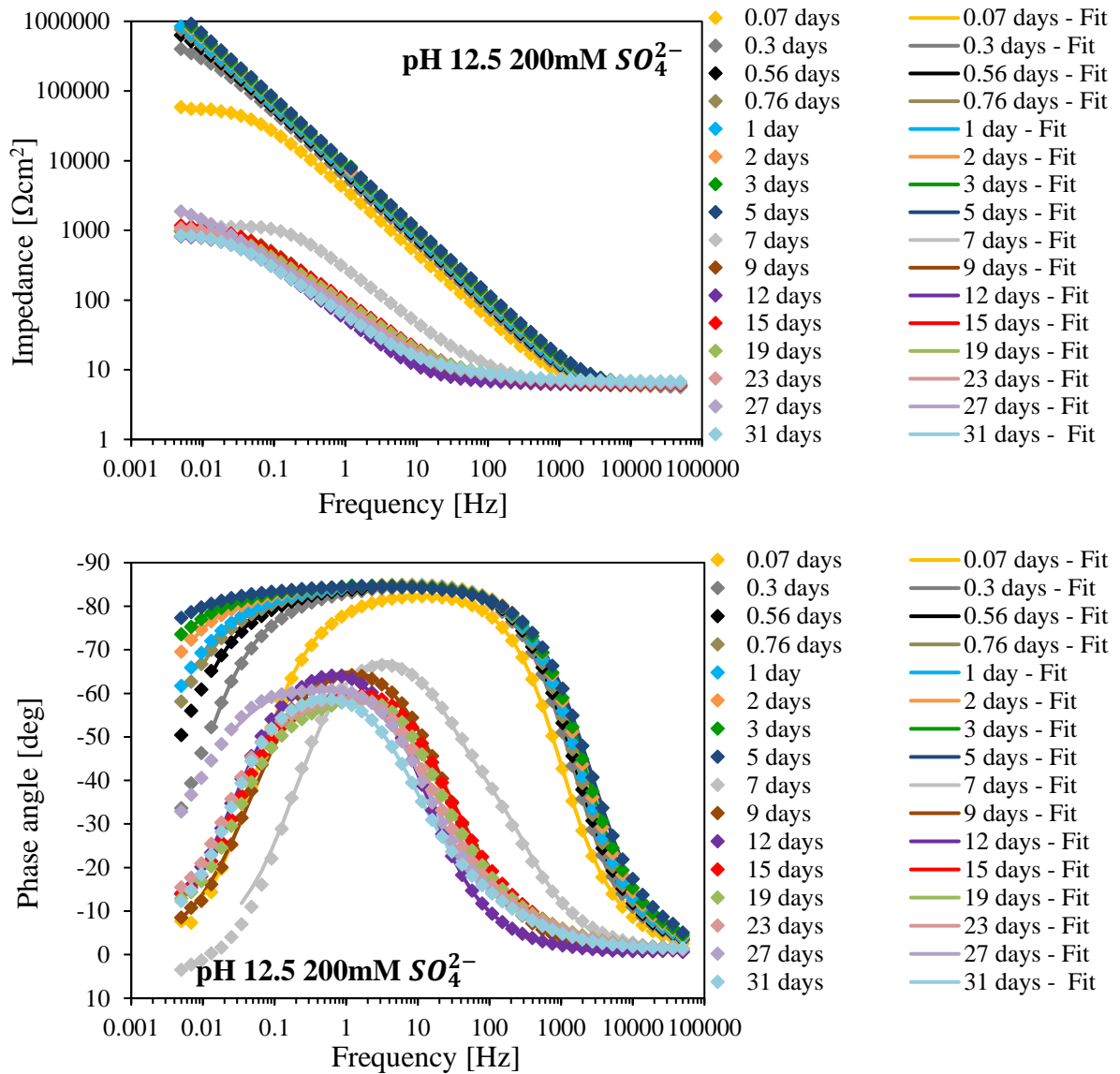
Figure 3.49: Bode spectra for modulus of Z (upper) and Phase angle (lower) – 200mM SO_4^{2-} solution at pH 11.5.

3.3.1.3 Visual observation

Figure 3.50 to Figure 3.61 report the images of the samples' surfaces immersed inside the simulating solutions, collected with Leica DMS 300 microscope. Visual observation tests confirm and support very well the electrochemical tests and the free corrosion potential evolution. At pH 10.5, in absence of sulfates, carbon steel sample shows the presence of corrosion products after 5 hours of immersion, which rapidly cover the surface with

yellowish-orange incoherent products. In presence of sulfates, the samples shows corrosion products since the first minutes after immersion: right after exposure they looked like light-yellowish spots and with increasing time, they covered the entire surface with incoherent orange products.
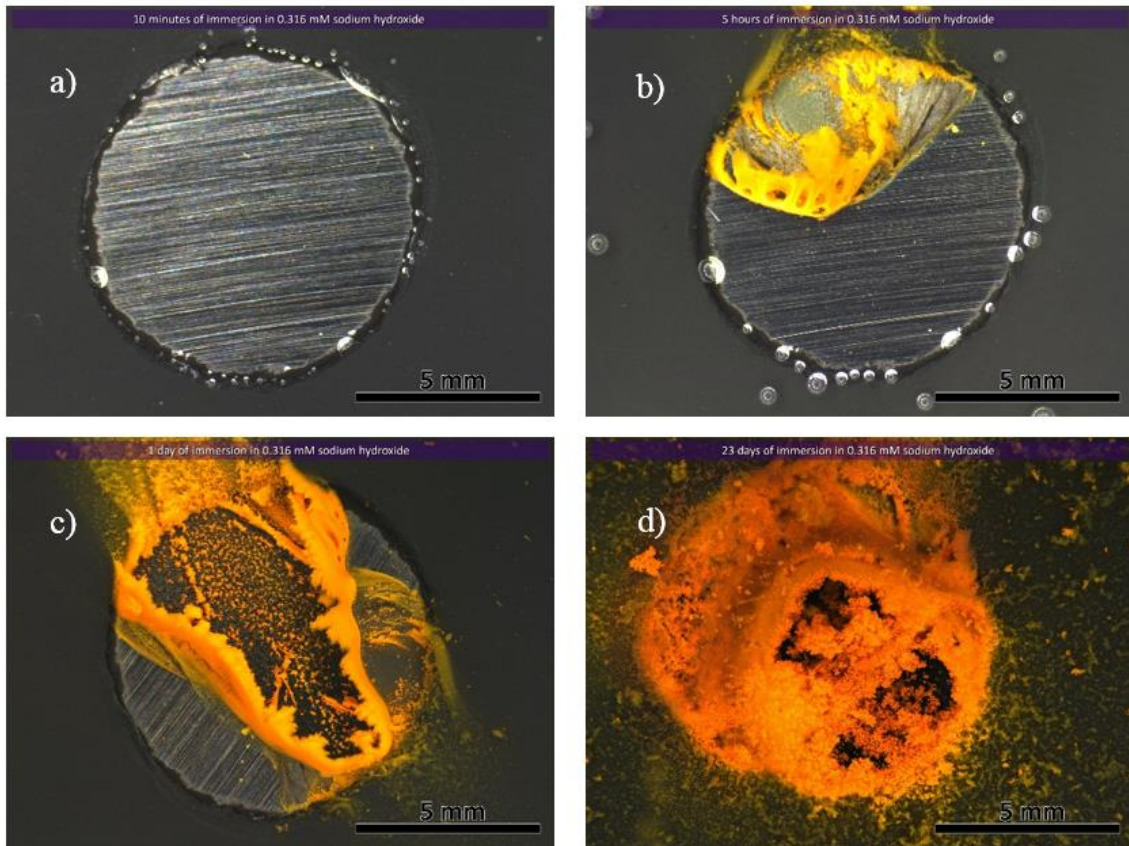
Figure 3.50: Carbon steel surface of sample immersed in blank solution at pH 10.5 after 10 minutes a), 5 hours b), 1 day c) and 23 days d) of immersion.
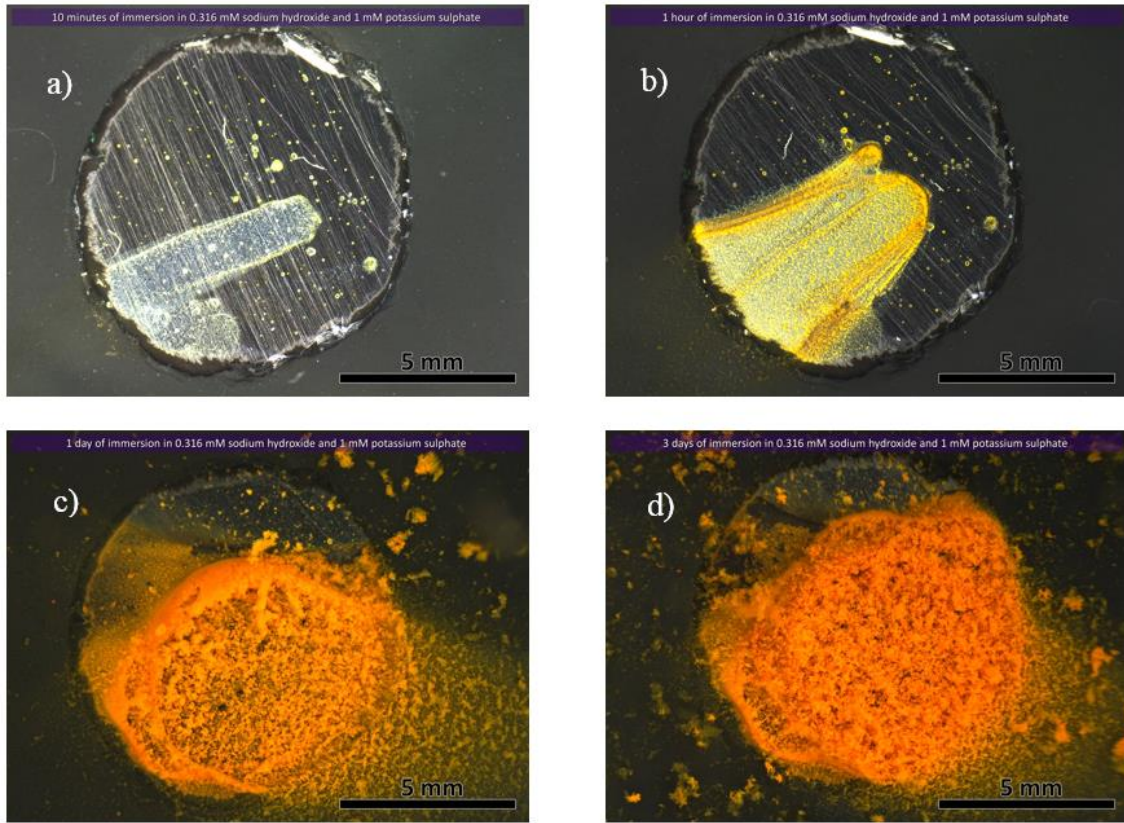
Figure 3.51: Carbon steel surface of sample immersed in 1mM SO_4^{2-} solution at pH 10.5 after 10 minutes a), 1 hour b), 1 day c) and 3 days d) of immersion.
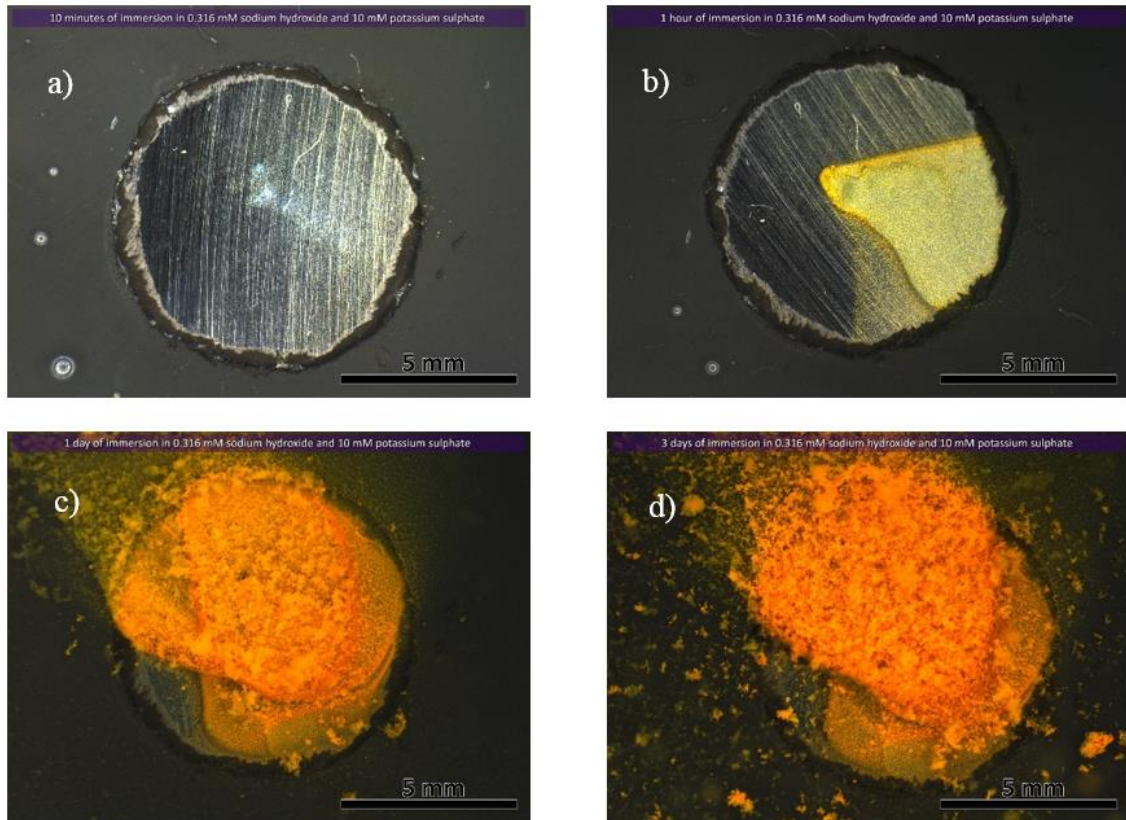
Figure 3.52: Carbon steel surface of sample immersed in 10mM SO_4^{2-} solution at pH 10.5 after 10 minutes a), 1 hour b), 1 day c) and 3 days d) of immersion.
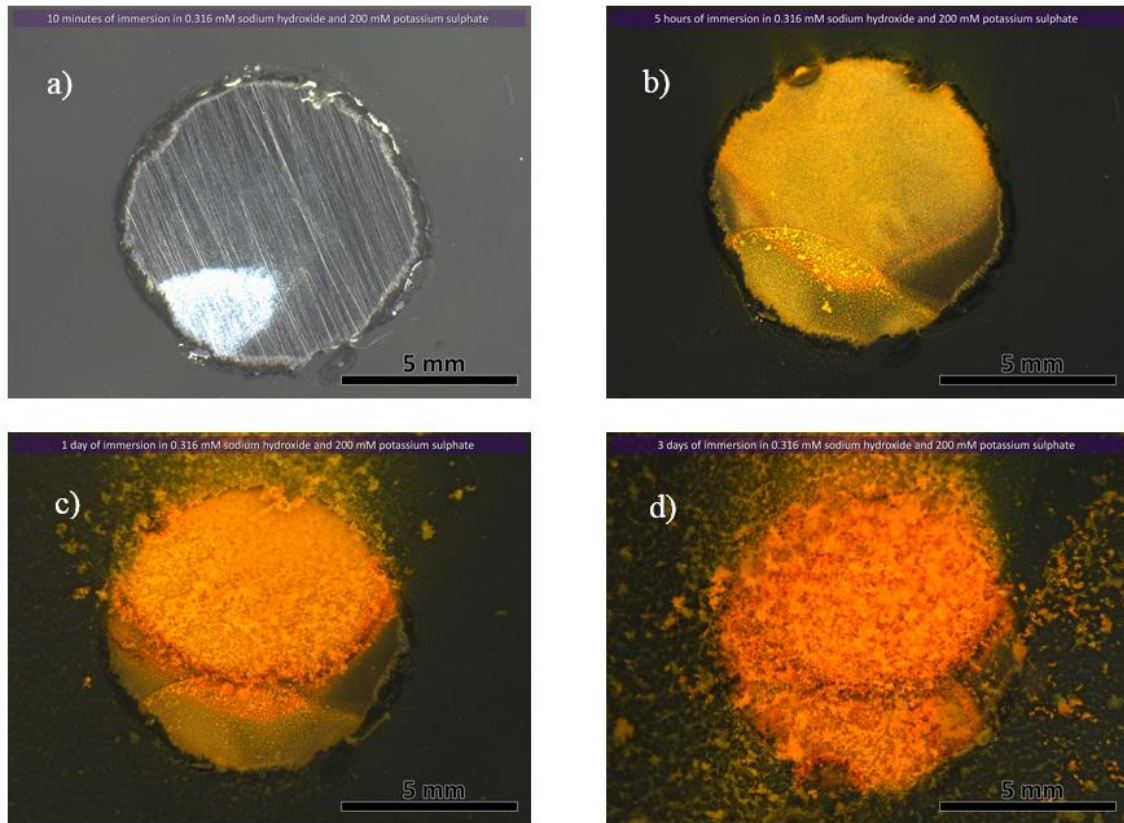
Figure 3.53: Carbon steel surface of sample immersed in 200mM SO_4^{2-} solution at pH 10.5 after 10 minutes a), 5 hours b), 1 day c) and 3 days d) of immersion.

In blank solution at pH 11.5, corrosion was observed only after 3 days of immersion while, for concentration of 1mM, during the second day. For SO_4^{2-} concentrations of 10mM and 200mM, corrosion products are visible after 5 hours and 10 minutes of exposure, respectively.
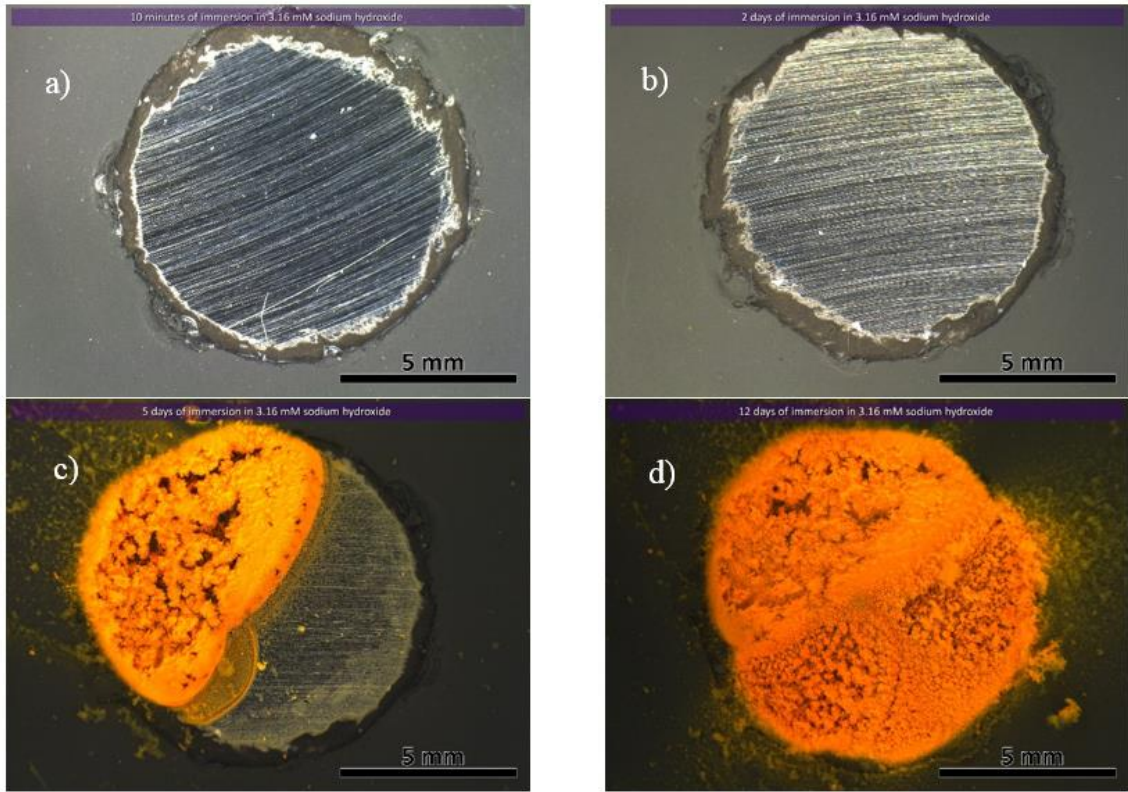
Figure 3.54: Carbon steel surface of sample immersed in blank solution at pH 11.5 after 10 minutes a), 2 days b), 5 days c) and 12 days d) of immersion.
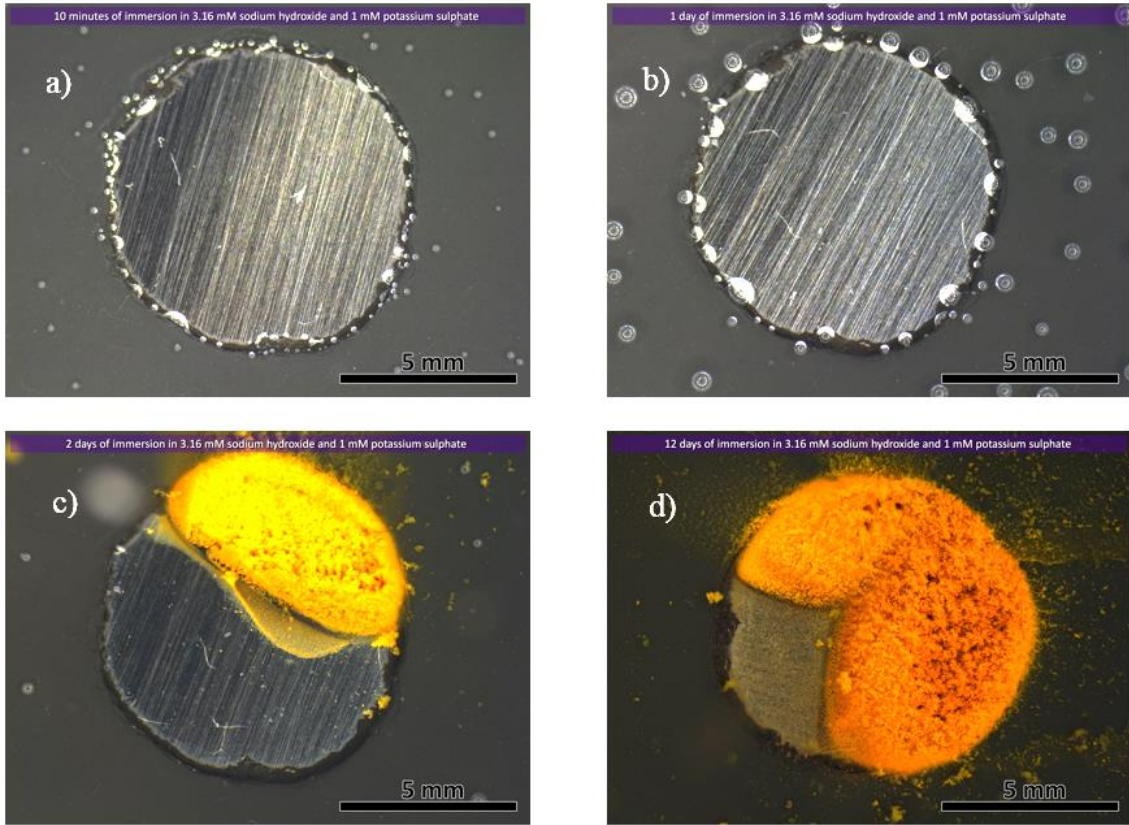
Figure 3.55: Carbon steel surface of sample immersed in 1mM SO_4^{2-} solution at pH 11.5 after 10 minutes a), 1 day b), 2 days c) and 12 days d) of immersion.
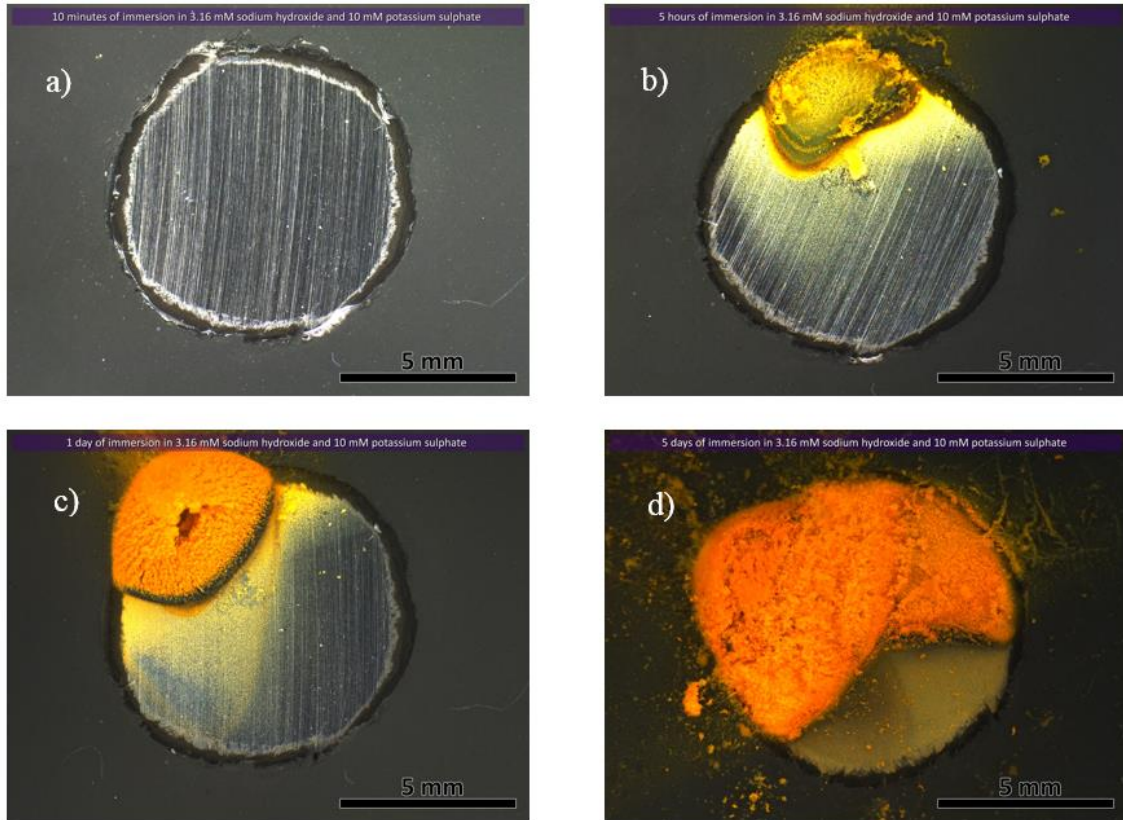
Figure 3.56: Carbon steel surface of sample immersed in 10mM SO_4^{2-} solution at pH 11.5 after 10 minutes a), 5 hours b), 1 day c) and 5 days d) of immersion.
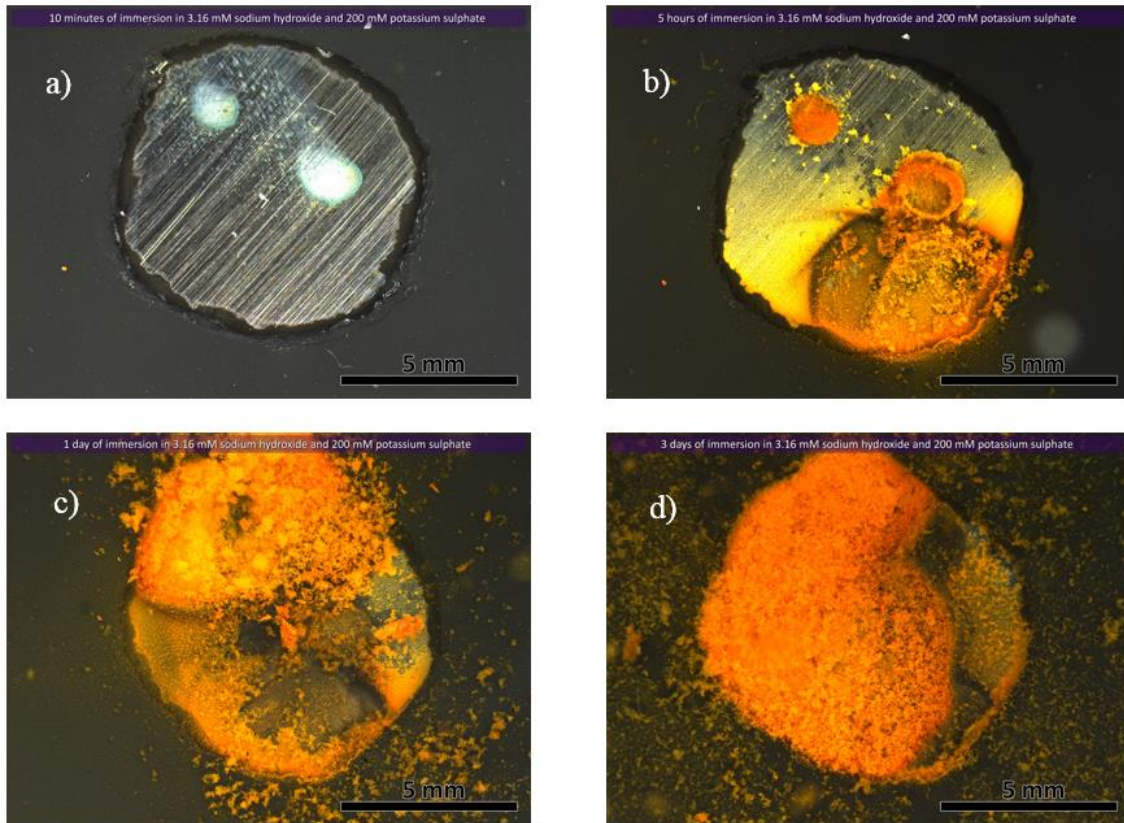
Figure 3.57: Carbon steel surface of sample immersed in 200mM SO_4^{2-} solution at pH 11.5 after 10 minutes a), 5 hours b), 1 day c) and 3 days d) of immersion.

At pH 12.5, likewise samples used for electrochemical tests, no corrosion was detected at sulfates concentration of 0mM and 1mM while, increasing the amount of this specie up to 10mM and 200mM, corrosion occurs after 12 days and 1 day, respectively. For this last case, the presence of crevice corrosion in correspondence of the border of the adhesive tape was evident.
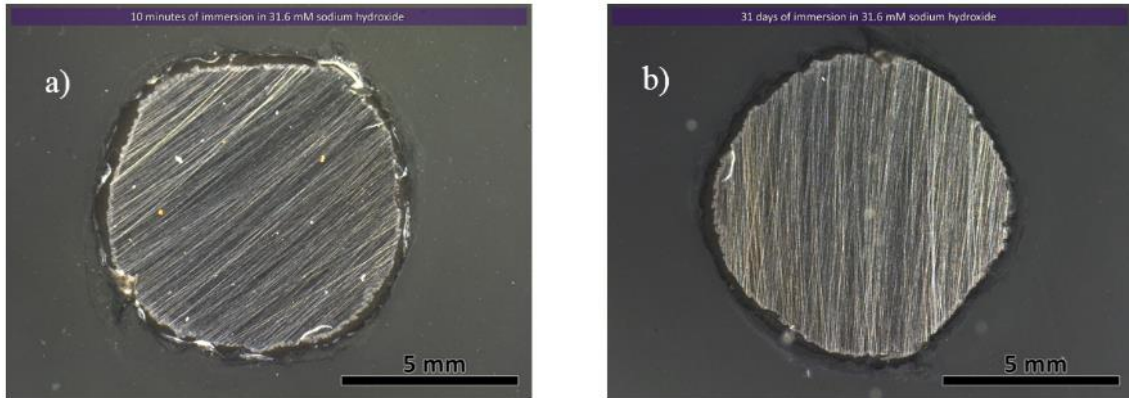
Figure 3.58: Carbon steel surface of sample immersed in blank solution at pH 12.5 after 10 minutes a) and 31 days b).
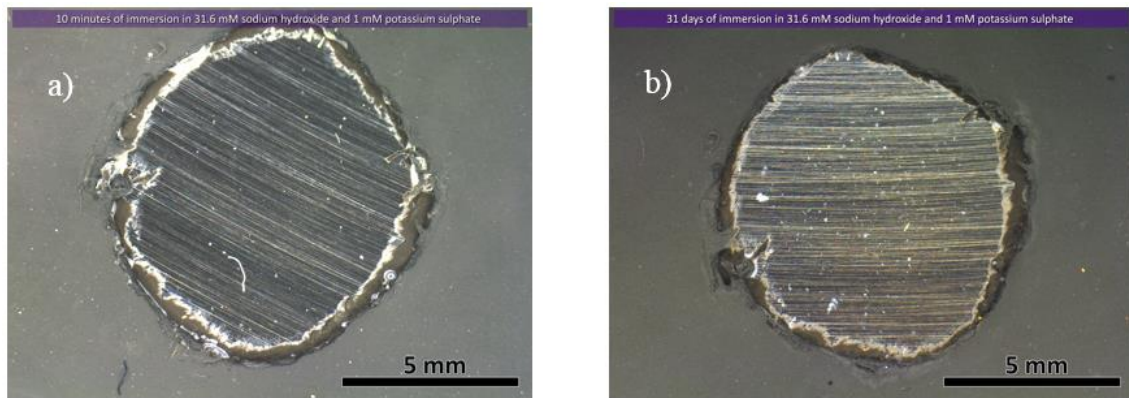
Figure 3.59: Carbon steel surface of sample immersed in 1mM SO_4^{2-} solution at pH 12.5 after 10 minutes a) and 31 days b).
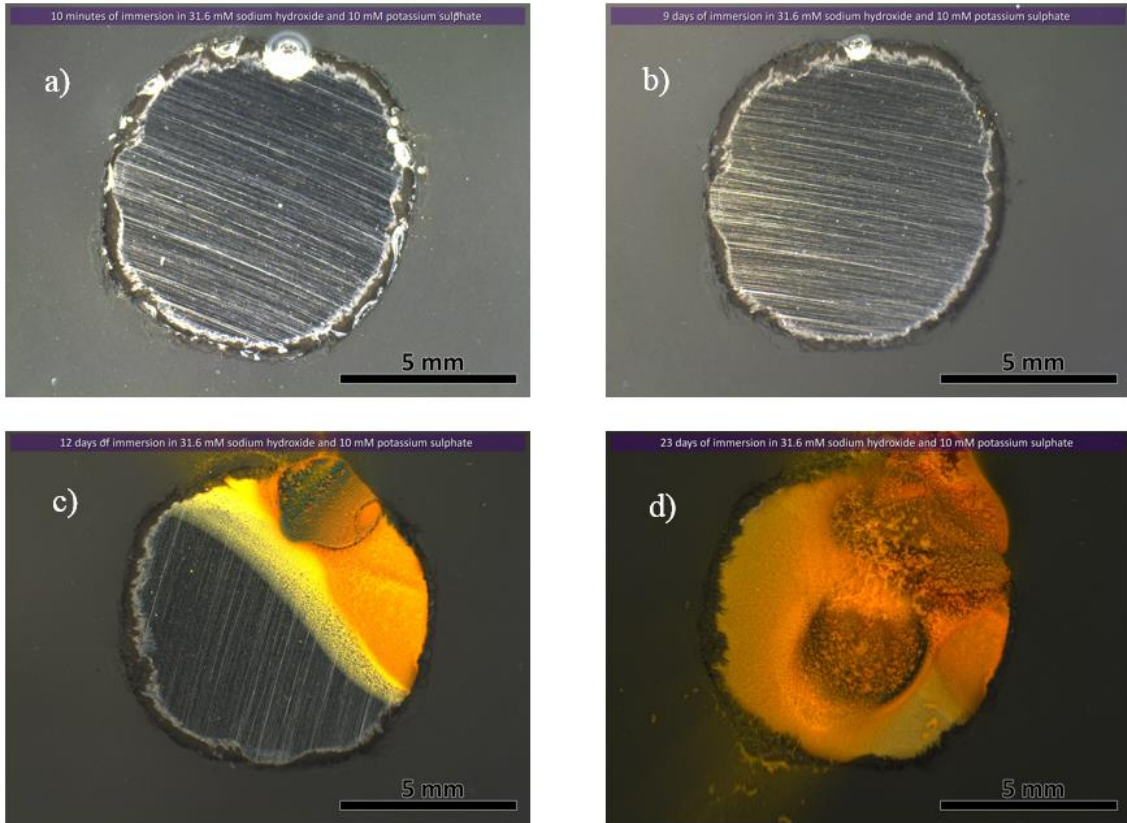
Figure 3.60: Carbon steel surface of sample immersed in 10mM SO_4^{2-} solution at pH 12.5 after 10 minutes a), 9 days b), 12 days c) and 23 days d) of immersion.
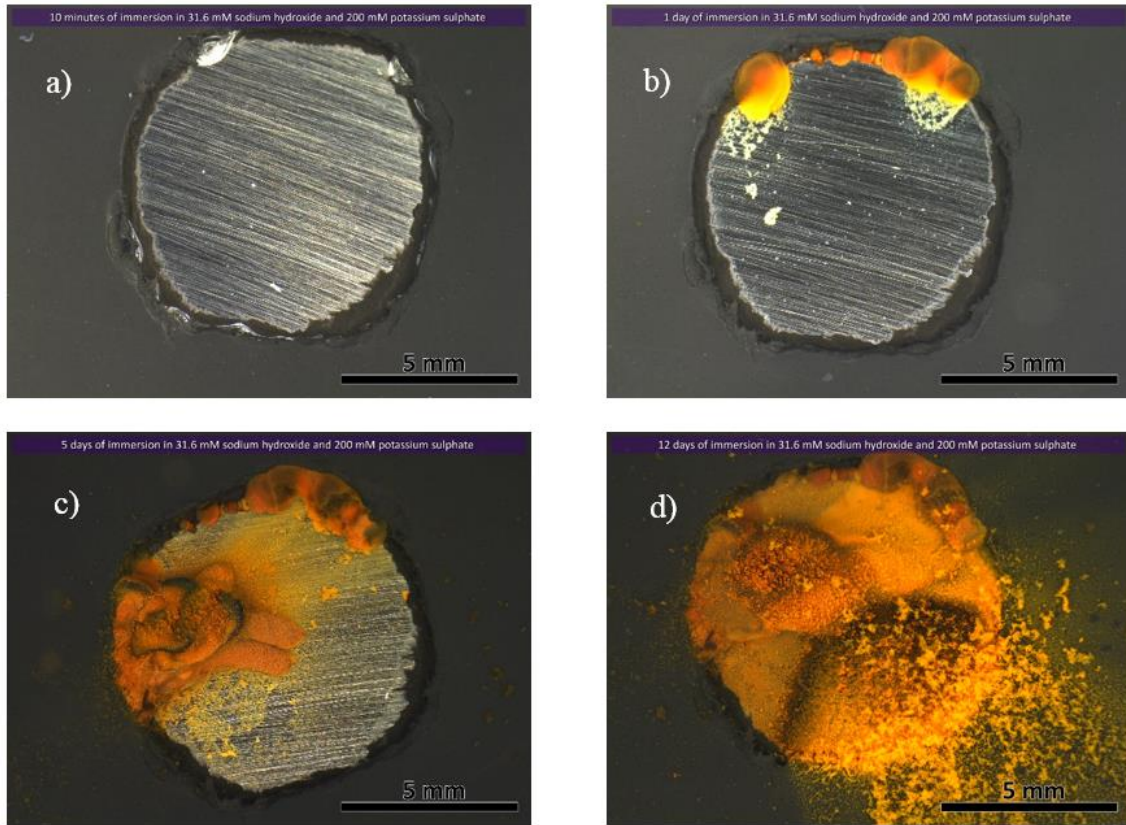
Figure 3.61: Carbon steel surface of sample immersed in 200mM SO_4^{2-} solution at pH 12.5 after 10 minutes a), 1 day b), 5 days c) and 12 days d) of immersion.

For all samples, general corrosion is the most common form corrosion and crevice corrosion was observed only at pH 12.5 at the highest concentration of sulfates.

CHAPTER **4**

---

4 ANALYSIS AND DISCUSSION

4.1 Effect of $C_4A_3\bar{S}$ (ye'elimite) content of the binder

In this paragraph, in order to study the effect of the use of CSA-based binder, characterized by different amount of ye'elimite, compared to reference concretes manufactured with Portland cement, experimental data of free potential evolution, EIS parameters, free corrosion potential evolution and pH are reported in function of mineral $C_4A_3\bar{S}$ amount inside the binder. In fact, $4CaO \cdot 3Al_2O_3 \cdot SO_3$ (ye'elimite or tetracalcium trialuminate sulfate) is the main constituent that characterize calcium sulfoaluminate cements.

Therefore, 0% was used to represent OPC concretes (or cement pastes) while, $C_4A_3\bar{S}$ percent of 15, 25 and 50 were used to represent concretes (or cement pastes) "EXP3", "EXP2" and "EXP1", respectively.

4.1.1 Effect of $C_4A_3\overline{S}$ (ye'elimite) content on pH

Figure 4.1 reports the effect of the ye'elemite content on pH, ███████████████ ██ of cement pastes characterized by water to cement ratio of 0.50. For $C_4A_3\overline{S}$ content inside the binder between 0% and 15%, no variations are visible and pH around 13.3 are measured. By increasing the amount of ye'elimite up to 25% and to 50%, the pH drops to values around 12.5 and 11.7, respectively.
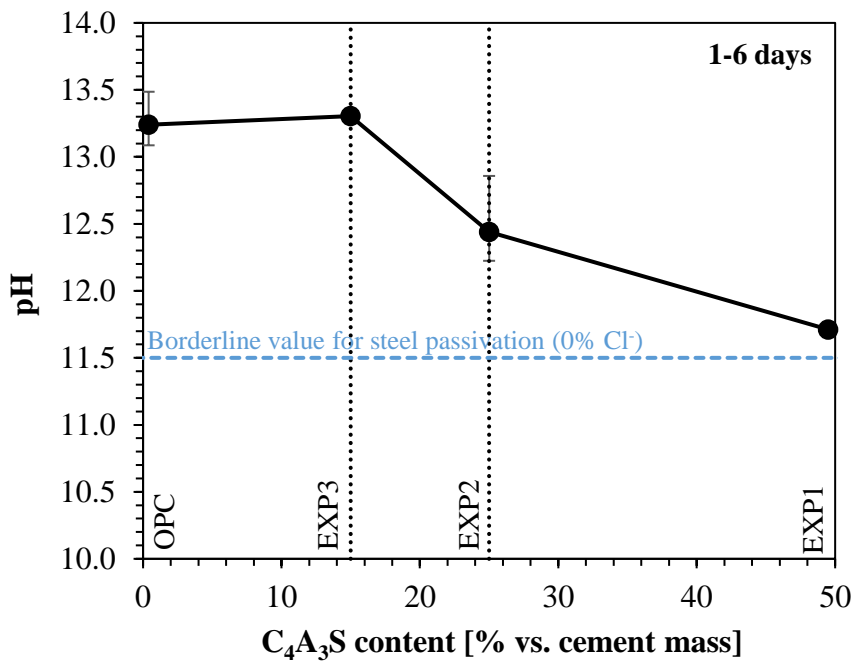
Figure 4.1: Effect of $C_4A_3\overline{S}$ on pH of cement paste (w/c 0.50) ████████████████████████.

4.1.2 Effect of $C_4A_3\bar{S}$ (ye'elimite) content on free corrosion potential

Figure 4.2 and Figure 4.3 report the effect of the ye'elemite content on the evolution of free corrosion potential, at different ageing, of carbon steel rebar embedded in single electrode cubic samples and in full-scale beams. The indicators that represent OPC and EXP1 concretes, show the mean value of the results collected with the two different water to cement ratios (0.55 and 0.50).

For rebar embedded in cubic samples, is possible to observe that, after 1 day of curing, by increasing the $C_4A_3\bar{S}$ content the corrosion potential decreases from -280 mV vs. SCE to -680 mV vs. SCE. After 28 days of curing this effect is still present, but only for addition of ye'elemite greater than 25%: corrosion potential is almost constant, around -170 mV vs. SCE, from percent of 0% to 25%, and for the maximum percent of 50% it decreases to -500 mV vs. SCE. After 280÷340 days of exposure, the effect is similar of that observed after 4 weeks, but nobler corrosion potential were measured in general. Figure 4.2 also reports the results collected considering the addition used with experimental binder EXP1 and with Portland cement: ███████████████ ██ ██ ████████████████████████ The use of calcium hydroxide (represented as the mean value of the two different addition of 2% and 4% vs. cement mass) and of lithium carbonate slightly increases, considering equal ageing, the corrosion potential of concretes manufactured with binder EXP1.
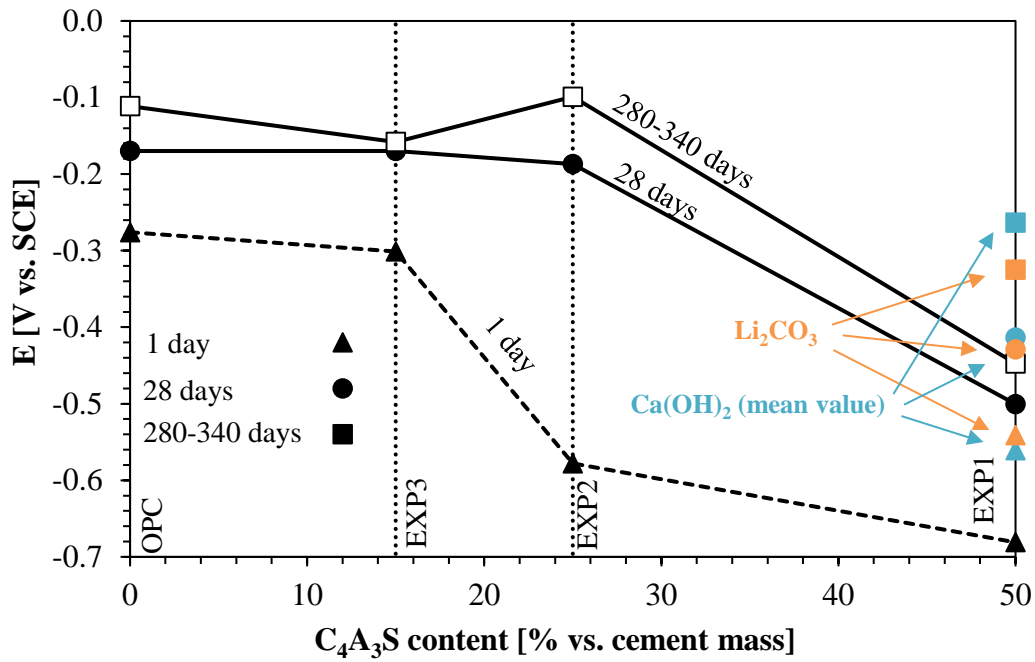
Figure 4.2: Effect of $C_4A_3\bar{S}$ on free corrosion potential evolution of carbon steel embedded in concrete cubic samples.

Regarding reinforcements embedded in full-scale beams (Figure 4.3), it is possible to observe a similar effect, compared to single electrode in cubic samples: after 1 day of exposure, a linear correlation between the decrease of corrosion potential and the increase of $C_4A_3\bar{S}$ content is visible. After 28 days of curing, the increment of ye'elemite to 15% decreases the corrosion potential from -80 mV to -135 mV vs. SCE while, increasing the percent up to 25% and 50%, the decrease is greater and corrosion potentials of -275 mV and -400mV vs. SCE are measured, respectively. After 300 days of exposure, the use of ye'elimite in percent lower or equal to 25% appears to be uninfluential on free corrosion potential variations while, the percent of 50%, causes a decrease of the corrosion potential from -80 mV vs. SCE (0% of $C_4A_3\bar{S}$) to -450 mV vs. SCE.
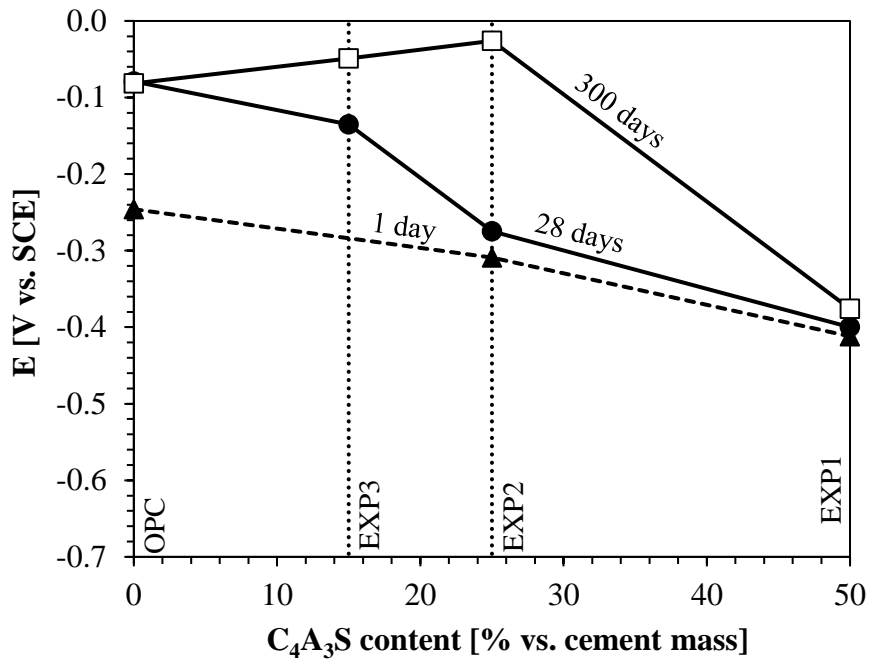
Figure 4.3: Effect of $C_4A_3\bar{S}$ on free corrosion potential evolution of carbon steel reinforcement embedded in full-scale beams.

Corrosion potential evolution is strictly dependent upon environmental conditions, which for laboratory tests were fixed over time while, for full-scale beams, varied in function of the natural climatic changes. Therefore, differences of behavior were noticed. However, a clear trend of the corrosion potential in function of the mineralogical composition can be outlined: by increasing the amount of ye'elimite inside the binder, is possible to observe, with both laboratory tests and field tests, a decrease of the free corrosion potential of the steel.

4.1.3 Effect of $C_4A_3\bar{S}$ (ye'elimite) content on R$_\Omega$ parameter

According to the simplest equivalent circuit to interpret EIS data by Randles, the Impedance (or modulus of Z) in the frequency range from 1000-20000 Hz represents the ohmic drop R$_\Omega$ ($|Z|_{1\,kHz}$) into the electrolyte (concrete) between the working electrode and reference electrode. This is valid also for passive material, because, in order to determine the ohmic drop, the behavior at low frequencies (where Randles model is able to fit EIS spectra of active materials) is not investigated.

Figure 4.4 reports the effect of the ye'elimite content of the binder on the R$_\Omega$ parameter, calculated from EIS spectra carried out on concrete cubic samples, which is related to the mechanical performances (Figure 3.6) but also to the environmental condition of relative humidity.

The figure represents the ohmic drop resistance of concretes stored in their formworks. All concretes show, at longer ageing, an increase of the ohmic drop, related to the microstructure of the cement paste that becomes more dense over time. By increasing the amount of $C_4A_3\bar{S}$ from 0% to 25%, no remarkable effect are observed and values around 780÷1570 Ωcm^2 and 3600÷4700 Ωcm^2 are measured at 1 day and 28 days, respectively. A strong increase of the ohmic drop is evident at the maximum ye'elimite concentration of 50%: after 1 day of curing it raches values around 7500 Ωcm^2 while, after 28 days, values close to 31400 Ωcm^2.

The use of lithium carbonate as set accelerator increases the ohmic drop only at 1 day to values close to those observed after 28 days of curing. The other additions does not cause significant changes when used with Portland cement or with binder EXP1.
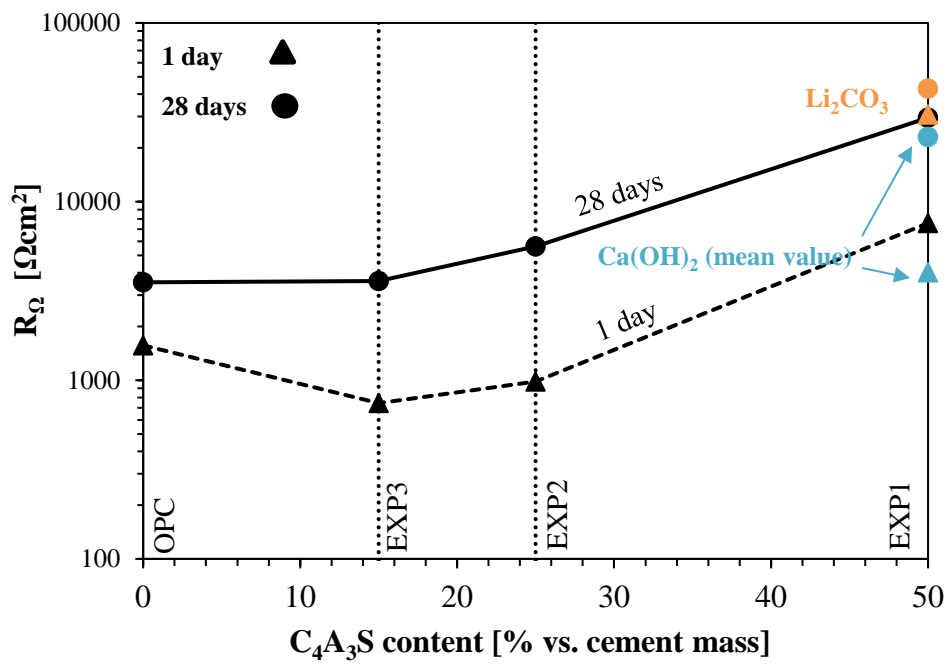
Figure 4.4: Effect of $C_4A_3\bar{S}$ on ohmic drop parameter R_Ω after 1 day and 28 days of curing.

4.1.4 Effect of $C_4A_3\overline{S}$ (ye'elimite) content on polarization resistance R_p parameter

At lowest frequencies Randles model defines a second stationary zone, which represents the sum of the polarization resistance (R_p) and the ohmic drop (|Z| at 1kHz). This model is valid to interpret active materials while, for material characterized by passive behavior, other equivalent circuits (as reported in paragraph 1.2.1) should be considered. EIS spectra results, supported by free corrosion potential and pH measurements suggested that carbon steel embedded in concretes manufactured with binder EXP1 without any other addition, and with addition of lithium carbonate, show a behavior that is typical of active material. Therefore, for these concretes, Randles model can be used to determine the polarization resistance R_p and consequently the corrosion rate, according to Equation 4.1:

Equation 4.1: Determination of corrosion rate with polarization resistance parameter.

$$I_{corr}[mA] = \frac{k\,[mV]}{R_p\,[m\Omega]}$$

Where k is a constant, which can be assumed equal to 26 mV for active steel behavior (while a value of 52 mV should be used for passive materials).

In order to define R_p value it is sufficient to subtract from the value of impedance obtained at 5 mHz (|Z|$_{5\,mHz}$) the impedance at 1000 Hz (|Z|$_{1\,kHz}$).

Finally, to estimate the corrosion rate is necessary to subdivide I_{corr} by the exposed area of working electrode (0.0016 m^2) and then multiply the i_{corr} by a conversion factor in order to obtain a corrosion rate expressed as μm/year.

In order to validate Randles model, EIS spectra of concrete "EXP1+Li$_2$CO$_3$" were fitted with ZView software. Table 4.1 reports the evolution of the fitting parameters over time while, Figure 4.5 reports the evolution of the ohmic resistance (R_Ω) and of the polarization resistance (R_p). Concrete manufactured with binder EXP1 and lithium carbonate as set accelerator develops a strong increase during the first hours of the ohmic drop to values around $2E^{+4}$ Ωcm^2; this is related to the cement paste behavior, that becomes denser within the first hours. The order of magnitude of the polarization resistance R_p settles

around low values of 4E^{+4} and 2E^{+5} Ωcm^2, for all the exposure time, meaning that passive film is not formed on steel surface.

Table 4.1: Evolution of fitting parameters of concrete "EXP1+Li$_2$CO$_3$" over time.

Time (hours)	R$_\Omega$ [Ωcm^2]	R$_p$ [Ωcm^2]	CPE-T	CPE-P
0.072	5.38E+02	1.11E+05	1.83E-03	7.68E-01
0.96	5.14E+02	9.92E+04	1.91E-03	7.79E-01
3.36	1.25E+04	2.94E+05	2.37E-03	6.28E-01
8.16	1.88E+04	3.49E+05	1.39E-03	7.21E-0
24	3.12E+04	2.10E+05	9.21E-04	7.18E-01
96	3.74E+04	7.99E+04	8.77E-04	6.78E-01
168	4.01E+04	6.38E+04	9.74E-04	6.62E-01
360	3.84E+04	7.27E+04	9.12E-04	6.87E-01
792	4.42E+04	5.07E+04	1.29E-03	6.14E-01
1320	5.02E+04	4.86E+04	1.72E-03	6.59E-01
1680	5.68E+04	5.81E+04	1.77E-03	6.71E-01
2160	6.42E+04	7.45E+04	1.79E-03	6.80E-01
2880	7.32E+04	9.69E+04	1.79E-03	6.82E-01
6144	1.43E+05	2.47E+05	1.57E-03	6.90E-01
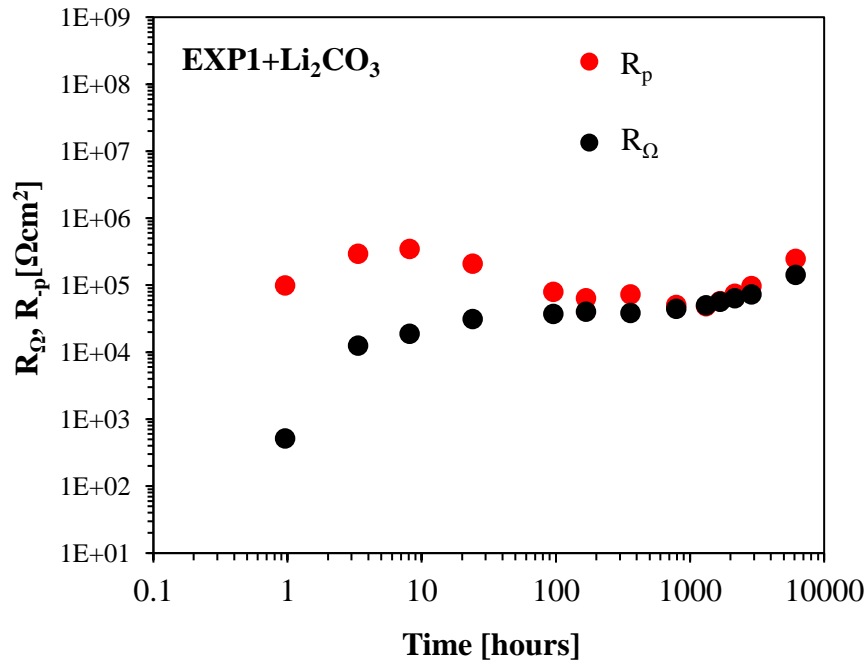
Figure 4.5: Evolution of R$_\Omega$ and R$_p$ parameters of concrete "EXP1+Li2CO3".

██████	██████	██████	████	████
▮	██████	██████	██████	██████
▮	██████	██████	██████	██████
▮	██████	██████	██████	██████
▮	██████	██████	██████	██████
▮	██████	██████	██████	██████
▮	██████	██████	██████	██████
▮	██████	██████	██████	██████

Figure 4.6: ████████████████████████████████

Anyway, it has been decided to interpret the EIS spectra of all concretes using the polarization resistance parameter. Moreover, the determination of R_p, calculated as the difference of the impedance at 1 kHz and 0.005 Hz, underestimates the real polarization resistance of passive behavior materials.

Figure 4.7 reports the effect of the ye'elimite content of the binder on the polarization resistance R_p (Ωcm^2) evaluated at short ageing. The higher is this parameter the lower is the corrosion rate, according to Equation 4.1.

At 1 day is possible to observe that increasing the mineralogical content of tetracalcium trialuminate sulfate the R_p parameter decreases from 280÷340 $k\Omega cm^2$ (at 0% and 15%) to 35÷38 $k\Omega cm^2$ (at 25% and 50%). The trend of the EIS spectra at 1 day (paragraph 3.1.1.3) revealed that concretes manufactured with binder EXP1 (█████████████████ ████████████████████████████) and EXP2 show active behavior. Therefore, for this concretes the corrosion rate was calculated, revealing values of about 8 μm/year.

██
██
████████████████████████████

After 28 days of exposure, the use of CSA-based binder characterized by a ye'elimite content lower or equal to 25% seems to be able for steel passivation. In fact, rather high polarization resistance parameters are determined, but in any case, they were lower than those of concretes manufactured with Portland cement. Moreover, the free corrosion potential values of concretes "EXP2" are low and reach noble values, close to those of OPCs, only after 21 days, meaning that different passivation kinetic occurs. This fact can be deleterious in presence of chlorides or sulfates, even in very low concentration, which could destroy the passive film and promote localized corrosion initiation. It must be noticed that very small amount of chlorides are usually present into both the mixing water or in raw materials while, concentrations of sulfates can be around 10÷30 mM during the first days [48] and, if pH is low, the weak passive film formed can be easily destroyed, causing localized corrosion initiation.

By increasing the amount of $C_4A_3\bar{S}$ up to 50% it is possible to determine low R$_p$ (around 30 kΩcm^2) and high corrosion rates around 10 μm/year, since EIS spectra of concretes "EXP1" and "EXP1+Li$_2$CO$_3$" showed active behavior, at 28 days (paragraph 3.1.1.3).

CSA concretes with calcium hydroxide (the blue indicators represent the mean value of the results collected with the different amounts of 2% and 4% vs. cement mass) show higher polarization resistances at 28 days.

In general, it is possible to outline that, the higher is the $C_4A_3\bar{S}$ content, the lower is the polarization resistance, meaning that the passive film is not forming or, if it has formed, it is less stable and protective compared to that formed in Portland cement.
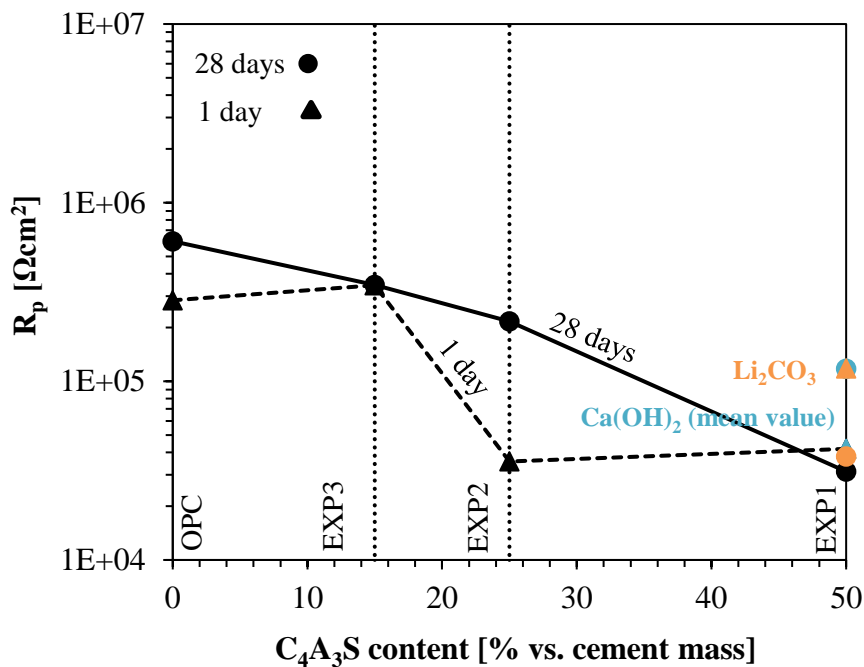
Figure 4.7: Effect of $C_4A_3\bar{S}$ on polarization resistance R$_p$ parameter after 1 day and 28 days of curing.

At long ageing, the increase of the ye'elimite binder up to 15% did not modify the polarization resistance, which was around 560 kΩcm^2 while, the percent of 25% decreased the R$_p$ to 265 kΩcm^2. After 150÷170 days of exposure, carbon steel embedded in concrete manufactured with the binder characterized by the highest amount of $C_4A_3\bar{S}$ developed low polarization resistances, around 27 kΩcm^2 that, after 280÷340 days increased up to 66 kΩcm^2.
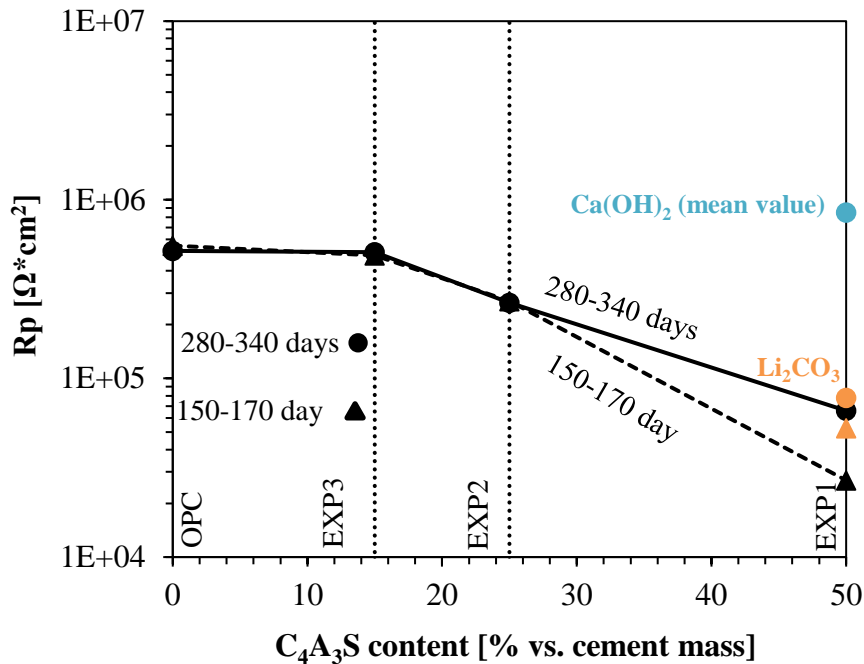
Figure 4.8: Effect of $C_4A_3\bar{S}$ on polarization resistance R_p parameter after 150÷170 days and 280÷340 days of curing.

Thus, it is evident that by increasing the amount of the mineralogical component $C_4A_3\bar{S}$ inside the binder lower polarization resistances are developed over time. Compared to concretes manufactured with Portland cement, which are characterized by R_p values of 600 kΩcm², a strong decrease, around one order of magnitude, is visible for CSA concretes manufactured with the binder characterized by the highest amount of ye'elimite.

Only after 280÷340 days of exposure concretes manufactured with binder EXP1 show an increase of the R_p but, it must be underlined that the determination of this parameter is dependent on many factors, such as the environmental conditions of relative humidity of the concrete (see paragraph 4.2.2). In order to estimate the corrosion rate of active material behavior, only R_p parameters at short ageing (1 and 28 days) were considered

and values around 8÷10 μ/year, typical of active corrosion in carbonated concrete, were determined for concretes with binder EXP1 (also with addition of Lithium carbonate). The use of calcium hydroxide seems to have a beneficial effect in combination with binder EXP1 ██ ██.

4.2   Effect of environmental conditions

The corrosion behavior of carbon steel reinforcements is strictly dependent on several characteristics of the concrete among which pH, mineralogical composition, presence of aggressive species, porosity, moisture of the admixture are the more important. Therefore, in order to attain a wide overview regarding the behavior of steel embedded in CSA-based concretes, different wet and dry environmental conditions were analyzed. Concrete "EXP1 w/c 0.50" showed, when exposed to dry environments, a greater water absorption compared to OPC (Figure 3.21) and also important variations of its open circuit potential (Figure 3.5) and of its EIS spectra (Figure 3.20) in function of the moisture of the matrix.

According to the simplest equivalent circuit to interpret EIS data by Randles, the ohmic drop R_Ω was calculated as the impedance (or modulus of Z) at the frequency of 1 kHz.

Figure 4.9 reports the evolution of the R_Ω parameter of concrete "EXP1 w/c 0.50" exposed to different wet and dry conditions. The ohmic drop is, at 20°C and relative humidity of 70%, $4E^{+4}$ Ωcm^2. When the sample is placed in water, at the same conditions of temperature and R.H. of the chamber, R_Ω decreases down to $1.6E^{+4}$ $\Omega*cm^2$ and, when the relative humidity of the chamber is increased up to 70%, a further decrease of the ohmic drop is observed, reaching values of about $1E^{+4}$ Ωcm^2.

When the sample is dried, first by storing it in a climatic chamber without water at 20°C and R.H. of 40%, later in an oven at 60°C for 24 hours, the ohmic drop increases to $2.76E^{+4}$ and $6.2E^{+4}$ Ωcm^2, respectively.
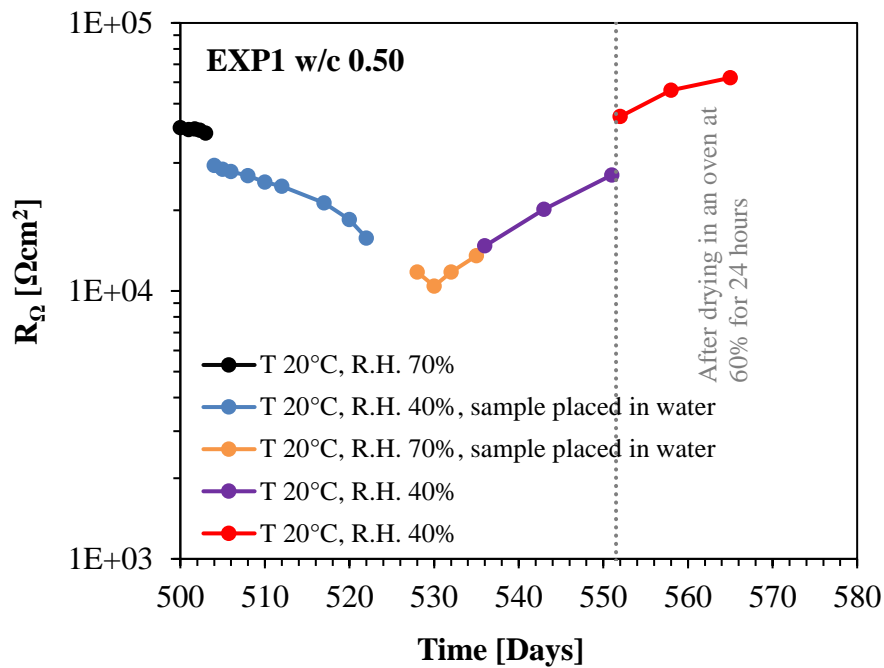
Figure 4.9: Evolution of ohmic drop R_Ω parameter of concrete "EXP1 w/c 0.50", exposed to wet and dry environmental conditions.

The polarization resistance R_p was also evaluated, according to Randles model, as the difference of the impedance at low frequencies (|Z| at 0.005 Hz) and the ohmic drop (|Z| at 1kHz). It must be considered that the sample, tested after 500 days in different wet and dry conditions, did not show any more a well defined active behavior such that observed at early and medium ageing. In fact, EIS spectra (Figure 3.20) does not show anymore the presence of a plateau at low frequencies, typical of active behavior material.

The evolution of R_p parameter (Figure 4.10), calculated as the difference of the impedance at low and high frequencies, is strictly dependent on the ohmic drop, which showed large variations in function of the environmental conditions. The polarization resistance reveals stable values, around $3.6E^{+4} \div 4E^{+4}$ Ωcm^2 considering a relative humidity of 40%, with and without the presence of water in touch with the sample for a depth of few centimeters. By increasing the relative humidity up to 70%, with the sample placed in water, the Rp decreases to $2.4E^{+4}$ Ωcm^2 and after natural and forced drying in an oven, it increases again up to values around $3.5 \div 4E^{+4}$ Ωcm^2.
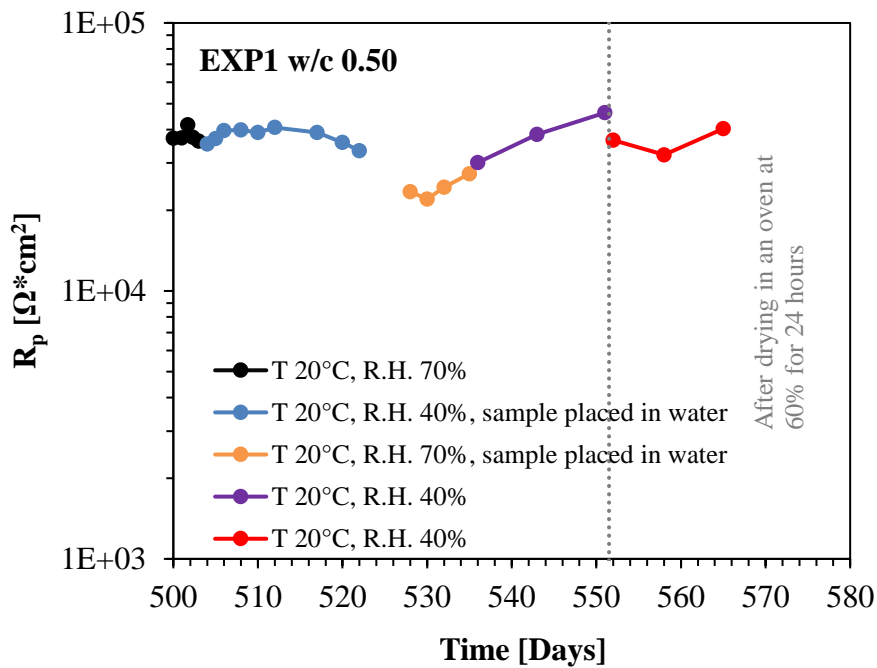
Figure 4.10: Evolution of polarization resistance R_p parameter of concrete "EXP1 w/c 0.50", exposed to wet and dry environmental conditions.

Table 4.3 reports the ohmic drop R_Ω and polarization resistance R_p parameters calculated, as the impedance at low frequencies and the difference of the impedance at low frequencies and that at high frequencies respectively, and fitted with ZView software. The R_Ω parameters both calculated and fitted show very similar values while, the polarization resistance parameters reveal higher values when fitted, compared to those calculated. However, the trend of R_p is the same both for calculated and fitted values.

Table 4.3: R_Ω and R_p parameters calculated and fitted with ZView software, of sample "EXP1 w/c 0.50" exposed to wet and dry environmental conditions.

Time (days)	Exposure conditions	Calculated R_Ω [Ωcm^2]	Fitted R_Ω [Ωcm^2]	Calculated R_p [Ωcm^2]	Fitted R_p [Ωcm^2]
500	T 20°C, R.H. 70%	4.06E+04	4.09E+04	3.72E+04	6.44E+04
501		4.00E+04	4.05E+04	3.73E+04	6.31E+04
501		4.02E+04	4.04E+04	4.16E+04	6.06E+04
502		3.98E+04	4.04E+04	3.74E+04	6.12E+04
503		3.88E+04	3.94E+04	3.62E+04	5.92E+04
504	T 20°C, R.H. 40%, Sample placed in water	2.94E+04	2.74E+04	3.53E+04	6.05E+04
505		2.84E+04	2.76E+04	3.70E+04	6.08E+04
506		2.79E+04	2.81E+04	3.96E+04	6.39E+04
508		2.69E+04	2.72E+04	3.98E+04	6.29E+04
510		2.54E+04	2.57E+04	3.90E+04	5.82E+04
512		2.46E+04	2.48E+04	4.07E+04	6.35E+04
517		2.13E+04	2.14E+04	3.90E+04	5.74E+04
520		1.84E+04	1.85E+04	3.58E+04	5.30E+04
522		1.57E+04	1.57E+04	3.34E+04	4.73E+04
528	T 20°C, R.H. 70%, Sample placed in water	1.18E+04	1.15E+04	2.34E+04	3.58E+04
530		1.04E+04	1.03E+04	2.20E+04	3.29E+04
532		1.17E+04	1.17E+04	2.44E+04	3.77E+04
535		1.35E+04	1.34E+04	2.74E+04	4.39E+04
536	T 20°C, R.H. 40%	1.47E+04	1.45E+04	3.01E+04	5.00E+04
543		2.02E+04	1.99E+04	3.84E+04	6.81E+04
551		2.71E+04	2.68E+04	4.62E+04	8.48E+04
Drying with an oven at 60°C and 24 hours					
552	T 20°C, R.H. 40%	4.47E+04	4.50E+04	3.65E+04	5.09E+04
558		5.61E+04	5.61E+04	3.22E+04	6.84E+04
565		6.24E+04	6.09E+04	4.03E+04	7.62E+04

4.2.1 Effect of the environmental conditions on free corrosion potential

Supposed that after 500 days of curing all hydration reactions of CSA-based concretes are exhausted, the effect of the moisture of the concrete was evaluated without taking account the effect of time, which was assumed, after 500 days, constant. Therefore, is possible to outline, for concretes manufactured with CSA-based cement containing the highest amount of ye'elimite of 50%, the effect of the relative humidity (and the presence or absence of water in contact with the sample) on free corrosion potential.

Figure 4.11 reports the corrosion potential in function of the relative humidity of the climatic chamber, in presence or absence of water in touch with the concrete. The environmental conditions are reported in a specific order that reasonably represents increasing moisture content inside the concrete sample. It is possible to observe that increasing the moisture content from a condition where the sample has been dried in an oven to another where the sample is exposed to R.H. values of 40% and 70%, the corrosion potential decreases from -380 mV vs. SCE down to -466÷-480 mV vs. SCE. The increment of the moisture content due to the presence of water in contact with concrete decreases the corrosion potential of the reinforcements down to -515 mV vs. SCE. The increase of the R.H. of the room up to 70% together with the presence of water in touch with the sample develops the lowest corrosion potential values, around -530 mV vs. SCE.

Thus, the marked shift of the corrosion potential of concretes manufactured with CSA binder EXP1 to nobler values must not be interpreted as the consequence of the formation of the passive film on the steel surface. A similar shift of the potential to nobler values is also visible at long ageing for cubic sample stored in the formwork and beam exposed to the environment manufactured with binder EXP1 and with w/c 0.55 (Figure 3.4 and Figure 3.22). Such increases are ascribed to the arise of the anodic overpotential.
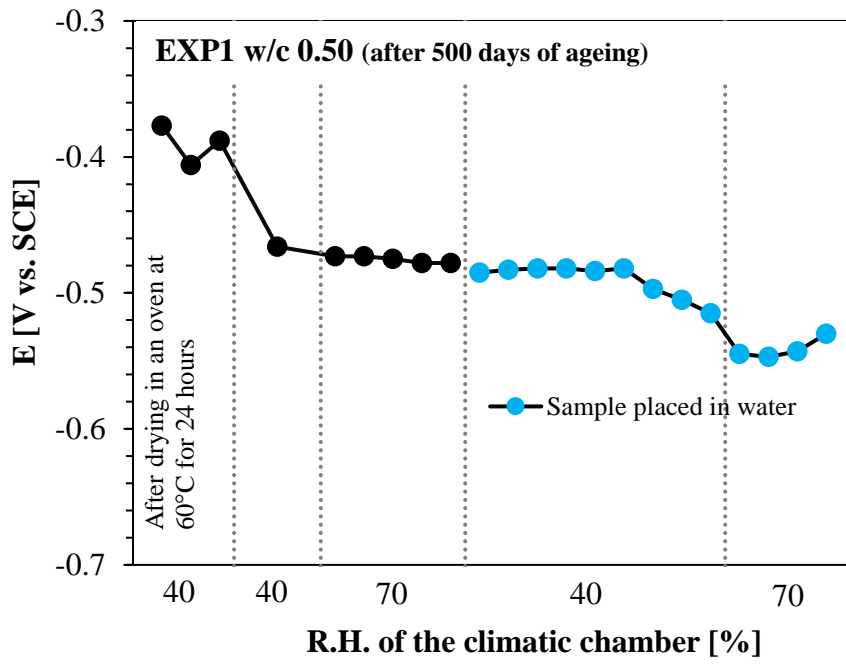
Figure 4.11: Effect of dry and wet environmental conditions on free corrosion potential of concrete "EXP1 w/c 0.50".

4.2.2 Effect of the environmental conditions on R_Ω and R_P parameters

After 500 days of curing, modifications of the ohmic drop, which at early ages is dependent on the hardening of the concrete when hydrations of the cement is still occurring, are mainly dependent on the environmental conditions.

Figure 4.12 shows the evolution of R_Ω. Increasing the moisture content of the concrete, the ohmic drop, between the working electrode and the reference electrode, decreases, as expected. The polarization resistance (Figure 4.13) shows constant values, and only at R.H. of 70% in presence of water in contact with concrete, lower values are observed, meaning that in these conditions higher corrosion rates should be expected.
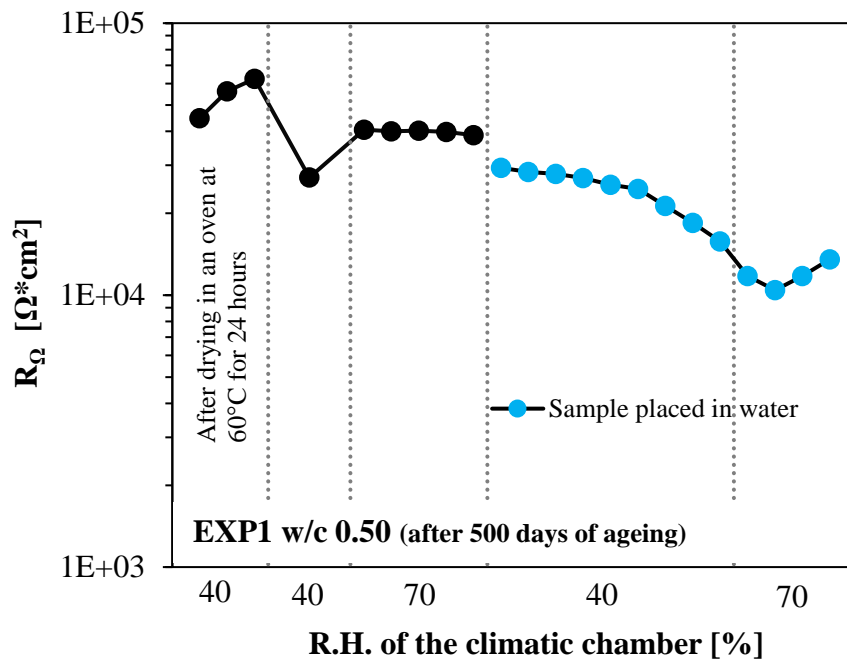
Figure 4.12: Effect of dry and wet environmental conditions on ohmic drop R_Ω parameter of concrete "EXP1 w/c 0.50".
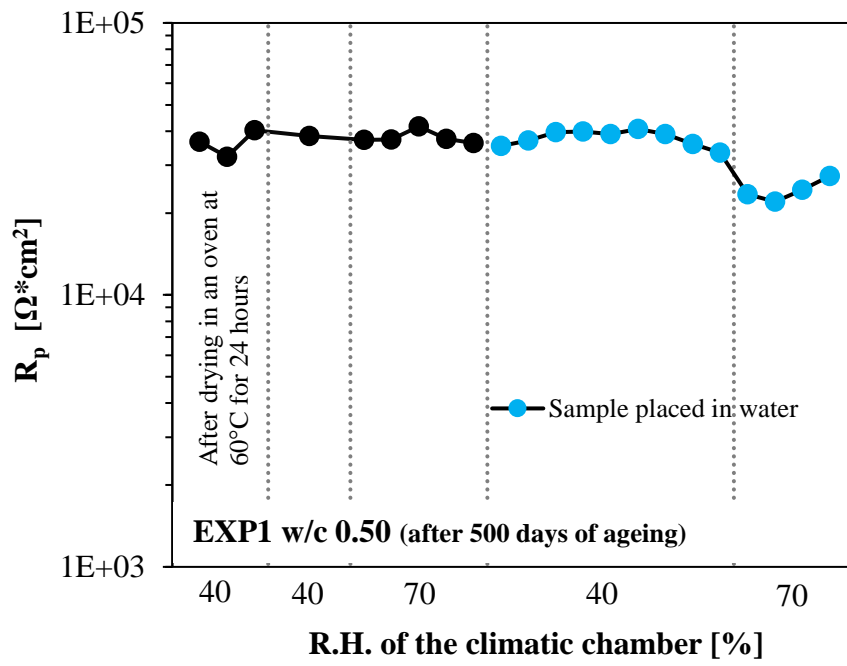
Figure 4.13: Effect of dry and wet environmental conditions on ohmic drop R_Ω parameter of concrete "EXP1 w/c 0.50".

4.3 Effect of SO_4^{2-} concentration

In this paragraph, in order to study the effect of sulfate on the corrosion behavior of carbon steel, results are reported in function of the sulfates concentrations of solutions that simulate different stages of CSA concretes pore solution.

Experimental data of free corrosion potential evolution, time of immersion to initiate corrosion and EIS parameters are reported in function SO_4^{2-} amount, at different pH values of 10.5, 11.5 and 12.5.

Concentration of 0.1 mM was used to represent blank solutions on x-axis.

4.3.1 Effect of SO_4^{2-} amount on free corrosion potential

Figure 4.14 to Figure 4.16 report the effect of the sulfates concentration on the free corrosion potential evolution measured before the beginning of the EIS tests, at the pH values of 10.5, 11.5 and 12.5.

At pH 10.5 the increase of sulfates concentrations from 0.1 (blank solution) to 1 mM, within 8 hours of immersion, decreases the corrosion potential of the specimen to negative values around -690 mV vs. SCE, typical of active corrosion process.

As expected, the same effect is observed for greater concentrations of sulfates. Also in blank solution a decrease of the corrosion potential to the same negative values occurs after 1 day of exposure, meaning that this alkalinity level is not sufficient to promote the formation of a stable protective oxide film.
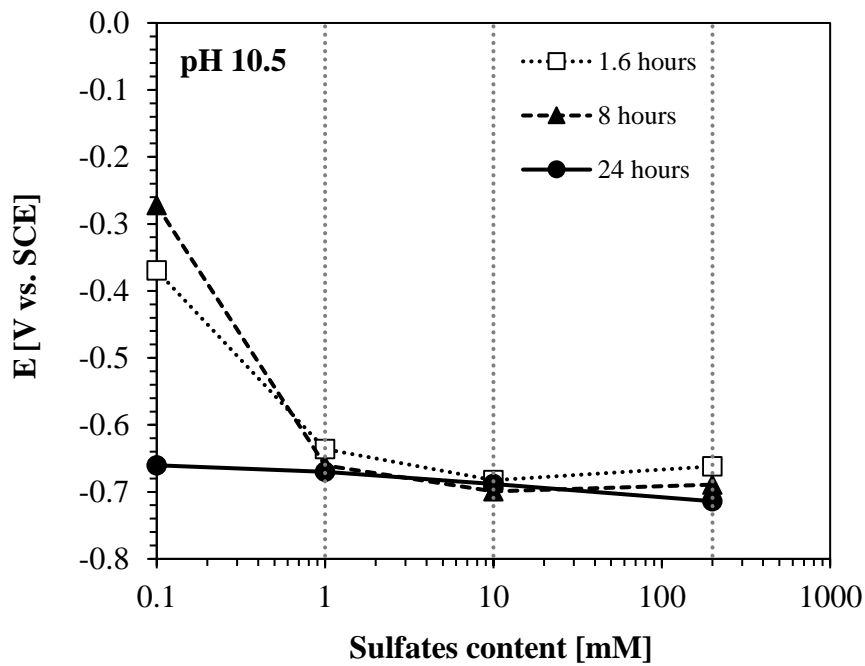
Figure 4.14: Effect of SO_4^{2-} on free corrosion potential over time at pH 10.5.

Considering the intermediate pH value of 11.5, it is possible to observe that the increase of sulfates up to 1 mM decreases the corrosion potential after 2 days of immersion while, greater additions decrease the potential down to -630÷-690 mV vs. SCE right after the immersion of the sample.

The solution's pH decreased over time of about 0.2÷0.3 points of pH and, therefore, also in blank solution low potentials were observed after 3 days of immersion, when corrosion occurred.
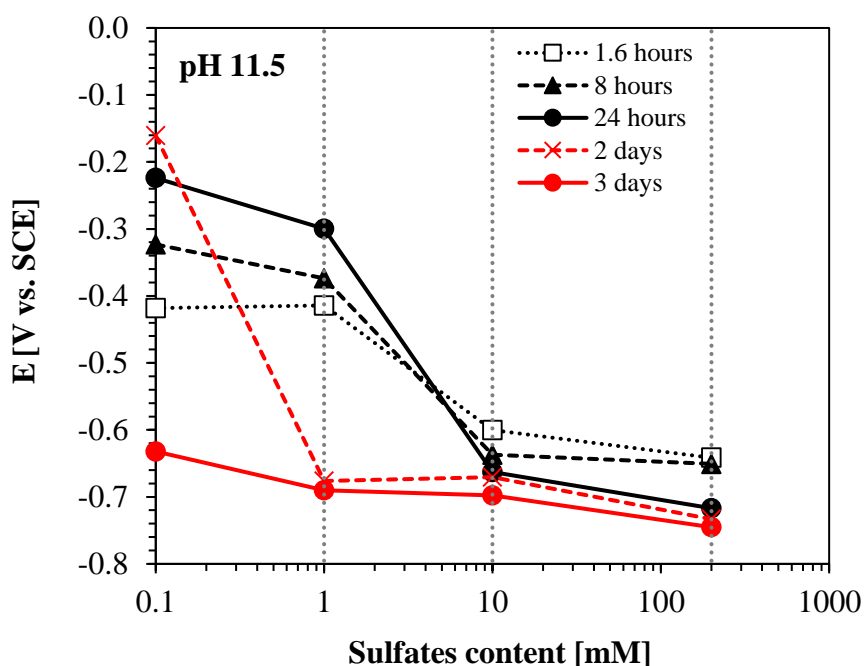
Figure 4.15: Effect of SO_4^{2-} on free corrosion potential over time at pH 11.5.

At the maximum pH value tested, no effects of sulfates are visible considering the concentration of 1 mM: carbon steel sample, similarly to blank solution, develops since the first hours of immersion high corrosion potential values, which increases over time until the end of the tests after 31 days, meaning that a protective passive film is forming on steel surface.

By increasing the SO_4^{2-} concentration up to 10 mM it os possible to observe a decrease of the corrosion potential from noble values down to -640 mV vs. SCE after two weeks of immersion, meaning that the breakdown of the passive film occurred. This effect is more remarkable at the greater concentration of sulfates, when corrosion occurs before one week from immersion of the sample.
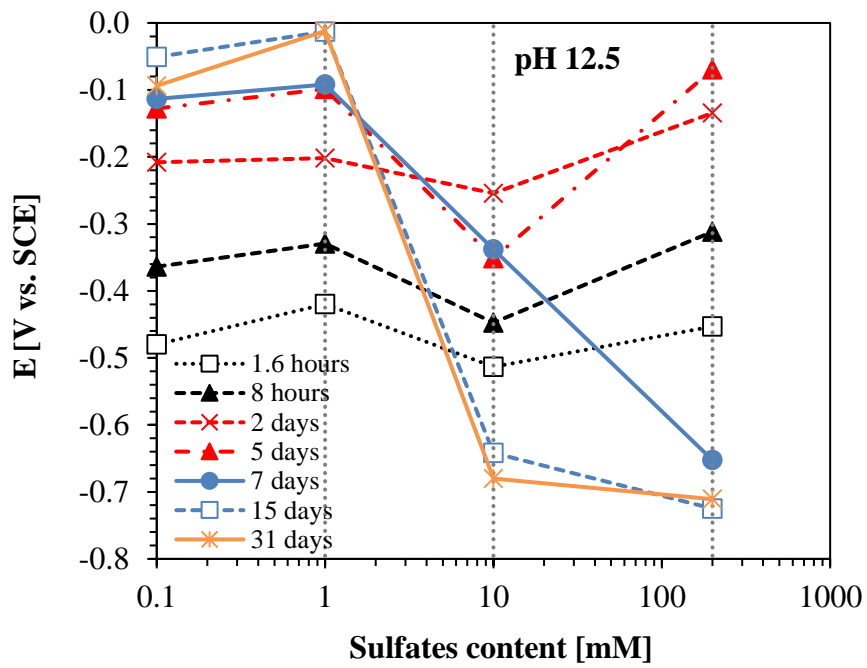
Figure 4.16: Effect of SO_4^{2-} on free corrosion potential over time at pH 12.5.

4.3.2 Effect of SO_4^{2-} amount on time to corrosion initiation

The effect of the amount of sulfates on time, at different pH values, necessary for corrosion to initiate is reported in Figure 4.17. In order to determine the time, it was considered the mean value of the time of immersion, for electrochemical solutions, when corrosion potential dropped to negative values around -600÷-700 mV vs. SCE and the time when corrosion was observed with optical tests.

At pH 10.5, in absence of sulfates, corrosion occurs only after 14 hours of immersion and, the addition of SO_4^{2-}, decreases the time necessary to initiate corrosion down to zero, independently on the concentration. At pH 11.5, carbon steel sample shows corrosion after 3 days, in blank solutions, and by increasing the amount the sulfates up to 1 mM, the time to corrosion initiation decreases to 48 hours. Greater additions (10 and 200 mM) promote corrosion right after immersion of the sample, similarly to samples immersed in solutions with pH of 10.5.

At the maximum pH of 12.5, in solutions without and with the lowest amount of sulfates (1mM), corrosion is not present until the end of the experimental tests. The increase of SO_4^{2-} amount up to 10 mM, promotes corrosion after around 14 days of immersion and after only 4 days considering the greatest concentration of 200 mM.

Therefore, it is possible to outline that sulfates have a negative effect on corrosion behavior of carbon steel samples, in simulating solution environments: by increasing their concentration, it decreases the time of immersion for corrosion to occur. Furthermore, considering the same time of exposure, the increase of the concentration of this specie decreases the free corrosion potential of the steel.

It must be underlined that the experimental tests were carried out in absence of chlorides, which, in concrete environment, could be present together with sulfates. The presence of both species should be deeply investigated and could slow down the corrosion process of carbon steel, due to the competition between chloride and sulfate ions in correspondence of the steel surface.
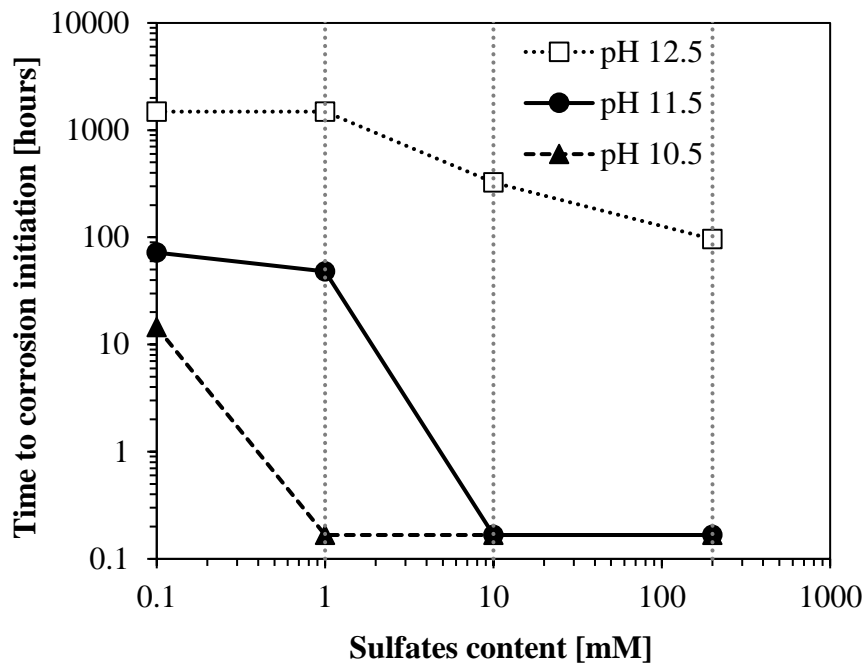
Figure 4.17: Effect of SO_4^{2-} on time to corrosion initiation.

4.3.3 Effect of SO_4^{2-} amount on charge transfer resistance R$_{-CT}$

In order to evaluate the effect of sulfates on corrosion behavior of carbon steel, at different pH, EIS spectra were fitted using the equivalent circuit reported in Figure 4.18. R$_s$ represents the ohmic drop of the electrolyte between the reference electrode and the working electrode, CPE$_{-OX}$ and R$_{-OX}$ represent the constant phase element and the resistance of the passive film, CPE$_{-DL}$ and R$_{-CT}$ represent the constant phase element of the double layer (passive film/steel interface) and the charge transfer resistance, respectively.
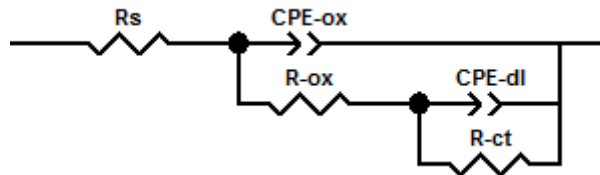
Figure 4.18: Equivalent circuit used to fit EIS spectra of carbon steel immersed in simulating solutions.

Figure 4.19, Figure 4.21 and Figure 4.23 reports the evolution of the oxide film resistance R$_{-ox}$ and of the charge transfer resistance R$_{-CT}$, at different pH values. The R$_{-CT}$ parameter, in particular, gives an information concerning the energy required for electron transfer from one phase (e.g. the anode of the steel surface) to another (e.g. the electrolyte where cathodic reaction will take place). Therefore, the higher is the value of the charge transfer resistance, the greater is the energy required for the process of transferring electrons from the electrode. As immersed, on the steel surface, which is not covered by a protective oxide layer, the electron transfer requires low energy. If the alkalinity of the environment is enough to promote the formation of a stable film, on the steel surface it will be formed a compact protective layer and, as consequence, the energy necessary for the electron transfer will increase together with the charge transfer resistance. If the conditions necessary to promote and preserve the passive film fail, the electron transfer will occur more easily and the charge transfer resistance will decrease.

Figure 4.20, Figure 4.22 and Figure 4.24 reports the effect of the sulfates concentration on the charge transfer resistance, at the different pH values of 10.5, 11.5 and 12.5.

At pH 10.5, the oxide film resistance is, for all the different concentrations of sulfate, in the range between 10 and 1000 Ωcm^2.

The charge transfer resistance R_{CT} increases, for blank solution at pH 10.5, during the first hours of immersion simultaneously with the growth of the oxide layer and then, when corrosion occurs, it decreases to 2800 Ωcm^2. The addition of sulfates, independently on the amount, strongly penalizes the charge transfer resistance, which shows constant and low values around 700 Ωcm^2, since the first minutes after immersion of the sample, meaning that the formation of the passive film is completely avoided (confirmed also by the low corrosion potential values).

Figure 4.19: Evolution of oxide film resistance R_{-OX} and of charge transfer resistance R_{-CT} values obtained by EIS spectra data fitting at different time of immersion, at pH 10.5.

Figure 4.20: Effect of SO_4^{2-} on R_{CT} parameter over time at pH 10.5.

Also for solutions characterized by pH of 11.5, fitting of EIS spectra showed oxide film resistance values in the range between 10 and 1000 Ωcm^2. The charge transfer resistance R_{-ct} increases both for blank and 1mM solutions up to $1E10^{+6}$ Ωcm^2 until 48 and 24 hours, respectively, meaning that passive oxide layer is forming on the steel surface. After this period of immersion, corrosion occurs and the value of R_{-CT} decreases to $1E10^{+3}$ Ωcm^2.

The presence of sulfates in concentrations equal or greater than 10mM, prevents the formation of the passive film and, therefore, low values of charge transfer resistance are calculated since the first instants after immersion, confirmed also by the low free corrosion potential values monitored over time.

174

Figure 4.21: Evolution of oxide film resistance R$_{-OX}$ and of charge transfer resistance R$_{-CT}$ values obtained by EIS spectra data fitting at different time of immersion, at pH 11.5.
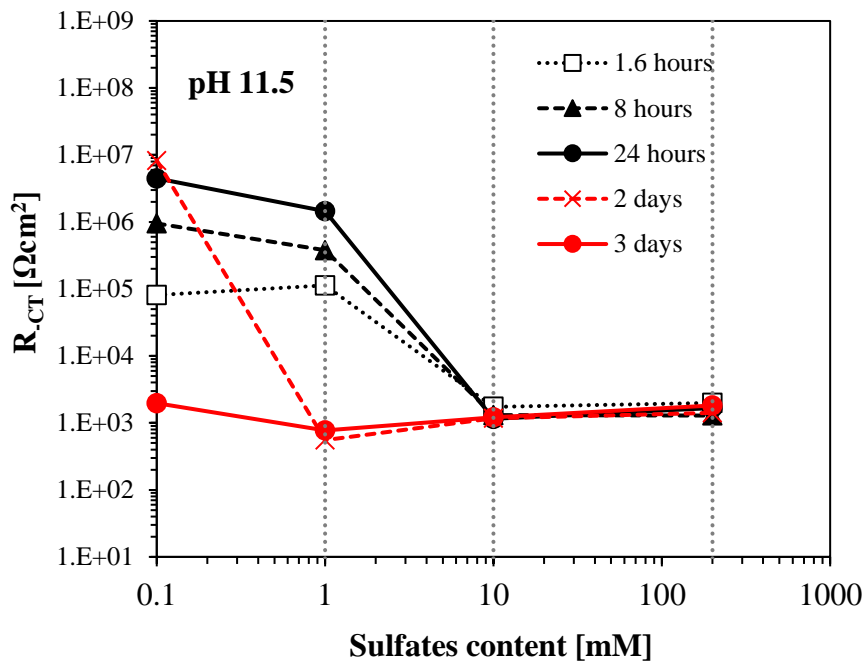
Figure 4.22: Effect of SO_4^{2-} on R_{CT} parameter over time at pH 11.5.

At the maximum pH of 12.5, the charge transfer resistance increases over time in absence of sulfates or in presence of sulfates considering the lowest concentration of 1mM. R_{-CT} reaches, at the end of the tests, values around $4E10^{+7} \div 2.5E10^{+7}$ Ωcm^2, meaning that a stable passive film formed on the steel surface. This is also confirmed by the open circuit potential monitoring that revealed high potential values over time and also by visual observation with optical microscope.

The increase of SO_4^{2-} up to 10mM, causes a drop of the charge transfer resistance after 12 days of immersion, meaning that the breakdown of the passive film occurs. The maximum concentration of sulfates promotes the failure of the oxide film after only 5 days of exposure, when the parameter R_{-CT} decreases from $4.6E^{+6}$ to $1.2E^{+3}$ Ωcm^2. Likewise solutions with pH 10.5 and 11.5, the values of the oxide film resistance are in the range of $10 \div 1000$ Ωcm^2.
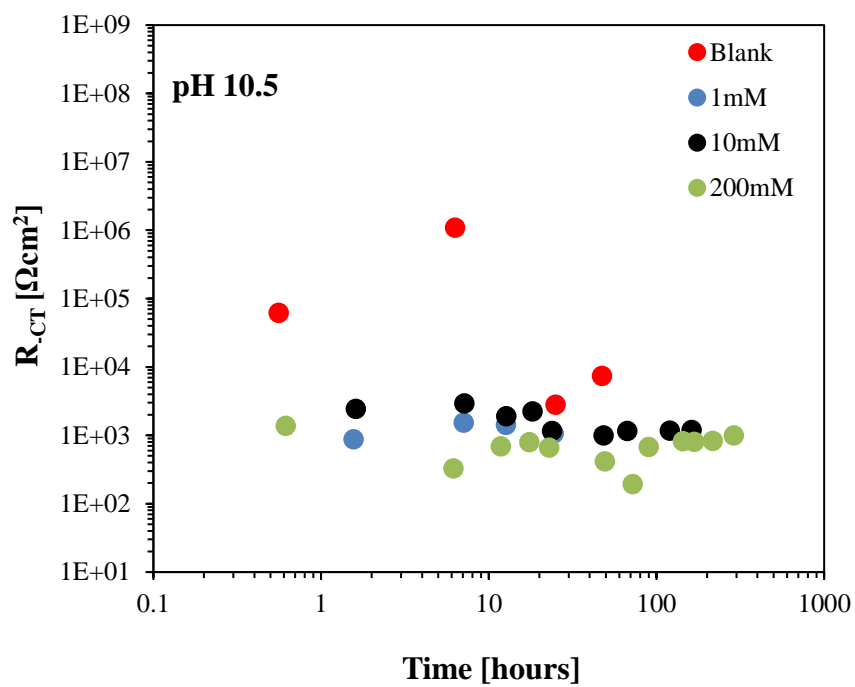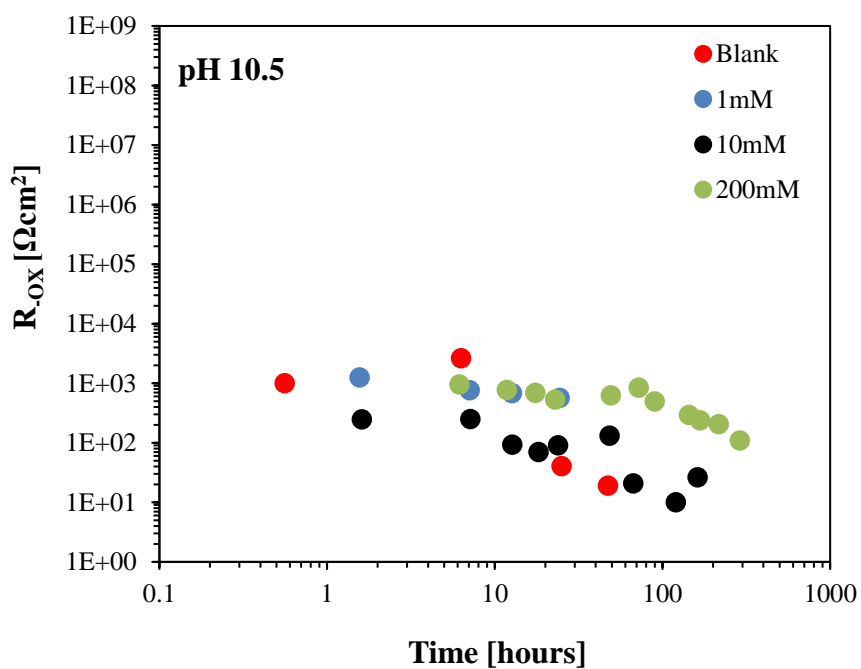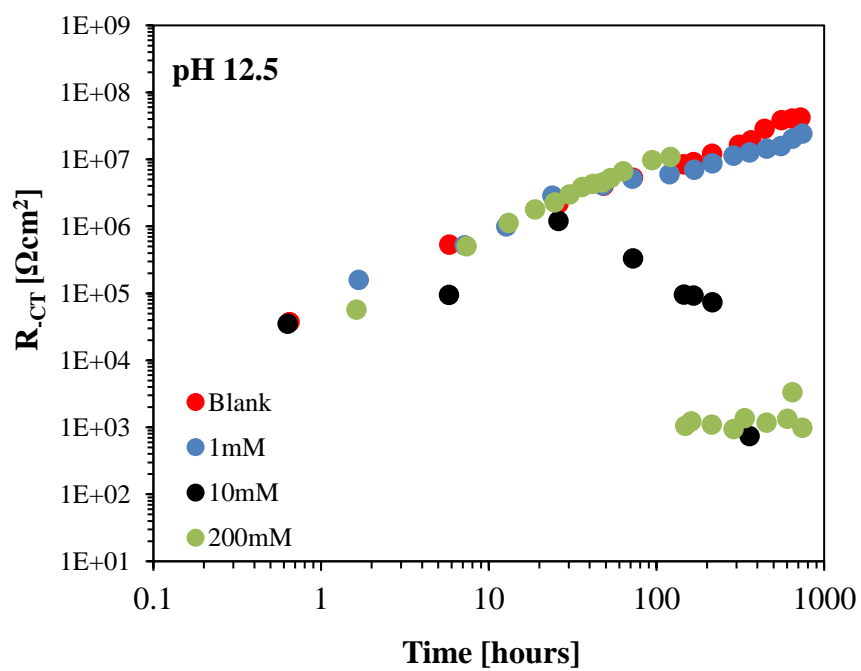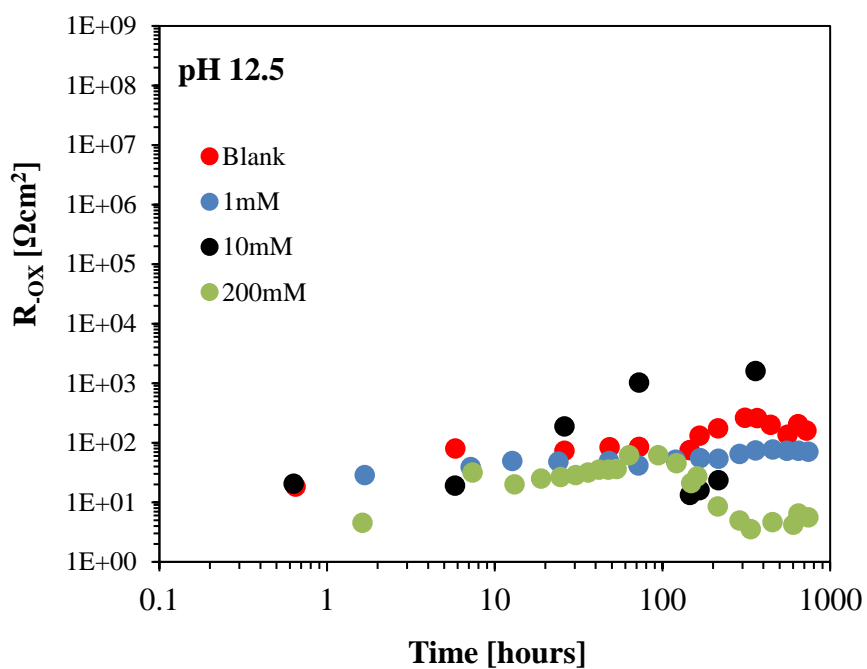
Figure 4.23: Evolution of oxide film resistance R_{-OX} and of charge transfer resistance R_{-CT} values obtained by EIS spectra data fitting at different time of immersion, at pH 11.5.
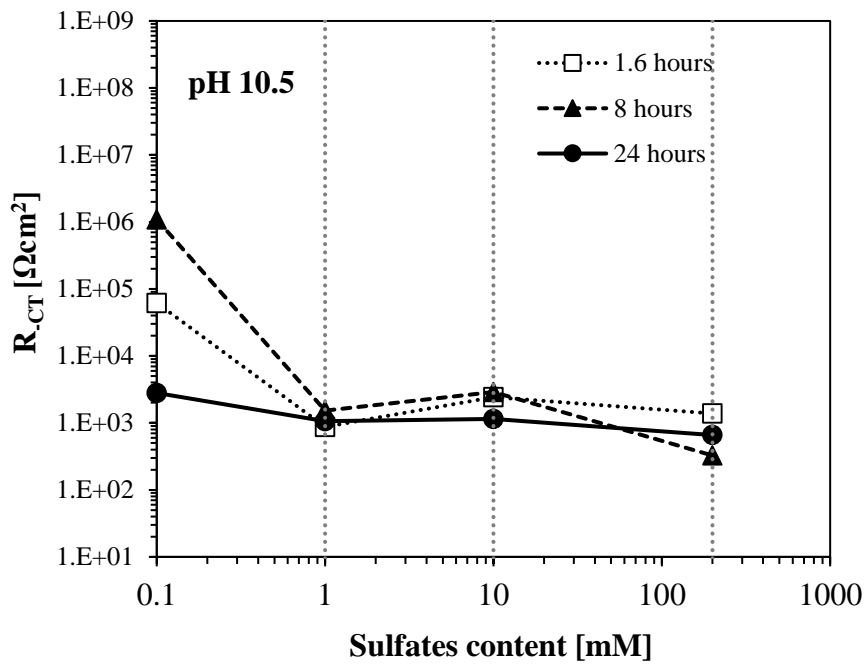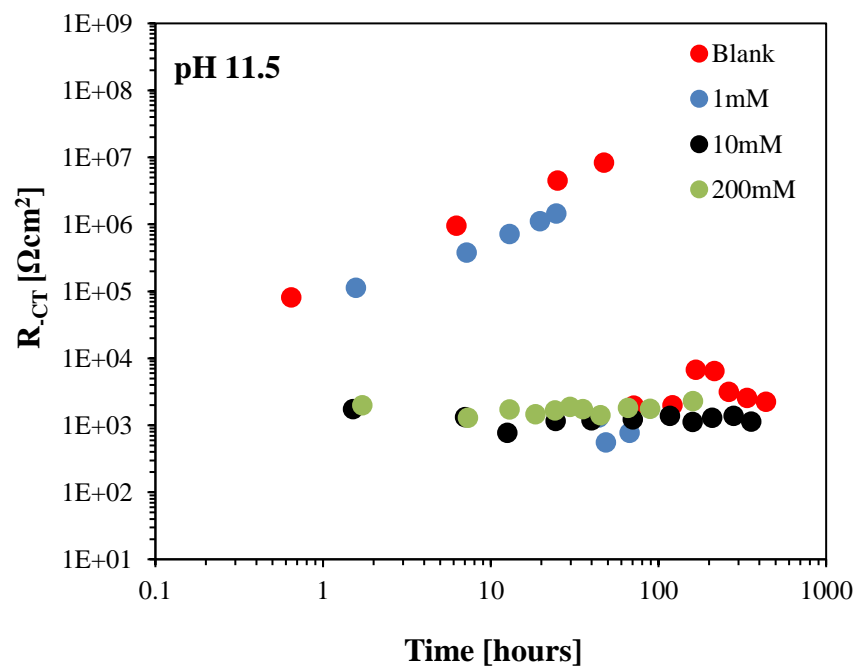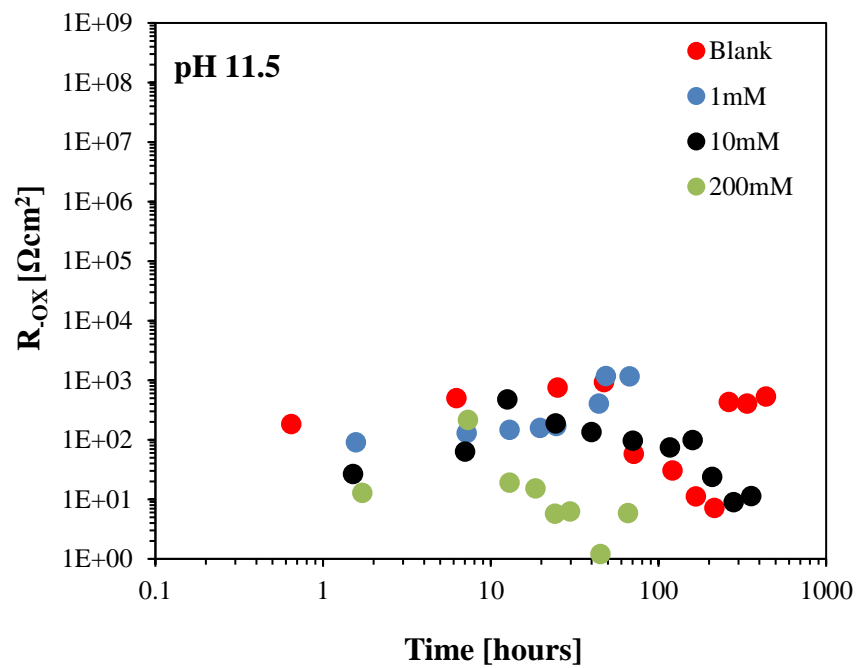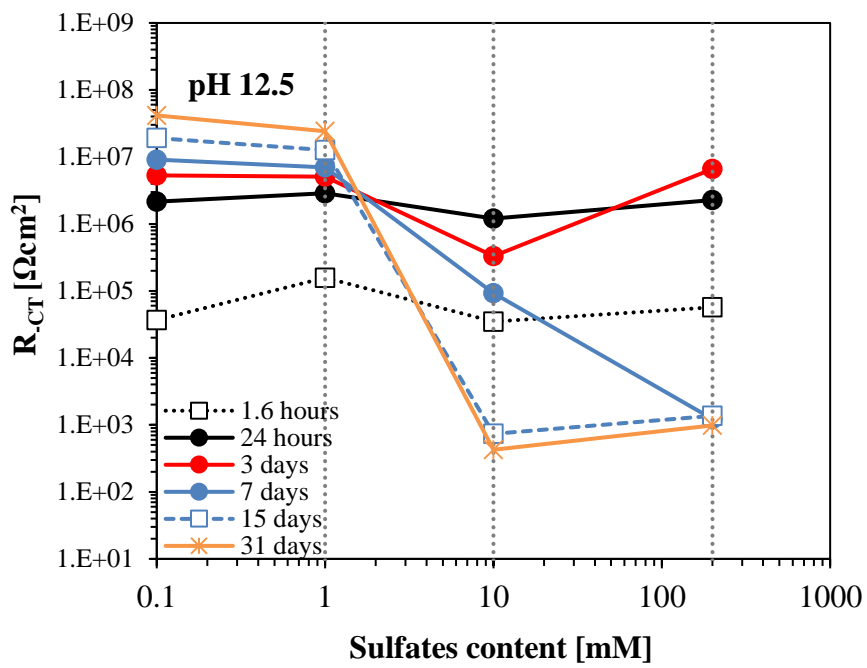
Figure 4.24: Effect of SO_4^{2-} on R_{CT} parameter over time at pH 12.5.

5   CONCLUSIONS

This doctoral thesis deals with the passivation capability of calcium sulfoaluminate (CSA) systems on carbon steel reinforcements.

Carbon steel embedded in CSA concretes shows both active and passive behavior, with slowed kinetic of passive film formation, depending on the amount of the mineralogical component ye'elimite in the binder. The peculiar mineralogical composition of CSA concretes determines different pH values, in the range of 11.7÷13.2, which are always lower compared to those of OPC concretes. In absence of aggressive species, these pH values could be sufficient to promote carbon steel passivation but, in presence of chlorides, lower pH values correspond to lower capacity to contrast them. Furthermore, the delayed kinetic for film formation can expose the surface of the steel to corrosion at early ages.

Carbon steel reinforcements embedded into CSA-based concretes, characterized by the greatest amount of its mineralogical component ye'elimite (50% vs. cement mass), shows an inability to passivate, due to the low pH developed by these admixtures, around 11.7. The corrosion rates derived by electrochemical impedance spectroscopy (EIS) data are in the range of 10 μm/year, typical of active corrosion in carbonated concrete, and low corrosion potential are measured. The decrease of the ye'elimite amount to an intermediate level (25% vs. cement mass) develops admixtures characterized by pH values around 12.5, which are able to passivate the steel, but only after 30 days of curing. CSA binders containing little amount of ye'elimite (15% vs cement mass) are able to

passivate the steel, due to a pH value close to 13.2. However, the kinetic of the film formation is slightly delayed, compared to reference ordinary Portland cement (OCP) concretes, which show pH around 13.3, able to guarantee the formation of a stable passive film on the surface of the steel.

Different additions were considered concerning CSA cement containing the greatest amount of ye'elimite. The use of calcium hydroxide and of lithium carbonate set accelerator does not promote the passivation of the steel, which reveal a similar behavior to CSA concretes without any addition. ████████████████████████████
██
███████

Furthermore, dry and wet environmental conditions play an important role on the corrosion behavior of steel reinforcements in CSA concrete. The drying of the concrete promotes an increase of the corrosion potential, due to the arise of the anodic overpotential. On the contrary, increasing the moisture content of the concrete, the corrosion potential decreases together with the polarization resistance, meaning that greater corrosion rates should be expected.

Secondly, the effect of dissolved sulfates in pore solution of CSA-based concretes on passive film formation at carbon steel rebar is studied. Results show that the increase of sulfate concentration affects and decreases the capability of the steel to passivate. At low pH values (10.5÷11.5), little amount of this specie is able to avoid the formation of the passive film while, at a greater pH value (12.5) the oxide film is formed and higher concentrations are necessary to affect and promote the breakdown of the passive film.

In order to study the corrosion behavior of steel reinforcements embedded in CSA-based concretes by means of electrochemical tests and corrosion potential measurements, embeddable probes suitable for concrete applications were developed and characterized. Titanium Mixed Metal Oxide electrodes (Ti-MMO) were used to manufacture Multi-Electrodes Probes (MEP), single electrode probes and Reference Mortar Electrode

(RME) probes. All the probes shows a great stability over time and also very similar correlations between their potential and the pH of the environment in which they are immersed. Therefore, their application is suitable both for laboratory testing and for field testing on real structure.

Two different methodologies were studied and developed in order to give a quantitative measure of the pH of hardened concretes/cement pastes and, therefore, to outline the capability of the admixture to passivate the reinforcements.

Indigo Carmine indicator showed an excellent response and suitability for pH determination of ordinary and alternative binders. Its color variation in function of pH can discriminate very well the alkalinity of the admixture, especially in the range of the borderline values necessary for steel passation. Its response and facility of application, when sprayed on hardened concrete' surface, make it an important tool both for real structures and for laboratory testing.

REFERENCES

[1] M. Schneider, M. Romer, M. Tschudin, and H. Bolio, "Sustainable cement production—present and future," *Cement and Concrete Research*, pp. 642-650, 2011.

[2] A. Saunders, Preview: The top 100 global cement companies and global per capita capacity trends, December 01, 2015.

[3] Wikipedia. [Online]. https://en.wikipedia.org/wiki/List_of_countries_by_cement_production

[4] (2016) Statista. [Online]. https://www.statista.com/statistics/267364/world-cement-production-by-country/

[5] J.G.J. Olivier, G. Janssens-Maenhout, M. Muntean, and J.A.H.W. Peters, "Trends in global CO2 emissions: 2015 Report," PBL Netherlands Environmental Assessment Agency Institute for Environment and Sustainability (IES) of the European Commission's Joint Research Centre (JRC), 2015.

[6] E. Gartner, "Industrially interesting approaches to "low-CO2" cements," *Cement and Concrete Research*, no. 34, pp. 1489-1498, 2004.

[7] J.S. Damtoft, J. Lukasik, D. Herfort, D. Sorrentino, and E.M. Gartner, "Sustainable development and climate change initiatives," *Cement and Concrete Research*, no. 38, pp. 115-127, 2008.

[8] Noor-ul-Amin, "Comparative study of Geopolymer and calcium sulfoaluminate as alternatives for Ordinary Portland cement (OPC)," *Journal of Basic and Applied Chemistry*, no. 4, pp. 1-10, 2014.

[9] G. Valenti. Leganti idraulici per calcestruzzi eco-compatibili e cementi innovativi a base di solfoalluminato di calcio. [Online]. http://www.enco-journal.com/journal/ej50/valenti.html

[10] S. Lorenzi, "Corrosione-erosione dell'acciaio in conglomerati cementizi allo stato fresco," University of Bergamo, Bergamo, PhD Thesis 2010.

[11] M. Cabrini, S. Lorenzi, and T. Pastore, "Studio elettrochimico della formazione del film di passività sulle armature nel calcestruzzo," in *Giornate Nazionali della Corrosione*, Napoli, 2013.

[12] U. Angst, B. Elsener, C.K. Larsen, and O. Vennesland, "Critical chloride content in reinforced concrete – A review," *Cement and Concrete research*, vol. 39, pp. 1122-1138, 2009.

[13] U. Angst and O. Vennesland, "Critical chloride content in reinforced concrete," Trondheim, COIN project report 2008.

[14] C.L. Page, "Mechanism of corrosion protection in reinforced concrete marine structures," *Nature*, vol. 258, pp. 514-515, 1975.

[15] M. Cabrini, S. Lorenzi, and T. Pastore, *Cyclic voltammetry evaluation of inhibitor for localised corrosion in alkaline solutions, Electrochim.*: Akta, 2013.

[16] M. Cabrini, S. Lorenzi, and T. Pastore, "Studio della corrosione localizzata degli acciai per armature in soluzioni alcaline inibite," *La metallurgia italiana*, vol. 105, pp. 21-31, 2013.

[17] D.A. Hausmann, "Steel corrosion in concrete - how does it occur?," *Material protection*, vol. 6, no. 11, pp. 19-23, 1967.

[18] V.K. Gouda, "Corrosion and inhibition of reinforcing steel: 1. Immersed in alkaline solution," *British corrosion journal*, vol. 5, no. 5, pp. 198-203, 1970.

[19] S. Goni and C. Andrade, "Synthetic Concrete Pore Solution Chemistry and Rebar Corrosion Rate in the Presence of Chlorides," *Cement and concrete research*, vol. 20, pp. 525-539, 1990.

[20] S. Diamond, "Chloride concentrations in concrete pore solutions resulting from calcium and sodium chloride admixtures," *Cement and concrete aggregate*, vol. 8, no. 2, pp. 97-102, 1986.

[21] T. Yonezawa, V. Ashworth, and R.P.M. Procter, "Pore Solution Composition and Chloride Effects on the Corrosion of Steel in Concrete," *Corrosion*, vol. 44, no. 7, pp. 489-499, 1988.

[22] M. Alonso and M. Sanchez, "Analysis of the variability of chloride threshold values in the literature," *Materials and corrosion*, vol. 60, no. 8, pp. 631-637, 2009.

[23] G.K. Glass and N.R. Buenfeld, "The presentation of the chloride threshold level for corrosion of steel in concrete," *Corrosion science*, vol. 39, no. 5, pp. 1001-1013, 1997.

[24] C. Arya, N.R. Buenfeld, and J. Newman, "Factors Influencing Chloride-binding in Concrete," *Cement concrete research*, vol. 20, pp. 291-300, 1990.

[25] R., S. Schrebler Guzmán, J., R. Vilche, and A., J. Arvia, "The potentiodynamic behavior of iron in alkaline solutions," *Electrochimica Acta*, vol. 24, no. 4, pp. 395-403, 1979.

[26] J., T. Hinatsu, W., F. Graydon, and F., R. Foulkes, "Voltammetric behavior of iron in cement II: effect of sodium chloride and corrosion inhibitor additions," *Journal of Applied Electrochemistry*, vol. 20, no. 5, pp. 841-847, 1990.

[27] S. Lorenzi, T. Pastore, and M. Cabrini, "Steel damaging in flowing mortar," *Corrosion Engineering Science and Technology*, vol. 51, pp. 596-605, November 2016.

[28] J.T. Hinatsu, W.F. Graydon, and F.R. Foulkes, "Voltammetric behavior of iron in cement. I. Development of a standard procedure for measuring voltammograms," *Journal of applied electrochemistry*, vol. 19, no. 6, pp. 868-876, 1988.

[29] F.R. Foulkes and P. McGrath, "A rapid cyclic voltammetric method for studying cement factors affecting the corrosion of reinforced concrete," *Cement and concrete research*, no. 29, pp. 873-883, 1999.

[30] M.L. Matteo, T. Fernandez Otero, and D.J. Schiffrin, "Mechanism of enhancement of the corrosion of steel by alternating currents and electrocatalytic properties of cycled steel surfaces," *Journal of Applied Electrochemistry*, vol. 20, pp. 26-31, 1990.

[31] C. Andrade, M. Keddam, X. Ramón Nóvoa, and H. Takenouti, "Electrochemical behavior of steel rebars in concrete: Influence of environmental factors and cement chemistry," *Electrochimica Acta*, no. 46, pp. 3905-3912, 2001.

[32] C.Y. Chao, L.F. Lin, and D.D. MacDonald, "A Point Defect Model for Anodic Passive Films," *Journal of the electrochemical society*, vol. 129, pp. 1874-1879, 1982.

[33] M. Bojinov, I. Kanazirski, and A. Girginov, "Proceedings of the Symposium on Passivity and Its Breakdown," , 1992.

[34] C. Gabrielli, M. Keddam, F. Minouflet, and H. Perrot, "Investigation of the anodic behavior of iron in sulfuric acid medium by the electrochemical quartz microbalanc under ac regime," *Material science*, pp. 185-188, 1995.

[35] P. Merino, X.R. Novoa, M.C. P´erez, L. Soler C. Andrade, *Material science forum*, pp. 192–194, 1995.

[36] M. Sánchez et al., "Electrochemical impedance spectroscopy for studying passive layers on steel rebars immersed in alkaline solutions simulating concrete pores," *Electrochimica acta*, vol. 52, pp. 7634-7641, 2007.

[37] R. Cabrera-Sierra, I. García, E. Sosa, T. Oropeza, and I González, "Electrochemical behavior of carbon steel in alkaline sour environments measured by electrochemical impedance spectroscopy," *Electrochimica acta*, vol. 46, pp. 487-497, 2000.

[38] C. Christodoulou, C.I. Goodier, S.A. Austin, J. Webb, and G. Glass, "On-site transient analysis for the corrosion assessment of reinforced concrete," *Corrosion science*, no. 62, pp. 176-183, 2012.

[39] M. Cabrini, S. Lorenzi, T. Pastore, S. Pellegrini, and D. Pesenti Bucella, "EIS and Voltammetric study of passive film formation on steel bar embedded in Portland cement and innovative cementitious binders," in *10th International Symposium on Electrochemical Impedance Spectroscopy*, Toxa, 2016, p. 116.

[40] C. Andrade and C. Alonso, "Test methods for on-site corrosion rate measurement of steel reinforcement in concrete by means of the polarisation resistance method," *Materials sctructures*, no. 37, pp. 623-643, 2004.

[41] M. Stern and A.L. Geary, "lectrochemical polarisation I: a theoretical analysis of the shape of polarisation curves," *Electrochemical science*, no. 104, pp. 55-63, 1957.

[42] S. Joiret, M. Keddam, X. Ramón Nóvoa, and H. Takenouti, "Use of EIS, ring-disk electrode, EQCM and Raman spectroscopy to study the film of oxides formed on iron in 1M NaOH," *Cement & Concrete Composites*, no. 24, 2002.

[43] M. Sánchez Moreno, J. Gregori, C. Alonso, and F. Vicente, "Anodic growth of passive layers on steel rebars in an alkaline medium simulating the concrete pores," *Electrochimica acta*, no. 52, pp. 47-53, 2006.

[44] U. Retter, A. Widmann, K. Siegler, and H. Kahlert, *Journal of electrochemical chemistry*, vol. 543, no. 87, 2006.

[45] J.R. Macdonald,., 1987.

[46] C. Monticelli, A. Frignani, and G. Trabanelli, "Corrosion inhibition of steel in chloride-containing alkaline solutions," *Journal of Applied Electrochemistry*, vol. 32, pp. 527-535, 2002.

[47] G.K. Glass, C.L. Page, N.R. Short, and J.Z. Zhang, "The analysis of potentiostatic transients applied to the corrosion of steel in concrete," *Corrosion science*, vol. 39, 1997.

[48] F.P. Glasser and L. Zhang, "High-performance cement matrices based on calcium sulfoaluminate–belite compositions," *Cement and Concrete research*, no. 31, pp. 1881-1886, 2001.

[49] J. Péra and J. Ambroise, "New applications of calcium sulfoaluminate cement," *Cement and Concrete Research*, no. 34, pp. 671-676, 2004.

[50] F. Winnefeld and B. Lothenbach, "Hydration of calcium sulfoaluminate cements — Experimental findings and thermodynamic modelling," *Cement and Concrete Research*, no. 40, pp. 1239-1247, 2010.

[51] P. Arjunan, M. R. Silsbee, and D. M. Roy, "Sulfoaluminate-belite cement from low-calcium fly ash and sulfur-rich and other industrial by-products," *Cement and Concrete Research*, no. 29, pp. 1305-1311, 1999.

[52] K. Quillin, "Performance of belite–sulfoaluminate cements," *Cement and Concrete Research*, no. 31, pp. 1341-1349, 2001.

[53] S. Ioannou, K. Paine, L. Reig, and K. Quillin, "Performance characteristics of concrete based on a ternary calcium sulfoaluminate–anhydrite–fly ash cement," *Cement & Concrete Composites*, no. 55, pp. 196-204, 2015.

[54] Y. Liao, X. Wei, and G. Li, "Early hydration of calcium sulfoaluminate cement through electrical resistivity measurement and microstructure investigations," *Construction and Building Materials*, no. 25, pp. 1572-1579, 2011.

[55] D. Gastaldi et al., "In situ tomographic investigation on the early hydration behaviorsof cementing systems," *Construction and Building Materials*, no. 29, pp. 284-290, 2012.

[56] D. Kalogridis, G.Ch. Kostogloudis, Ch. Ftikos, and Ch. Malami, "A quantitative study of the influence of non-expansive sulfoaluminate cement on the corrosion of

steel reinforcement," *Cement and concrete research*, vol. 30, pp. 1731-1740, 2000.

[57] D. Gastaldi et al., "Hydraulic Behavior of Calcium Sulfoaluminate Cement Alone and in Mixture with Portland Cement".

[58] P.K. Mehta, "Mechanism of expansion associated with ettringite formation," *Cement and Concrete Research*, vol. 3, pp. 1-6, 1973.

[59] G. Bernardo, A. Telesca, and G. L. Valenti, "A porosimetric study of calcium sulfoaluminate cement pastes cured at early ages," *Cement and Concrete Research*, no. 36, pp. 1042-1047, 2006.

[60] D. Zhang , D. Xu, X. Cheng, and W. Chen, "Carbonation Resistance of Sulphoaluminate Cement-based High Performance Concrete," *Journal of Wuhan University of Technolotgy-Mater. Sci. Ed.*, pp. 663-666, 2009.

[61] Q. Zhou, N.B. Milestone, and M. Hayes, "An alternative to Portland Cement for waste encapsulation—The calcium sulfoaluminate cement system," *Journal of Hazardous Materials*, no. 136, pp. 120-129, 2006.

[62] F. Glasser and M. Andac, "Pore Solution Composition of Calcium Sulfoaluminate Cement," *Advances in cement research*, vol. 11, pp. 23-26, January 1999.

[63] A. Vollpracht, B. Lothenbach, R. Snellings, and J. Haufe, "The pore solution of blended cements: a review," *Materials and Structures*, vol. 49, pp. 3341–3367, 2016.

[64] J. Shi and W. Sun, "Effect of Sulfate Ions on the Corrosion Behavior of Steel in Concrete Using Electrochemical Methods," *Advanced material research*, pp. 3049-3054, 2010.

[65] G. Le Saout, B. Lothenbach, A. Hori, T. Higuchi, and F. Winnefeld, "Hydration of Portland cement with additions of calcium sulfoaluminates," *Cement and concrete research*, vol. 43, pp. 81-94, 2013.

[66] L. Pelletier-Chaignat, F. Winnefeld, B. Lothenbach, and G. Le Saout, "Influence of the calcium sulphate source on the hydration mechanism of Portland cement–calcium sulphoaluminate clinker–calcium sulphate binders," *Cement & concrete composites*, vol. 33, pp. 551-561, 2011.

[67] M.C.G. Juenger, F. Winnefeld, J.L. Provis, and J. Ideker, "Advances in alternative cementitious binders," *Cement and concrete research*, vol. 41, pp. 1232-1243, 2011.

[68] T. Pastore, M. Cabrini, S. Lorenzi, S. Pellegrini, and L. Coppola, "Valutazione del comportamento a corrosione i calcestruzzi confezionati con leganti innovativi," in *Giornate Nazionali sulla Corrosione e Protezione – XI Edizione*, 2015.

[69] T. Pastore, L. Coppola, and S. Lorenzi, "Qualificazione dei Nuovi Leganti per il confezionamento di Calcestruzzi in Relazione alla Protezione delle Armature in Acciaio," in *AIMAT, Nuovi orizzonti della ricerca LEGANTI, CALCETSRUZZI E MATERIALI INNOVATIVI PER COSTRUIRE SOSTENIBILE, in Onore di Giuseppe Frigione*, Cosenza, 2015.

[70] I. Janokta and L. Krajči, "An experimental study on the upgrade of sulfoaluminate—belite cement systems by blending with Portland cement," *Advances in cement research*, vol. 11, pp. 35-41, January 1999.

[71] PCA America's Cement Manufactures. Chemical Admixtures. [Online]. http://www.cement.org/cement-concrete-basics/concrete-materials/chemical-admixtures

[72] J.A. Mihell and J.K. Atkinson, "Planar Thick-film pH electrodes based on ruthenium dioxide hydrate," *Sensors and Actuators B*, no. 48, pp. 505-511, 1998.

[73] V.V. Panić, T.R. Vidaković, A.B. Dekanski, V.B. Mišković-Stanković, and B.Ž Nikolić, "Capacitive properties of RuO2-coated titanium electrodes prepared by the alkoxide ink procedure," *Journal of Electroanalytical Chemistry*, no. 609, pp. 120-128, 2007.

[74] G.M. da Silva et al., "Development of low-cost metal oxide pH electrodes based on the polymeric percursor method," *Analytica Chimica Acta*, no. 616, pp. 36-41, 2008.